

“Oligodendrocytes as active modulators of neuroinflammation”

Von der Fakultät für Mathematik, Informatik und Naturwissenschaften der RWTH Aachen University zur Erlangung des akademischen Grades einer Doktorin der Naturwissenschaften genehmigte Dissertation

vorgelegt von

Diplom-Biologin

Katharina Henriette Janssen geborene Berger

aus Witten

Berichter: Universitätsprofessor Dr. rer. biol. hum. Cordian Beyer

Berichter: Universitätsprofessor Dr. rer. nat. Hermann Wagner

Tag der mündlichen Prüfung: 7. April 2014

Diese Dissertation ist auf den Internetseiten der Hochschulbibliothek online verfügbar

Meiner Familie

Ein Gelehrter in seinem Laboratorium ist nicht nur ein Techniker; er steht auch vor den Naturgesetzen wie ein Kind vor der Märchenwelt.

- Marie Curie

Index	
Abbreviations	4
1. Introduction	6
1.1 Multiple sclerosis: autoimmunity versus oligodendroglipathy	6
1.2 Oligodendrocytes in multiple sclerosis	7
1.3 Chemokines in multiple sclerosis	10
1.4 Microglia in multiple sclerosis	12
2. Scope of the study	14
3. Materials and Methods	15
3.1 Mice and demyelination	15
3.2 Tissue preparation: transcardial perfusion and paraffin-embedding	15
3.3 Immunohistochemistry (IHC) and cell parameter quantification	17
3.4 Immunocytochemistry (ICC)	20
3.5 Electron microscopy	21
3.6 <i>In situ</i> hybridization (ISH)	21
3.7 Cell culture and treatment	22
3.7.1 Primary cultures of glial cells	22
3.7.2 Oligodendrocyte precursor cells	22
3.7.3 Rat OLN93 cells	24
3.7.4 Mouse embryonic stem cell-derived microglial cells	24
3.7.5 Primary mouse astrocyte cultures	25
3.7.6 Isolation of mouse peritoneal macrophages	25
3.8 Migration and Phagocytosis Assay	25
3.9 CellTiter Blue® Cell viability and CytoTox non-radioactive cytotoxicity assay	26
3.10 Microarray analysis	26
3.11 Real-time reverse transcriptase-polymerase chain reaction (<i>rt</i> RT-PCR)	27
3.12 Genotyping of CCL2/3 ^{-/-} mice	29
3.13 Enzyme-linked immunosorbent assay (ELISA)	30
3.14 SDS polyacrylamide gel electrophoresis (SDS-PAGE) and Western Blot	31
3.15 Statistical analysis	33
4. Results	34
4.1 Oligodendrocyte-derived chemokine CXCL10 triggers microglial activation in the cuprizone animal model of multiple sclerosis	34

4.1.1 Oligodendrocyte loss occurs early in the cuprizone model	34
4.1.2 Chemokines are dynamically regulated in cuprizone-treated mice	37
4.1.3 CXCL10- but not CCL2- or CCL3-deficient mice display less severe early microglia activation	39
4.1.4 CXCL10 is expressed and secreted by oligodendrocytes	40
4.1.5 CXCL10 does not affect mature oligodendrocyte cell death	45
4.1.6 CXCL10 does not regulate microglia proliferation	47
4.1.7 CXCL10 induces microglia attraction and activation, but not phagocytosis	49
4.2 The growth factors FGF-2 and PDGF α are involved in oligodendrocyte maturation and homeostasis <i>in vitro</i>	53
4.2.1 FGF-2 and PDGF α inhibit myelin gene expression in oligodendrocytes possibly via ERK signalling	53
4.3 The chemokines CCL2 and CCL3 regulate cortical myelin integrity in the cuprizone model	56
4.3.1 CCL2/3 ^{-/-} mice are viable, fertile and show no gross physical or behavioural abnormality	56
4.3.2 CCL2 and CCL3 expression is disrupted in CCL2/3 ^{-/-} mice	58
4.3.3 CCL2/3 ^{-/-} mice display normal brain morphology	60
4.3.4 CCL2/3 ^{-/-} mice display less severe demyelination, astrogliosis and oligodendrocyte loss in the cortex after cuprizone-induced acute demyelination	62
5. Discussion	67
5.1 Oligodendrocyte-derived chemokine CXCL10 triggers microglial activation in the cuprizone model	67
5.2 The growth factors FGF-2 and PDGF α are involved in oligodendrocyte maturation and homeostasis <i>in vitro</i>	69
5.3 The chemokines CCL2 and CCL3 regulate cortical myelin integrity in the cuprizone model	70
6. Work contribution	73
7. References	74
8. Summary	85
9. Curriculum vitae & publications	88
10. Danksagung	90

Abbreviations

18s	18s ribosomal RNA
A. dest.	Aqua destillata
APC	adenomatous poliposis coli
bp	base pairs
BSA	bovine serum albumine
CA2	carbonic anhydrase 2
Casp3	Caspase-3
CC	corpus callosum
CCL2 ^{-/-}	CCL2 knockout
CCL2/3 ^{-/-}	CCL2/CCL3 double knockout
CCL2/MCP1	monocyte chemotatic protein-1
CCL3 ^{-/-}	CCL3 knockout
CCL3/MIP1 α	macrophage inflammatory protein-1 α
cDNA	complementary desoxyribonucleic acid
CNPase	2',3'-cyclic-nucleotide 3'-phosphodiesterase
CNS	central nervous system
CNTF	ciliary neurotrophic factor
CO	control
Ct	cycle threshold
Cx	cortex
CXCL10 ^{-/-}	CXCL10 knockout
CXCL10/IP10	interferon-inducible protein-10
CYCA	cyclophilin A
DAB	di-aminobenzidine
DIFF	basal primary oligodendrocyte medium containing CNTF & T3
DMEM	Dulbecco's modified eagle medium
EAE	experimental autoimmune encephalomyelitis
ELISA	enzyme-linked immunosorbent assay
EM	electron microscopy
ERK1/2	extracellular signal-regulated kinase 1/2
ESdM	embryonic stem cell-derived microglial cells
FCS	fetal calf serum
FC	fold change
FGF-2	basic fibroblast growth factor
GAPDH	glyceraldehyde 3-phosphate dehydrogenase
GF	basal primary oligodendrocyte medium containing FGF-2 & PDGF α
GFAP	glial fibrillary acidic protein
GPCR	G-protein coupled receptor
HE	haematoxylin eosin
HIER	heat-induced epitope retrieval
Hip	Hippocampus
HRP	horse reddish peroxidase

IBA1	ionized calcium binding adaptor molecule-1
ICC	Immunocytochemistry
IHC	Immunohistochemistry
IFN γ	interferon- γ
iNOS	inducible nitric oxide synthase
ISH	<i>in situ</i> hybridisation
KO	Knockout
LDH	lactate dehydrogenase
LPS	Lipopolysaccharide
MAC3/LAMP2	surface antigen MAC3/ lysosomal-associated membrane protein-2
MAG2	myelin associated glycoprotein-2
MBP	myelin basic protein
mOL	mature oligodendrocyte
mRNA	messenger ribonucleic acid
MS	multiple sclerosis
Mut	mutant i.e. knock out
NAWM	normal appearing white matter
OLIG2	oligodendrocyte transcription factor-2
OPC	oligodendrocyte precursor cell
P/S	penicillin/streptomycin
PBS	phosphate buffered saline
PCNA	proliferating cell nuclear antigen
PDGFR α	platelet-derived growth factor receptor α
PDGF α	platelet-derived growth factor α
PLP	proteolipid protein
RIN	RNA integrity number
rtRT-PCR	real time reverse transcriptase- polymerase chain reaction
SDS-PAGE	SDS-polyacrylamide gelelectrophoresis
SEM	standard error of the mean
sqRT-PCR	semi-quantitative reverse transcriptase-polymerase chain reaction
T3	triiodo-L-thyronine
TBS	tris-buffered saline
TBST	tris-buffered saline/ 0.05% Tween20®
TNF α	tumor necrosis factor α
WT	wild type

1. Introduction

1.1 Multiple sclerosis: autoimmunity versus oligodendroglipathy

Multiple sclerosis (MS) is an inflammatory disease of the central nervous system (CNS) characterized by myelin loss, oligodendrocyte death, inflammation and various degrees of axonal damage [1]. Oligodendrocytes as the principal target in MS pathology maintain the myelin sheath of up to 40 neighbouring axons. In consequence, oligodendrocyte death and destruction of the myelin sheath result in disturbances of saltatory conduction, axon degeneration and neuronal loss and thus lead to the variety of neurological symptoms observed in MS patients [2]. MS occurs usually in young adults between 20 and 40 years of age with a particular higher prevalence in women. With 2 to 2.5 million people affected worldwide it is the most-common chronic inflammatory disease of the CNS [3-4]. The first clinico-pathological description was given in 1868 by the French neurologist Jean-Martin Charcot (1825-1893) and almost 150 years later the cause of MS is still unknown [3].

For long MS was exclusively discussed as an autoimmune disorder with autoreactive T-cells directed against myelin components as the disease trigger [5]. This view was partially build on and supported by research obtained in one of the most common MS animal models: experimental autoimmune encephalomyelitis (EAE) [6]. EAE is a model that leads to T-cell driven inflammatory demyelination in the spinal cord due to immunization with myelin proteins or spinal cord homogenates [7-9]. Although MS and EAE have some features in common, like involvement of the adaptive immune response in CNS inflammation or clinical disease course, several differences exist between the model and the disease, which cannot be explained with an exclusive autoimmune view of the disease [10-13]. In the past ten years researchers have investigated biopsies and autopsies of MS patients and made a significant discovery: in CNS tissue of MS patients pathological changes occur in the absence of T-cell driven inflammation and demyelination [14-20]. Among others, they found activation of microglial cells [14-15, 21] as well as increased expression of anti-apoptotic genes in oligodendrocytes and apoptotic oligodendrocytes [19, 22]. Based on this observations some researchers claimed that the different lesion patterns described in MS [23] should not be considered as different types of the disease, but rather as different time points in disease development [11-12]. In this view, early pathological changes (microglia activation and oligodendroglipathy) with no or very little adaptive immune response precede the formation of an active demyelinating lesion with strong adaptive immune response, finally followed by the development of a chronic lesion with decreasing inflammation [1, 20]. The responsible

trigger causing this early changes is completely unknown, but different genetical and environmental risk factors have long been discussed in the context of MS, for example viruses, chemicals or lack of vitamin D, but none was proven so far [24-29]. Suggesting that oligodendroglipathy and activation of microglial cells as the major cells of CNS innate immune response [30-32] are the first steps in MS lesion development, leads to the question what factors are responsible for microglia activation in the absence of demyelination and thus myelin debris? For instance, it has been shown that the small heat shock protein α -B-Crystallin is expressed in oligodendrocytes in the normal appearing white matter (NAWM) of MS patients and is able to activate microglial cells [33]. It is likely that further factors, such as cytokines or chemokines, are also involved in the observed microglia activation. The initial activation of microglial cells might alter the integrity of the blood brain barrier leading to activation and recruitment of peripheral immune cells as found in active demyelinating MS lesions. Since the EAE model is primarily an adaptive immune driven model, other animal models are necessary to study details of this scenario, where the adaptive immune response plays no or only a minor role. A well described model to study demyelination *in vivo*, which is not of an autoimmune origin is the cuprizone model. In the past years, the cuprizone model was extensively characterized with respect to de- and remyelination properties and the complex cell-cell interactions during these processes [34-39]. Feeding of cuprizone, chemically a copper chelator, induces demyelination of many CNS white and grey matter regions, notably the corpus callosum (CC) [34]. In this model, oligodendroglipathy results in significant oligodendrocyte apoptosis with concomitant microglial activation, astrogliosis, and finally active demyelination [35-36, 40-41]. The underlying biochemical and cellular mechanisms of these alterations are, however, still poorly understood. Extensive investigations of these mechanisms will help to understand the molecular changes during oligodendroglipathy and microglia activation not only in the cuprizone model, but also in MS. This has further implications for the understanding of disease mechanisms and for the development of future treatment strategies.

1.2 Oligodendrocytes in multiple sclerosis

In the central nervous system functionality of neurons depends on the integrity of the myelin sheath. The myelin sheath is build up by oligodendrocytes that tightly enwrap neuronal axons with concentric loops of their plasma membrane. Disturbance of the myelin sheath leads to severe failure in action potential conduction and thus problems on various levels such as cognitive, sensory- and motorfunctions. Myelinating oligodendrocytes originate from

oligodendrocyte progenitor cells (OPCs) which are generated in the ventral epithelium of the neural tube in early embryonic life [42-43] and in the dorsal spinal cord, hindbrain and telencephalon in late embryonic development and early post-natal life [44-47]. During development OPCs migrate into the developing white matter [48-50], exit the cell cycle, undergo differentiation into mature oligodendrocytes and begin to express a subset of myelin-associated proteins [51-52]. When an oligodendrocyte gets in close contact to an unmyelinated axon it starts to enwrap it with flat membrane sheets. Myelin components are synthesized and transported to the appropriate region within the sheath. Finally, when the axon is wrapped, the myelin membrane is compacted such that myelin leaflets are practically fused and almost devoid of cytoplasm [53-56]. In the CNS, one single oligodendrocyte can produce up to 40 myelin segments on different axons. This means, myelinating oligodendrocytes produce as much as $5\text{-}50 \times 10^3 \mu\text{m}^2$ of membrane per day [57]. It is clear that maintaining this membrane needs a continual high turnover of myelin and is correlated with high levels of myelin gene expression long after the completion of the myelination process [58-59]. The maintenance of this enormous membrane makes oligodendrocytes particularly vulnerable to pathologic changes as they are confronted with several metabolic challenges. First, oligodendrocytes have an extremely high metabolic rate and consume large amounts of ATP and oxygen, which leads to the production of hydrogen peroxide and reactive oxygen species as by-products [60]. Second, many of the myelin synthetic enzymes require iron as a co-factor [61] which can under unfavourable conditions evoke free radical formation and lipid peroxidation [62-63]. The problem of oxidative stress is even more severe as oligodendrocytes exhibit only low levels of the anti-oxidative enzyme glutathione [64]. Third, the endoplasmatic reticulum of oligodendrocytes works on the upper limit of its capacity due to high myelin protein synthesis. Already small changes in the amount of a single protein can easily result in missfolding and accumulation of other proteins in this organelle, leading to endoplasmatic reticulum stress and, if not eliminated by corresponding rescue pathways, possibly apoptosis [65-67]. Taken together these unique metabolic features of oligodendrocytes makes them a vulnerable cell population under pathological changes in the CNS.

In MS the destruction of myelin and oligodendrocyte apoptosis leads to the typical demyelinating lesions. Whether lesions develop due to inflammation in an autoimmune manner or due to high vulnerability of oligodendrocytes to a still unknown trigger with inflammation as a secondary phenomenon, is topic of a controversial debate (see 1.1). Nevertheless, recent findings suggest that oligodendrocyte apoptosis and accompanying

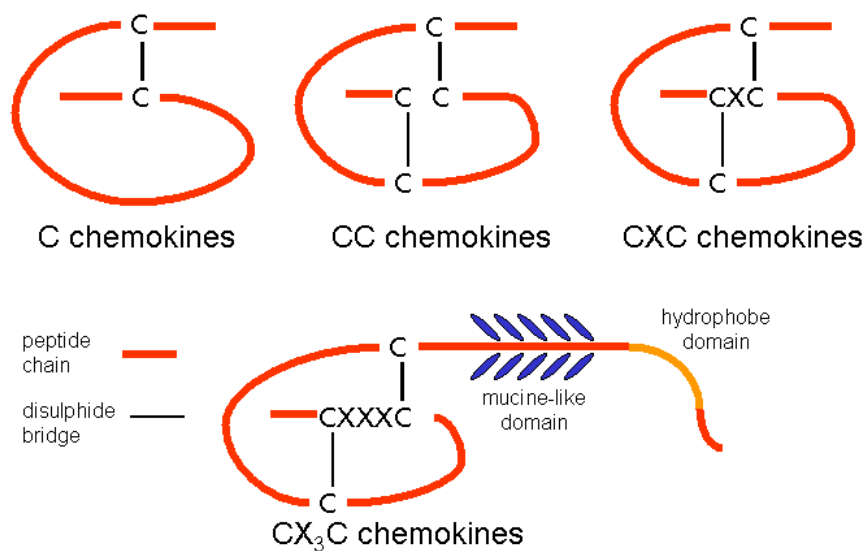
microglia activation precede the infiltration of the brain parenchyma with peripheral immune cells like macrophages and T-cells and the formation of demyelinating plaques [19, 68-69]. Therefore, the view that oligodendrocytes are only 'passive victims' during MS lesion development and progression should be reconsidered. For example, experimental studies showed that the absence of oligodendrocyte protective factors increases oligodendrocyte susceptibility to injury and augments the inflammatory reaction [70]. In addition, mice lacking pro-apoptotic genes, or over-expressing anti-apoptotic molecules, exclusively in oligodendrocytes, display resistance to EAE [71-72]. This resistance is paralleled by reduced numbers of infiltrating T-cells and macrophages/microglia in the EAE lesions [71]. These examples promote the view that myelinating oligodendrocytes can control neuroinflammatory and demyelinating processes in the brain. Whether this control is a passive effect due to less oligodendrocyte apoptosis or if it is actively controlled by the secretion of inflammatory factors was not systematically investigated in these studies. In this context the cuprizone model is of particular interest to study the microenvironment during oligodendrocyte damage, as it displays a primary oligodendroglialopathy with significant oligodendrocyte apoptosis and concomitant microglia activation [35-36, 40-41, 73]. Thus, the cuprizone model provides the pathological conditions needed to investigate the presence of oligodendrocyte-derived inflammatory factors and possible effects on microglia activation.

Another important aspect of oligodendrocyte biology in the context of MS is their capacity to remyelinate axons after demyelination [74]. During remyelination OPCs, which are located throughout the adult grey and white matter [75-76], proliferate and migrate into the demyelinated lesion site, differentiate to mature oligodendrocytes and start to enwrap demyelinated axons. This important repair mechanism is jointly responsible to retrieve axonal function and restore clinical disability in MS patients to a certain extent. For the majority of MS patients this repair mechanism ultimately fails leading to persistent demyelination, axonal loss and progressive clinical decline. Why remyelination failure occurs in MS is poorly understood [77], but it seems that the differentiation of OPCs is inhibited, preventing their maturation and thus myelination [78]. The process of remyelination involves different signalling pathways which influence proliferation and differentiation of OPCs. For example the growth factors platelet derived growth factor α (PDGF α) and basic fibroblast growth factor (FGF-2) are involved in OPC proliferation, suppress differentiation and myelin protein production [79-84] and have been described to be expressed after demyelination [85]. Among others, both factors might be involved in remyelination failure in MS. A better understanding what factors drive OPC proliferation and possibly inhibit OPC differentiation, would offer

novel clues for therapeutic intervention to promote OPC differentiation and thus remyelination.

1.3 Chemokines in multiple sclerosis

Chemokines represent a group of chemotactic proteins, playing important roles during leucocyte attraction and activation under inflammatory conditions [86-89]. Chemokines are relatively small proteins with a molecular weight from 8 to 14 kDa. They can be subdivided into four groups, depending on the number and spacing of conserved cysteine residues in their amino termini (compare Fig. 1) [90-91]. Today, approximately 50 chemokines [92] and 20 corresponding receptors [93] have been described in human, with orthologs in other mammalian species [89, 94].



© Kohidai, L.

Figure 1 Structure of chemokine classes

Chemokines consist of four subfamilies which are distinguished by the number and spacing of conserved cysteine residues in their amino termini. The largest chemokine classes are the CC and CXC chemokines, whereas the C and CX₃C chemokine families consist only of two or one member, respectively.

Chemokines signal through a group of seven-transmembrane G-protein coupled receptors (GPCRs), which are expressed on various cells including immune cells as well as astrocytes, oligodendrocytes, microglia and neurons [95]. Due to the diversity of down-stream GPCR signalling, chemokines may control a broad spectrum of cellular functions, among cell migration [96-97]. Furthermore, most chemokines display affinity for more than one receptor making their action more complex compared to other cytokines. Beside the classical GPCRs atypical receptor-like molecules exist, which do not show classical chemokine receptor function but significantly regulate the complex chemokine network, making chemokine functions even more versatile [98-100]. In addition, chemokine function can be negatively

regulated by chemokine receptor desensitization and internalization upon ligand binding [101-102].

Beside their role in immune response chemokines execute a variety of functions in the CNS. They are involved in migration and development of neural stem cells [103-104], regulate the growth of axons during neuronal development [105-106], are discussed to influence electrical activity in neurons [107-108] and have been shown to co-ordinate the communication between neurons and microglial cells under distinct neuropathological conditions [109]. Furthermore, chemokines induce proliferation [110-111] and migration of astrocytes *in vitro* [112-116] indicating a role during the formation of astrogliosis. The induction of chemokines and their receptors in various pathologies of the CNS, like Alzheimer's disease, Behçet's disease, HIV-1-associated dementia, human T-cell leukemia virus-1-associated myelopathy or brain injury [117-118] argue for an important role of the chemokine system in neuropathology. Regarding MS, a variety of chemokines and chemokine receptors is induced in this demyelinating disease and has been demonstrated in both acute and chronic MS lesions (reviewed in [119]). This included among others monocyte chemoattractant protein-1 (MCP1 or CCL2), macrophage inflammatory protein-1 α (MIP1 α or CCL3) and interferon-inducible protein-10 (IP10 or CXCL10) [119], all described to be involved in immune cell activation.

Through construction of transgenic and knockout mice, much progress has been made in our understanding of chemokine action *in vivo*. Several research groups have used EAE to probe CNS chemokine expression and function. CCL2-deficient mice were markedly resistant to EAE, and showed a significant reduction in macrophage recruitment into the CNS [120]. Karpus and colleagues showed that anti-CCL3 antibodies suppress initial attacks of adoptive-transfer EAE, while anti-CCL2 antibodies inhibit subsequent relapses, indicating that specific chemokines execute no redundant functions in these disease models [121-123]. Furthermore, CXCL10 levels have been correlated with the development of EAE, and the recruitment of T-cells expressing the CXCL10 receptor CXCR3. In mice treated with anti-CXCL10 antibodies a lower accumulation of inflammatory mononuclear cells and decreased incidence of EAE were observed [124]. These results could not be confirmed in a more recent study using anti-CXCL10 antibodies and CXCL10 deficient mice were even more susceptible to EAE [125-127], highlighting the complex role of chemokines under pathological conditions. Moreover, one should consider that EAE does not fully reflect the situation in MS, but it is highly probable that chemokines and their receptors are involved in MS pathogenesis [128].

Taking together, the role of chemokines in MS has been mainly discussed in terms of inflammatory recruitment of leukocytes across the blood brain barrier during lesion

progression [129-130]. However, the effects of these chemokines in the initial phase of lesion development on brain parenchymal cells, in particular microglia and astrocytes, remain to be elucidated.

1.4 Microglia in multiple sclerosis

Microglial cells are the brain resident immune cells with capacity of antigen presentation and phagocytosis [30-32]. During embryonic development and early postnatal life it is believed that monocytes invade the brain parenchyma and transform into microglial cells with similar properties as macrophages in other tissues [131]. During life microglia might be replaced either by cell division [132] or by recruitment of blood-borne monocytes, which then transform into new microglia [133]. Under physiological conditions the so called “ramified” microglia are highly dynamic cells, which send out or withdraw their numerous processes to control and observe the brain parenchyma [134-135]. Upon an insult targeted movement of microglia processes was observed and the number of responding cells was proportional to the severity of the insult [134, 136]. Under pathological conditions such as MS the activated microglia undergoes morphological changes from a ramified cell with long and thin processes to a cell with fewer and thicker processes [137]. Furthermore microglial cells migrate through the tissue towards the site of injury for instance to clear cellular debris (i.e. myelin). In addition the cells also release cytokines, radicals as well as neurotrophic factors [31-32, 138-139] thus are able to influence the injury site in various ways. Beside the activation of CNS-intrinsic microglia, blood-borne monocytes enter the CNS perivascular spaces and parenchyma upon an injury and transform into a macrophage phenotype. Since there are no specific immunohistochemical markers it is difficult to discriminate both cell types, therefore the cells are often referred to as “macrophages/microglia”.

The accumulation of macrophages/microglia in the injured CNS has been examined in various diseases of the CNS e.g. Alzheimer’s disease, MS and spinal cord injury [140-141]. In EAE microglia activation coincided with an increase of pro-inflammatory monocytes in the blood followed by their entry into the CNS just prior to the development of clinical signs [142]. The entry of monocytes may guide the infiltration of T-cells into the CNS parenchyma as supported by the findings of Tran *et al.* who chemically depleted macrophages in EAE leading to reduced infiltration of lymphocytes in the spinal cord parenchyma as they were trapped in the perivascular space unable to cross the glia limitans formed by astrocytes [143]. These findings indicate that macrophages/microglia play an important role during disease development in this model. Furthermore, in EAE and MS disease severity positively

correlates with the presence of activated macrophages in the CNS [144]. In active demyelinating MS plaques the number of macrophages/microglia exceeds the number of lymphocytes by as much as 10-20 times [23, 145-146] and is still remarkable at the borders of chronic active plaques and a histopathological hallmark of this lesion type [147]. The resting state microglia in the healthy CNS tissue changes rapidly under detrimental conditions such as disruption of the blood brain barrier, alterations in neurotransmitter levels or when they detect danger signals from damaged cells [32, 137]. This activation of microglia together with a tremendous influx of macrophages may account for detrimental effects observed in CNS injury. For example in MS there is evidence that in some lesions microglia promote lesion development long before the infiltration of immune cells from the periphery [19]. Additionally, it is reported that microglia can kill oligodendrocytes [148-149] and that myelin is stripped off axons by macrophages/microglia in active MS lesions [150-151].

In contrast to this “negative” view of microglia/macrophage action in MS are data from studies showing that reduced microglia/macrophage activity has a detrimental outcome for remyelination, the endogenous repair process following demyelination [152]. Acute inflammation even enhances local remyelination in areas of chronic demyelination mainly due to the elevated response of macrophages/microglia [153]. Activated macrophages/microglia release a multitude of neurotrophic factors which might account for the beneficial effects observed in these studies. Furthermore the clearance of myelin debris, a significant hindrance in the process of remyelination, is mandatory for effective remyelination, as shown in studies using lysophosphatidylcholine or cuprizone to induce demyelination. In these studies depletion of macrophages resulted in impaired remyelination [154-155]. Taken together macrophages/microglia play a bilateral role during MS and in its various animal models. Understanding the fine balance between detrimental and beneficial effects of macrophages/microglia would significantly improve our knowledge of inflammatory and repair processes in the CNS and makes them promising targets for disease modifying treatments.

2. Scope of the study

During the first part of this thesis I aimed to characterize the early effects of cuprizone-treatment focusing on the role of oligodendrocytes as possible modulators of inflammatory processes. Therefore, I characterized histopathological changes in the corpus callosum of short-term (two days up to one week) cuprizone treated mice. I investigated the early oligodendroglialopathy, which is present shortly after initiating the cuprizone-diet and the paralleling activation of microglial cells. My main focus was on the question if oligodendrocytes actively contribute to microglia activation for example by the secretion of microglia activating factors (e.g. chemokines).

As described in the introduction the progenitor status of oligodendrocytes is maintained by the growth factors FGF-2 and PDGF α . A finding I could confirm during the first part of this work. Since a balanced maintenance of oligodendrocyte proliferation and maturation is fundamental for repair mechanisms in the demyelinated CNS (i.e. remyelination). During the second part of this thesis I was interested whether FGF-2 and PDGF α may influence the gene expression of primary oligodendrocytes and the oligodendrocyte-like cell line OLN93. Therefore I investigated in a second part of the study, if treatment with FGF-2 and PDGF α changes the expression of oligodendrocyte marker genes *in vitro* and which pathways might be involved in this process.

Recent and ongoing research in our laboratory focuses on the role of chemokines as possible modulators of inflammatory processes during demyelination. In the third part of the study I investigated two chemokines (i.e. CCL2 and CCL3) under demyelinating conditions, which have already been described to play important roles in the context of MS, as well as in animal models of MS (i.e. EAE and cuprizone). As mentioned in the introduction chemokines can have redundant functions and thus one chemokine might conceal an important disease mechanism of another chemokine. Therefore I generated a double knockout mouse of CCL2 and CCL3. My work focused on the basic characterization of the mice together with a first five-week cuprizone trial.

3. Materials and Methods

3.1 Mice and demyelination

C57BL/6J mice were obtained from The Jackson Laboratory's stock (000664) at Charles River (Sulzfeld, Germany) and served as controls for CCL2, CCL3, CCL2/3 and CXCL10 knockout (ko; CCL2^{-/-}, CCL3^{-/-}, CCL2/3^{-/-}, CXCL10^{-/-}) mice. CCL2^{-/-} and CCL3^{-/-} single deficient mice were obtained from The Jackson Laboratory (B6.129S4-Ccl2^{tm1Rol}/J, B6.129P2-Ccl3^{tm1Unc}/J). CXCL10^{-/-} deficient mice were kindly provided by Dr. U. Christen (*Pharmazentrum Frankfurt/ZAFES, Klinikum der Goethe Universität, Frankfurt am Main, Germany* [156]). CCL2/3^{-/-} double deficient mice were generated by extensive cross breeding of CCL2 and CCL3 single knockout mice. Mice were kept under standard laboratory conditions according to the Federation of European Laboratory Animal Science Association's recommendations. The procedures were approved by the Review Board for the Care of Animal Subjects of the district government (Nordrhein-Westfalen, Germany) and performed according to international guidelines on the use of laboratory mice. Demyelination was induced by feeding 8-week-old (19-21 g) male or 10-week-old female mice a diet containing 0.2 % or 0.25 % cuprizone (bis-cyclohexanone oxaldihydrazone, Sigma-Aldrich Inc., Germany) mixed into ground standard rodent chow (SNIFF Spezialdiäten, Germany) for the indicated period as published previously [34-35]. Control mice were fed ground standard chow. Details about sex, number of mice and the concentration of cuprizone used are indicated in the respective figure legends.

3.2 Tissue preparation: transcardial perfusion and paraffin-embedding

For histological and immunohistochemical studies, mice were transcardially perfused with 2 % paraformaldehyde perfusion solution containing:

100 ml Formaldehyde (37%, Roth, Germany)

4.6 g NaH₂PO₄ (Roth, Germany)

8 g Na₂HPO₄ (Roth, Germany)

filled up to 1 L with A. dest.

The pH was adjusted to 7.0-7.4 and the solution was filtered and cooled down to 4°C. Before perfusion, mice were intraperitoneally injected with 20 µl of Clexane (heparin, Sanofi-Aventis, Germany) diluted 1:5 in phosphate buffered saline (PBS, Biochrom, Germany). The

mice were deeply anesthetized, fixed and the thorax opened using forceps and scissors. A small cut was placed in the right heart atrium and a small needle was inserted into the left heart ventricle to perfuse the mice with 20 ml cold perfusion solution with low pressure using a syringe. Afterwards 130 ml perfusion solution was applied at low undefined pressure using a drip. The tissue of interest was stored in perfusion solution over night at 4°C and prepared the day after for immediate embedding.

Paraffin-embedding of mice tissue samples was performed by dehydration with several ethanol bathes of increasing concentration followed by incubation in xylene to eliminate ethanol residues. Finally, the tissue was incubated in paraffin wax, which was changed three times to eliminate xylene residues. The incubation times in increasing ethanol, xylene and paraffin were as follows:

70 % ethanol	2 × 40 min
96 % ethanol	3 × 40 min
100 % ethanol	1 × 40 min
100 % ethanol	2 × 60 min
xylene	3 × 40 min
paraffin	2 × 30 min
paraffin	at least 2 days

Incubation in ethanol and xylene was performed at room temperature under a fume hood and constant agitation. Paraffin incubation was performed in a 60°C incubator. The tissue samples were then embedded in paraffin using tissue molds and stored at 4°C.

Embedded brains were coronary sectioned into 5 µm sections from approximately the levels 215 to 275 (short-term cuprizone experiments with wild type, CCL2^{-/-}, CCL3^{-/-} and CXCL10^{-/-} mice), 215 to 525 (characterization of CCL2/3^{-/-} mice) and 255 to 295 (5 weeks cuprizone treatment with wild type and CCL2/3^{-/-} mice) according to the mouse brain atlas of Sidman *et al.* (<http://www.hms.harvard.edu/research/brain/atlas.html>).

For gene expression analyses, mice were transcardially perfused with ice-cold PBS, brains subsequently removed, and the entire corpus callosum (CC) was dissected from the cortex (Cx) using a stereomicroscopic approach [38, 157]. Tissues were immediately snap frozen in liquid nitrogen and kept at -80°C until further used.

3.3 Immunohistochemistry (IHC) and cell parameter quantification

For IHC, paraffin sections were placed on advanced adhesive slides (Starfrost, Knittel Glas, Germany) and dried over night at 37°C. Sections were deparaffinized and rehydrated as follows:

xylene	4 × 5 min
100 % ethanol	3 × 3 min
96 % ethanol	2 × 3 min
70% ethanol	1 × 3 min
A. dest.	1 × 3min

Depending on the primary antibody used, heat induced epitope retrieval (HIER) was performed in Tris/EDTA buffer pH 9 or citrate buffer pH 6. Some antibodies, however, did not need any HIER, and this step was thus omitted.

Tris/EDTA buffer:

- 1.21 g Tris-(hydroxymethyl)-aminomethan (Roth, Germany)
- 0.37 g Ethylendiamintetraacetic acid (Roth, Germany)
- 0.5 ml Tween®20 (Sigma-Aldrich, Germany)
- filled up to 1 L with A. dest

Citrate buffer:

- 2.94 g Sodium citrate dehydrate (Sigma-Aldrich, Germany)
- 0.5 ml Tween®20 (Sigma-Aldrich, Germany)
- filled up to 1 L with A. dest.

Sections were placed in the respective buffer and boiled using a microwave for 10 min.

After HIER sections were cooled, washed three times in PBS and blocked with PBS containing 1 % normal horse, goat or donkey serum for 1 hour. Incubation with primary antibody was performed overnight at 4°C with the primary antibodies diluted in blocking solution. Primary antibodies, corresponding HIER and dilutions used in the study are given in Table 1.

Tab. 1 Primary antibodies used for IHC/ICC

Antibody	Host	Directed against	Dilution	AGR	Supplier cat. No.
APC	Mouse	adenomatous polyposis coli (oligodendrocytes)	1:200	Tris/EDTA	Calbiochem, OP80
CA2 (used for ISH/IHC double staining)	Rabbit	carbonic anhydrase-2 (oligodendrocytes)	1:2000	None	Dr. Said Ghandour, (University of Strasbourg, France)
Caspase-3	Rabbit	Activated caspase-3 (apoptotic cells)	1:300	Tris/EDTA	Abcam Ab13847
CNPase	Mouse	2',3'-cyclic-nucleotide 3'-phosphodiesterase (oligodendrocytes)	1:250	None	Abcam ab6319
GFAP	Rabbit	glial fibrillary acidic protein (astrocytes)	1:1000	Tris/EDTA	Encore, RPCA-GFAP
GFAP (used for ISH/IHC double staining)	Rabbit	glial fibrillary acidic protein (astrocytes)	1:1000	None	Millipore (Chemicon) AB5804
IBA1	Rabbit	ionized calcium binding adaptor molecule-1 (microglia/macrophages)	1:500 (used 1:1000 for ISH/IHC double staining)	Tris/EDTA	Wako, 019-19741
MAC3	Rat	surface antigen MAC3 (phagocytic microglia/macrophages)	1:25	Tris/EDTA	BD Pharmingen, 550292
OLIG2	Rabbit	oligodendrocyte transcription factor 2 (oligodendrocytes)	1:2000	Tris/EDTA	Millipore, AB9610
PCNA	Mouse	proliferating cell nuclear antigen (proliferating cells)	1:2000	Tris/EDTA	Abcam, ab29
PLP	Mouse	proteolipid protein (myelin)	1:500	None	AbD Serotec, MCA839G

After washing three times with PBS and blocking of endogenous peroxidase in 0.3 % hydrogen peroxide (in PBS) for 30 min, sections were washed three times in PBS and incubated with appropriate biotinylated secondary antibodies for 1 hour diluted in blocking solution. Sections were washed again three times, followed by peroxidase-coupled avidin-biotin-complex for 1 hour according to the supplier's recommendation (ABC kit, Vector

Laboratories). The di-amino-benzidine-reaction (DAB; DAKO Deutschland GmbH, Germany) was used to visualize peroxidase-avidin-biotin complexes according to the supplier's recommendations. Sections were counterstained with standard haematoxylin to visualize cell nuclei if appropriate. Secondary antibodies and dilutions used are given in Table 2. Before mounting of slides in DEPEX (Serva, Germany), sections were dehydrated in bathes with increasing ethanol concentrations and xylene as follows:

70 % ethanol	2 × 3 min
96 % ethanol	2 × 3min
100 % ethanol	3 × 3 min
xylene	3 × 3 min

Haematoxylin and eosin (HE) staining was performed on deparaffinized sections for evaluation of apoptosis using well defined morphological criteria such as condensed and fragmented cell nuclei [35, 158]. Sections were placed in haematoxylin solution for 30 s and blue color was developed under running tap water for 5 min. Thereafter, slides were placed in eosin solution for 30 s followed by increasing alcohol bathes and mounting in DEPEX as described above.

For fluorescence double-labeling experiments, slides were deparaffinized, HIER was performed if appropriate and blocked with 5 % bovine serum albumin (BSA, Roth, Germany)/PBS for 1 hour and incubated overnight at 4°C with primary antibodies diluted in 1 % BSA /PBS. After washing three times with PBS slides were incubated with Alexa Fluor 488 anti-mouse and Alexa Fluor 568 anti-rabbit antibodies (1:500, Life Technologies, Germany) diluted in 1 % BSA/PBS for 2 hours followed by three washing steps in PBS. Cell nuclei were counterstained for 5 min with Hoechst 33342 (1:100,000 in PBS, Life Technologies, Germany). Slides were washed again in PBS and mounted with FluoPreserve™ mounting medium (EMD Biosciences, USA).

DAB-stained sections were analyzed using a Nikon ECLIPSE 80i microscope. Fluorescence stained slides were analyzed with the Fluid cell imaging station (Life Technologies, Germany). Z-stack and confocal images were captured using the LSM710 laser scanning microscope station (Carl Zeiss AG, Germany).

For cell-parameter quantification, two consecutive sections per mice were evaluated in the medial and lateral parts of the CC and values averaged. Quantification in the Cx area was as

well performed on two consecutive sections in the layer 4 of the somatosensory Cx and the average calculated. Ionized calcium binding adaptor molecule-positive (IBA1⁺) microglia and glial fibrillary acidic protein-positive (GFAP⁺) astrocytes were only counted when a haematoxylin-stained nucleus was clearly visible. The area and the staining intensity of the region of interest was quantified using ImageJ 1.45 (National Institute of Health, USA) and cell numbers are given in cells per mm². Counting of cells according to this procedure was performed twice by two independent, blinded examiners and results were averaged. Determination of microglial cell area was performed using ImageJ 1.45 and the auto-detect area tool. Approximately 10 randomly chosen microglial cells per section were measured in the medial CC at 400 x magnification by blinded examiners and the results averaged.

Tab. 2 Secondary antibodies for IHC/ICC

Antibody	Host	Directed against	Dilution	Supplier cat. No.
Biotinylated anti-mouse IgG	Horse	mouse IgGs	1:50	Vector Lab. BA-2000
Biotinylated anti-rabbit IgG	Goat	rabbit IgGs	1:50	Vector Lab. BA-1000
Biotinylated anti-rat IgG	Mouse	rat IgGs	1:25	BD Pharmingen
Anti-mouse Alexa Fluor 488	Donkey	mouse IgGs	1:500	Life Technologies, A21202
Anti-rabbit Alexa Fluor 568	Goat	rabbit IgGs	1:500	Life Technologies, A11011

3.4 Immunocytochemistry (ICC)

For ICC, cells were seeded on poly-ornithine-coated glass coverslips, treated as indicated, fixed with 3.7 % formalin for 20 min at room temperature, washed three times with PBS, permeabilized with 0.2 % Tween®20 (Sigma-Aldrich, Germany) in PBS for 10 min and blocked with 5 % BSA/PBS for 30 min. Coverslips were subsequently incubated with primary antibodies diluted in 1 % BSA/PBS overnight at 4°C. After washing three times with PBS, coverslips were incubated with secondary antibodies in 1 % BSA/PBS for 2 hours at room temperature. After 3 washing steps, cell nuclei were counterstained with Hoechst 33342 1:100000 diluted in PBS. Coverslips were washed ones in distilled water and then mounted in FluoPreserveTM (EMD Biosciences, USA). Dilutions for primary and secondary antibodies used for ICC are given in Table 1 and 2, respectively.

3.5 Electron microscopy

Electron microscopy (EM) was performed in collaboration with Prof. Werner Baumgartner (*Department of Cellular Neurobiology, Institute for Biology II RWTH Aachen, 52056 Aachen, Germany*) as published previously [159]. Two days cuprizone fed and control mice were perfused with EM perfusion buffer:

EM perfusion solution:

- 100 mM cacodylate pH 7.2 (Fluka, Germany)
- 1.5 % formaldehyde (AppliChem, Germany)
- 1.5 % glutaraldehyde (Fluka, Germany)
- 5.8 g/ L NaCl

Trimmed brain sections were post-fixed for 1 hour in 1 % (w/v) OsO₄ (Fluka, Germany) in PBS, dehydrated and embedded in Epon 812 (Epon mix, Serva, Germany). Thin sections were cut, contrasted with uranyl acetate and lead citrate, and myelination of axons was analyzed with a Zeiss EM10C electron microscope.

3.6 In situ hybridization (ISH)

Fluorescence labeled ISH was performed using the QuantiGene® View RNA ISH tissue assay (Affymetrix, USA) according to the manufacturer's protocol. Briefly, 5 µm paraffin-embedded tissue slices were post-fixed for 60 min in 10 % formaldehyde, deparaffinized and boiled for 10 min in pretreatment solution. After washing in distilled water, slides were incubated in a wet chamber in protease solution for 20 min at 40°C (hybridization oven), washed with PBS and fixed again with 4 % formaldehyde for 5 min. After fixation and washing, the slides were incubated with the probe set hybridization mix directed against *Plp*, *Cxcl10* or *Ubiquitin* (reference gene) for 3 hours at 40°C. Appropriate negative controls were incubated with probe set diluent only. After hybridization of target gene probes, slides were washed in washing buffer and signal amplification and probe labeling was performed according to the manual. For visualization, the slides were incubated with enhancer solution for 5 min followed by 30 min incubation with fast red substrate at 40°C. After washing once in PBS the slides were fixed in 4 % formaldehyde for 5 min, washed again in PBS, counterstained with Hoechst 33342 (1:100,000 diluted in PBS) for 5 min and mounted in FluoPreserve™ (EMD Biosciences, USA).

ISH with radioisotopic labeled riboprobes was performed in collaboration with Prof. Luc Vallières (*Department of Neurosciences, Laval University Hospital Research Center, Quebec G1V 4G2, QC, Canada*) as described previously [160]. Two days cuprizone-treated and control mice were perfused with a buffer containing 4 % paraformaldehyde, 0.1 M sodiumtetraborate (Sigma, Germany) pH 9.5, post-fixed over night and send to Prof. Vallières for further analysis. Riboprobes were synthesized from linearized plasmids containing a fragment of mouse *Ccl2*, *Ccl3*, or *Cxcl10* cDNA. In some experiments, immunostaining for IBA1 (microglia marker), GFAP (astrocyte marker) or carbonic anhydrase-2 (CA2, mature oligodendrocyte marker) and *in situ* hybridization were sequentially performed on the same sections with modifications reported by Villeneuve and colleagues [160].

3.7 Cell culture and treatment

All cells were kept at 37°C and 5 % CO₂ in a humidified incubator.

3.7.1 *Primary cultures of glial cells* were prepared from the brains of one to two day-old Wistar rats. Meninges were carefully removed from cerebral hemispheres and the tissue mechanically disrupted using a pipette. Single-cell suspensions were transferred to culture flasks (1 brain/75 cm²) and kept for 12-14 days in basal glia medium:

- Dulbecco's Modified Eagle Medium, (DMEM, Gibco, Life Technologies, Germany)
- 10 % heat-inactivated fetal calf serum (FCS, PAA Laboratories GmbH, Germany)
- 50 U/ml penicillin, and 50 µg/ml streptomycin (P/S) (Gibco, Life Technologies, Germany)

The medium was replaced every other day.

3.7.2 *Oligodendrocyte precursor cells* (OPCs) were isolated and further purified from the flasks after 12-14 days as described by Richter-Landsberg and Vollgraf with minor modifications [38, 161-162]. For OPC separation, medium was replaced, cells incubated for 1 hour in the incubator and flasks were shaken for two hours at 100 rpm to remove cell debris and loosely attached microglia. Flasks were washed with pre-warmed PBS and incubated with fresh medium for 1 hour. Afterwards, OPCs were separated from the underlying astrocytic cell layer by vigorous shaking (for 16 hours at 240 rpm) at 37°C. The next day, the medium was collected, the flasks washed with pre-warmed PBS and medium and PBS were combined for centrifugation (10 min at 800 g). For differential adherence the cells were resuspended in 20 ml basal glia medium and plated on uncoated 10 cm plastic petri-dishes for 30-45 min in

the incubator. During this procedure astrocytes and microglia attach to the plastic surface, whereas OPCs remain unattached (i.e. differential adherence). Afterwards the OPCs were harvested under slow movement of the plate with the medium and the cell number was counted using a Neubauer counting chamber. OPCs were replated on poly-ornithine-coated culture dishes (2×10^5 cells/ well of a 6-well plate) and kept for 2 hours in DMEM supplemented with 10 % FCS. Medium was then changed to serum free proliferation medium containing of:

Basal primary oligodendrocyte medium:

- DMEM
- 1 × N2 supplement (Gibco, Life Technologies, Germany)
- 10 nM Biotin (Sigma-Aldrich, Germany)
- 0.1 % BSA (Roth, Germany)
- 1 % P/S
- 5 µg/ml N-acetyl-L-cysteine (Sigma-Aldrich, Germany)

Supplemented with:

- 10 ng/ml human recombinant fibroblast growth factor 2 and platelet derived growth factor α (FGF-2, PDGF α , both PeproTech, Germany).

To obtain highly purified and proliferating OPC cultures, cells were cultured under these conditions for 3 days and half of the medium was changed at the second day. On the third day, cells were treated as indicated or the medium was changed to a differentiation medium to induce mature oligodendrocytes (mOL) differentiation. Differentiation medium consisted of basal oligodendrocyte medium supplemented with:

- 15 nM 3,3',5-triiodo-L-thyronine (T3, Sigma-Aldrich, Germany)
- 10 ng/ml rat recombinant ciliary neurotrophic factor (CNTF, PeproTech, Germany).

Cells were allowed to differentiate for 3 days until morphological changes (high number of cellular processes) were clearly visible [163]. Purity of primary oligodendrocyte cultures was determined by means of immunocytochemistry. Cultures contained 0.3676 ± 0.3673 % IBA⁺ microglia and 8 ± 1.225 % GFAP⁺ astrocytes (values are given as arithmetic mean of n = 3 experiments \pm SEM).

3.7.3 *Rat OLN93 cells* were a kind gift from Prof. Christiane Richter-Landsberg (*Carl von Ossietzky Universität Oldenburg, Institut für Biologie und Umweltwissenschaften, AG Molekulare Neurobiologie/ Neurochemie, Oldenburg, Germany* [164]). Cells were seeded in uncoated 6-well plates at a density of 1.5×10^5 cells per well and cultured in basal glia medium supplemented with 1 % sodium pyruvate [164].

Primary rat oligodendrocytes or OLN93 cells were stimulated with either 100 ng/ml lipopolysaccharide (LPS, L4391, Sigma-Aldrich, Germany.), 100 U/ml rat recombinant interferon- γ (IFN γ , Peprotech, Germany for primary oligodendrocytes and ELISA or Hycult, Netherlands for migration assay), 100 ng/ml tumor necrosis factor α (TNF α , Invitrogen, Germany), 10 μ M H₂O₂ (Roth, Germany) or 1 mM glutamate (Roth, Germany) for 24 hours in serum-free DMEM/F12 medium containing:

DMEM/F12 medium:

- DMEM/F12 medium (Gibco, Life Technologies, Germany)
- $1 \times$ N2 supplement
- 0.48 mM L-glutamine (Gibco, Life Technologies, Germany)
- 5.3 μ g/ml D-glucose (Roth, Germany)
- 100 μ g/ml P/S

Supernatant was collected, filtered through a 0.45 μ m filter (VWR, Germany) and stored at -80°C until used.

3.7.4 *Mouse embryonic stem cell-derived microglial cells* (EsdM [165]) were a kind gift from Prof. Harald Neumann (*Neural Regeneration Group, Institute of Reconstructive Neurobiology, University of Bonn, 53127 Bonn, Germany*). Cells were cultivated in serum-free DMEM/F12 medium. Treatment of microglial cells for gene expression studies was performed in collaboration with Dr. Clara Beutner and Prof. Harald Neumann (*Neural Regeneration Group, Institute of Reconstructive Neurobiology, University of Bonn, 53127 Bonn, Germany*). 2×10^5 cells were seeded in a 6-well plate and stimulated for 24 hours with 10 ng/ml mouse recombinant CXCL10 or supernatant from IFN γ stimulated OLN93 cells. To block CXCL10-induced gene expression, an anti-rat CXCL10 antibody (1 μ g/ml, Peprotech, Germany) was added to the supernatants before incubation with microglial cells. Medium with or without IFN γ and control IgGs served as negative controls for OLN93 supernatants and blocking experiments, respectively.

3.7.5 Primary mouse astrocyte cultures were prepared from the brains of one to two day-old wild type or CCL2/3^{-/-} mice as published previously [166]. Briefly, meninges were carefully removed from cerebral hemispheres and the tissue mechanically disrupted using a pipette. Single-cell suspensions were transferred to culture dishes (3 brains/ 10 cm dish) and kept in basal glia medium until confluency was reached. The medium was replaced every other day. Before starting the experiment, cells were subcultured 1:10 in fresh 10 cm dishes to minimize microglial contamination and grown till 80-90 % confluency. For treatment cells were seeded into 6-well plates grown to 80 % confluency and treated with 1-10 µg/ml LPS for 24 hours.

3.7.6 Isolation of mouse peritoneal macrophages was performed from adult wild type and CCL2/3^{-/-} mice. Mice were killed by cervical dislocation and the abdominal skin carefully removed leaving the peritoneum intact. 5 ml of PBS containing 3 % FCS was injected with a 25 gauge needle into the peritoneal cavity. After gently massaging the abdominal walls for a few minutes the liquid was removed with a 25 gauge needle and placed in a falcon tube on ice. The peritoneal cavity was opened and the remaining liquid carefully removed with a syringe without aspirating blood. The number of isolated macrophages was approx. 10⁶ cells per mouse. The suspension was centrifuged for 5 min at 400 g, washed once with PBS and resuspended in 10 ml RPMI (Gibco, Life Technologies, Germany) containing 10 % FCS and P/S. 2 × 10⁵ cells were seeded per well of a 6-well plate and placed in the incubator. To remove dead cells and debris the medium was changed after 2 hours. After overnight incubation cells were treated with 1 µg/ml LPS for 2 hours in RPMI containing 10 % FCS and P/S. After treatment supernatant was removed and stored at -80°C until further used.

3.8 Migration and Phagocytosis Assay

Migration assays were performed in collaboration with Dr. Bettina Linnartz-Gerlach and Prof. Harald Neumann (*Neural Regeneration Group, Institute of Reconstructive Neurobiology, University of Bonn, 53127 Bonn, Germany*) following a published protocol [165]. Briefly, for the migration assay, 1 × 10⁵ cells were seeded into the upper chamber of a transwell system (8 µm pore size, Merck Millipore, Germany) and the lower chamber was filled with medium containing 50 ng/ml recombinant mouse CXCL10 (R&D Systems) or supernatant of IFNγ-stimulated OLN93 cells. To block CXCL10-induced microglia migration, an anti-rat CXCL10 antibody (1 µg/ml, Peprotech, Germany) was added to the supernatants in the transwell system. Cells were incubated for 3 hours and migrated ones (cells on the lower side of the membrane) were counted using a Neubauer counting chamber. Results from direct CXCL10 stimulation were normalized to results obtained from control wells without CXCL10. Results

from experiments with supernatants of OLN93 cells were normalized to results from corresponding wells containing either control EsdM medium or EsdM medium with IFN γ to exclude direct effects of IFN γ on microglial migration.

For phagocytosis assays, 1.5×10^5 microglia were seeded into 6-well plates and stimulated with either 500 ng/ml LPS (positive control), 10 ng/ml CXCL10 (Peprotech, Germany) or LPS and CXCL10 in combination for 24 hours. Cells were then incubated with fluoresbrite polychromatic red 1.0 μ m latex beads (yellow fluorescence under 545-610 nm filter, Polysciences, Inc., USA) for 1.5 hours. Flow cytometry was performed using the BD LSRFortessa cell analyzer (BD Biosciences, USA) and results were analyzed using FlowJo 7.6.5 (Tree Star Inc., USA). Forward and sideward scatter were calibrated using unstimulated control cells. Fluorescence was then measured using the 488 nm laser with PE filter settings (575 nm) and on the basis of the fluorescence intensity of the cells, the amount of cells that phagocytised three or more beads was calculated. Therefore, all cells that represent the fourth peak (intensity $\geq 10^4$) in the flow cytometry histogram or higher (compare Fig. 12A, Results 4.1.7) were counted as phagocytic active cells and the percentage of all fluorescent cells was calculated.

3.9 CellTiter Blue® Cell viability and CytoTox non-radioactive cytotoxicity assay

Cell viability and cytotoxicity assays were performed according to the manufacturer's protocol (Promega, USA). In brief, cells were treated as indicated and 30 μ l of supernatant was used for lactate-dehydrogenase-based cytotoxicity assays. After 30 min incubation at room temperature in dark, lactate dehydrogenase (LDH) activity was monitored with a Tecan infinite 200 plate reader at 490 nm after addition of STOP-solution. Results were normalized to lysis control (100%) and subsequently expressed as percentage of control. The remaining cells were incubated with CellTiter Blue® solution for approximately 4 hours. Fluorescence-intensity of resorufin in supernatants was then measured at 560/590 nm with a Tecan infinite 200 plate reader, mean value of lysis control was subtracted from all samples as background and treated samples were normalized to control samples (100%).

3.10 Microarray analysis

Regulation of gene expression in different treatment groups was analyzed using Affymetrix GeneChip® whole mouse genome microarrays as published previously [167-169]. The array and subsequent statistical analysis was performed in collaboration with Dr. Bernd Denecke (*Interdisciplinary Centre for Clinical Research (IZKF) Aachen, RWTH Aachen University*,

52074 Aachen, Germany). Total RNA (n = 3 per treatment group) was isolated and the quality assessed using RNA NanoChips with the Agilent 2100 Bioanalyzer (Agilent, USA). The RNA integrity number (RIN) of the samples was in the range of 8.5 to 8.9. Samples with lower RIN were excluded from the array. Probes for the GeneChip® Mouse Gene 1.0 ST Arrays (Affymetrix, USA) were prepared and hybridized to the arrays according to the Affymetrix GeneChip® Whole Transcript Sense Target labeling Assay Manual. Raw image data were analyzed with AGCC (Affymetrix, USA) and gene expression intensities were normalized and summarized with RMA algorithm [170]. Only genes expressed more than 3-fold compared to array internal negative controls were taken into consideration. Genes up-regulated in the two days cuprizone-treated group versus the control group were identified according to the following criteria: expression of genes in cuprizone-treated samples is at least 2-fold higher compared to control samples and the adjusted *p*-value for changes in expression is smaller than 0.05.

3.11 Real-time reverse transcriptase-polymerase chain reaction (rtRT-PCR)

Gene expression levels were further investigated using the *rtRT*-PCR technology (BioRad, Germany), SensiMix SYBR Green (Bioline, Germany), and a standardized protocol as described previously [39, 166, 169]. Isolation of total tissue RNA was performed with the Qiagen Lipid tissue Kit (Qiagen, Germany) according to the manufacturer's protocol. For cell culture experiments with OLN93 cells and primary oligodendrocytes, RNA was isolated with a standard phenol/chloroform extraction using PeqGold (PeqLab, Germany) and subsequent extraction of RNA with ice-cold Isopropanol. RNA was washed twice with 70 % ethanol, dried and resuspended in Rnase-free water. RNA isolation from microglial cells (EsdM) was performed using the Qiagen Rneasy mini Kit (Qiagen, Germany) according to the manufacturer's protocol. RNA concentration and purity was measured using the OD260 and OD260/OD280 ratio, respectively. Reverse transcription was performed with the Invitrogen MMLV RT-Kit and random hexanucleotide primers (both Invitrogen, Germany) according to the supplier's protocol. The PCR reactions were done in a reaction mixture containing:

- 2 µl cDNA (1:10 diluted in DNase-free water)
- 2 µl Rnase-free water
- 5 µl SensiMix SYBR Green (Bioline, Germany)
- 0.5 µl of each sense and antisense primer (100 pmol/µl, Life Technologies, Germany)

Primer sequences and respective annealing temperatures are given in Table 3. PCR with the MyIQ *rt*PCR Detection System (BioRad, Germany) was performed under following conditions:

- 10 min enzyme activation at 95°C
- 40 cycles of:
 - 15 s denaturation at 95°C
 - 30 s annealing at individual temperatures
 - 30 s amplification at 72°C
 - 5 s fluorescence measurement at 80°C.

Relative quantification was performed using the Δ Ct method, which results in ratios between target gene and a reference gene. Expression levels of the ribosomal RNA 18s (*18s*), glyceraldehyde 3-phosphate dehydrogenase (*Gapdh*) or Cyclophilin A (*Cyca*) were used as reference genes for mouse or rat samples as indicated in the figure legends. Constant expression of these reference genes under the given experimental conditions was routinely tested in our laboratory (not shown). In each run internal standard curves were generated by several fold dilutions of generated cDNA. The concentration of the target genes were calculated by comparing Ct values in each sample with Ct values of the internal standard curve. Finally, data were expressed as the ratio of the amount of each transcript versus the concentration of the reference gene. Melting curves and gel electrophoresis of the PCR products were routinely performed to determine the specificity of the PCR reaction (not shown).

For semi-quantitative reverse transcriptase PCR (*sq*RT-PCR) a related protocol was used. The PCR reaction was done in a PCR reaction mix containing:

- 1 μ l cDNA (undiluted)
- 1.25 μ l 10 \times PCR buffer (Bioline, Germany)
- 0.38 μ l MgCl₂ (50nM, Bioline, Germany)
- 0.25 μ l dNTPs (10 nM, Bioline, Germany)
- 0.25 μ l of each sense and antisense primer (100 pmol/ μ l, Life Technologies, Germany)
- 9.3 μ l Dnase free water

PCR was performed under following conditions with the Eppendorf Mastercycler epgradient S (Eppendorf, Germany):

- 3 min initial denaturation 95°C
- 18-40 cycles of:
 - 40 s denaturation at 95°C
 - 40 s annealing at individual temperatures
 - 45 s amplification at 72°C
- Followed by 2 min final elongation at 72°C

Visualization of *sq*RT-PCR products was performed using 2 % agarosegel in 1 × TAE buffer with ethidium bromide and electrophoresis at 120 V for 40 min. Images were captured with the E-Box VX2 (Peqlab, Germany).

Tab. 3. List of primers used for *rt*RT-PCR and *sq*RT-PCR

Name	Forward sequence 5'-3'	Reverse sequence 5'-3'	AT
<i>Ccl2</i> mouse	TTA AAA ACC TGG ATC GGA ACC AA	GCA TTA GCT TCA GAT TTA CGG GT	60°C
<i>Ccl3</i> mouse	TTC TCT GTA CCA TGA CAC TCT GC	CGT GGA ATC TTC CGG CTG TAG	62°C
<i>Cxcl10</i> mouse	CCA AGT GCT GCC GTC ATT TTC	GGC TCG CAG GGA TGA TTT CAA	60°C
<i>Cxcl10</i> rat	CTC TCG CAA GAA CGG TGC GCT	CAG CAC TGT GGC GAG TGG CTT	60°C
<i>Plp</i> mouse & rat	TGG CGA CTA CAA GAC CAC CA	GAC ACA CCC GCT CCA AAG AA	56°C
<i>Mag2</i> rat	TGA ACG AGA CAG AGA GGG AGT T	CTG GGT GAT GTA GCA GAC AAT G	60°C
<i>Mbp</i> mouse	CCC AAA GAA TAA CTG GCA AGG C	GAA GCT CGT CGG ACT CTG AG	56°C
<i>Mbp</i> rat	CCA TCC AAG AAG ATC CCA CA	CCT GTC ACC GCT AAA GAA GC	59°C
<i>Pdgfra</i> rat	AGG CTT GGG GCT CAC TTT TT	TCA GCG GCA CAA TCT TCT CA	61°C
<i>Cnpase</i> rat	TGG CGA AGA AGA TGG AAG TCA	GTG GGT GAA GGA ACT GAT GGT T	61°C
<i>Cyca</i> rat	GGC AAA TGC TGG ACC AAA CAC	TTA GAG TTG TCC ACA GTC GGA GAT G	62°C
<i>18s</i> mouse	CGG CTA CCA CAT CCA AGG AA	GCT GGA ATT ACC GCG GCT	60°C
<i>18s</i> rat	CGT GAG AGT GTC TAA CGG G	CGA GTC AGG CAT TTG GTC C	60°C
<i>inos</i> mouse	AAG CCC CGC TAC TAC TCC AT	GCT TCA GGT TCC TGA TCC AA	60°C
<i>Tnfa</i> mouse	TCT TCT CAT TCC TGC TTG TGG	AGG GTC TGG GCC ATA GAA CT	60°C
<i>Gapdh</i> mouse	ACA ACT TTG GCA TTG TGG AA	GAT GCA GGG ATG ATG TTC TG	60°C

3.12 Genotyping of *CCL2/3*^{-/-} mice

Genotyping was performed using *sq*PCR with genomic DNA isolated from a small piece of mouse tail. For DNA isolation, the Nucleospin tissue Kit (Macherey-Nagel, Germany) was used according to the manufacturer's recommendations for rat and mouse tails.

The PCR reaction mix consisted of the following:

- 2 µl genomic DNA (undiluted)
- 0.125 µl of each primer (100 pmol/µl)
- 0.125 µl BioXAct short DNA polymerase (Bioline, Germany)
- 5 µl of 2 × PCR reaction buffer G, C or I (PCR optimization Kit Bioline, Germany)
- Filled up to 10 µl with DNase free water

The primer sequences, product sizes and the buffer used for PCR reaction are given in Table 4. PCR with 40 cycles and following visualization of PCR products was performed as mentioned above.

Tab. 4 List of primers and buffers used for genotyping

Name		Sequence 5'-3'	Size [bp]	Buffer	AT
<i>Ccl2</i> Mut s	s	GCC AGA GGC CAC TTG TGT AG	179	G	60°C
<i>Ccl2</i> WT s	s	TGA CAG TCC CCA GAG TCA CA	287		
<i>Ccl2</i> Common as	as	TCA TTG GGA TCA TCT TGC TG			
<i>Ccl3</i> WT s	s	ATA CAA GCA GCA GCG AGT ACC	150	C	60°C
<i>Ccl3</i> WT as	as	ATG GCG CTG AGA AGA CTT G			
<i>Ccl3</i> Mut s	s	TAA AGC GCA TGC TCC AGA CT	600	I	56°C
<i>Ccl3</i> Mut as	as	AGA GTC CCT CGA TGT GGC TA			

3.13 Enzyme-linked immunosorbent assay (ELISA)

CCL2, CCL3 mouse and CXCL10 rat and mouse ELISA (Peprotech, Germany) were carried out according to the manufacturer's protocol. Color development of the ABTS substrate (Sigma-Aldrich, Germany) was monitored with a Tecan infinite 200 plate reader at 405 nm with a wavelength correction at 650 nm. Chemokine release was normalized to total protein content of cell or brain lysate as determined with the Pierce BCA protein Assay (Thermo Fisher Scientific, Germany). For measurement of CXCL10 protein in protein lysates of mouse brain tissue, lysates were prepared from cortex and corpus callosum samples of control mice or mice treated for two days with cuprizone. Briefly, brains were homogenized in ice-cold PBS containing protease-inhibitor cocktail (Roche, Germany) using precellys® tissue homogenizer (15 s at 2000 rpm, PeqLab, Germany). Brain lysates were subsequently centrifuged twice for 20 min at 12000 g at 4°C and the supernatant was stored at -80°C until use.

3.14 SDS polyacrylamide gel electrophoresis (SDS-PAGE) and Western Blot

Protein levels were semi-quantitatively measured using SDS-PAGE and Western Blot analysis. Protein isolation was performed with RIPAplus buffer:

RIPAplus buffer

- 50 mM Tris HCl pH 8.0
- 150 mM NaCl
- 1 % NP-40 (Roth, Germany)
- 0.5 % sodium deoxycholat (Roth, Germany)
- 0.1 % SDS (Roth, Germany)
- 1 × complete Mini protease inhibitor cocktail (Roche, Germany)
- 200 nM Sodium orthovanadate (phosphatase inhibitor, Sigma-Aldrich, Germany).

Lysed cells were centrifuged for 20 min at 12000 g at 4°C and supernatant was used for Pierce BCA protein assay and SDS-PAGE.

For electrophoresis, 10 % Acrylamide (Rotiphorese gel 40, Roth, Germany) resolving gels and 5 % stacker gels were used. Gels were prepared as follows:

Resolving gel:

- 2 ml water
- 1 ml 40 % Acrylamide
- 1 ml resolving buffer (1.5 M Tris-OH, 0.4 % SDS, pH 8.8)
- 40 µl 10 % APS (Sigma-Aldrich, Germany)
- 4 µl Temed (Roth, Germany)

After polymerization of the resolving gel, the stacker gel was casted as follows:

Stacker gel:

- 0.78 ml water
- 0.16 ml 40 % Acrylamide
- 0.31 ml stacker buffer (0.6 M Tris-Cl, 0.4% SDS, pH 6.8)
- 12.5 µl 10 % APS
- 1.2 µl Temed

After complete polymerization the gel was loaded with equal amounts of protein (5-10 µg) diluted in Laemmli buffer and denaturated for 5 min at 95°C. Proteins were separated in a Biorad SDS-PAGE system with SDS-run buffer pH 8.3 containing:

SDS-run buffer:

- 3 g Tris
- 14.4 g Glycin
- 1 g SDS
- filled up to 1 L with A. dest.

The gel was run at 80 V until proteins passed the stacker gel followed by 120 V for approximately 1.5 hours.

For subsequent Western Blot analysis separated proteins were blotted onto a nitrocellulose membrane (Hybond, Amersham Biotech, UK) for 1 hour at 10 V using the following buffer:

Transfer buffer:

- 0.9 g Tris
- 4.3 g glycine
- 60 ml methanol
- filled up to 300 ml with A.dest.

The membrane was blocked after washing in Tris-buffered saline (TBS) with 5 % fat-free milk solution in TBS containing 0.05 % Tween20 ® (TBST) for 1 hour. The membranes were then incubated in primary antibodies diluted in 5 % BSA/TBST over night at 4°C, washed three times with TBST for 10 min and further incubated with appropriate secondary HRP-coupled antibodies in 5% BSA/TBST for 2 hours at room temperature (see Table 5 for antibodies and dilutions). After three additional extensive washing steps with TBST and one wash with TBS visualization was performed with commercial enhanced chemoluminescence reagent kit (ABC Kit, Amersham Bioscience, UK) and exposure to X-ray film (Kodak, Germany).

Tab. 5 Primary and secondary antibodies used for Western Blot

Antibody	Host	Directed against	Dilution	Supplier cat. No.
CNPase	Mouse	2',3'-cyclic-nucleotide 3'-phosphodiesterase (oligodendrocytes)	1:500	Abcam ab6319
P44/42 MAPK (Erk1/2)	Rabbit	total p44/42 MAP kinase (Erk1/Erk2) protein	1:4000	Cell signalling 4695S
Phospho-p44/42 MAPK (Erk1/2) (Thr202/Tyr204)	Rabbit	p44/p42 MAP Kinase (Erk1/Erk2) when dually phosphorylated at Thr202 and Tyr204 of Erk1 (Thr185 and Tyr187 of Erk2) or singly phosphorylated at Thr202.	1:1000	Cell Signalling 4370S
Actin	Rabbit	Actin protein (cytoskeleton)	1:1000	Sigma A2066
Anti-mouse HRP	Rabbit	mouse IgGs	1:1000	Abcam 6728
Anti-rabbit HRP	Goat	rabbit IgGs	1:4000	Biorad 170-6515

3.15 Statistical analysis

Statistics were performed using absolute data. Intergroup differences were tested by ANOVA followed by Tukey's or Bonferroni post hoc test using GraphPad Prism 5 (GraphPad Software Inc.) if not stated otherwise. All data are given as arithmetic means \pm SEM. *P*-values are indicated as * = $p \leq 0.05$, ** = $p \leq 0.01$, *** = $p \leq 0.001$. Number of experiments performed or mice used are given in the figure legends.

4. Results

4.1 Oligodendrocyte-derived chemokine CXCL10 triggers microglial activation in the cuprizone animal model of multiple sclerosis

4.1.1 Oligodendrocyte loss occurs early in the cuprizone model

In a first set of experiments, I studied the temporal and spatial relationship of oligodendrocyte stress and early microglia activation using the cuprizone mouse model [34]. Mice were fed with cuprizone for two days or one week and brain sections were immunohistochemically analyzed. The principal region included in the study was the midline of the white matter tract corpus callosum (CC).

Numerous apoptotic oligodendrocytes with condensed and/or fragmented nuclei in an interfascicular position were seen as early as two days after cuprizone feeding (arrow in Fig. 2A). Several of the apoptotic nuclei were positive for the oligodendrocyte-specific transcription factor OLIG2 after one week cuprizone feeding (arrows in Fig. 2B). Apoptotic cells were absent in control mice. In addition double staining against activated caspase-3 and the myelin marker protein CNPase verified early oligodendrocyte apoptosis in this model (arrows in Fig. 2C). Apoptotic cells were virtually absent in control animals (data not shown). In parallel, I found a marked decrease in the number of adenomatous polyposis coli (APC)-expressing mature oligodendrocytes (Fig. 2D). Immunohistochemical evaluation of myelination with antibodies directed against proteolipid protein (PLP) revealed that overt demyelination was not yet evident on the histological level (Fig. 2E). However, ultrastructural analysis revealed signs of a dying back oligodendrogliopathy with a splitting of the inner myelin lamella (Fig. 2F) in the CC of cuprizone-exposed mice. Such alterations were absent in control mice. Oligodendrocyte dysfunction was further confirmed by gene transcription studies (*rt*RT-PCR) of the myelin protein-encoding gene transcripts proteolipid protein (*Plp*) and myelin basic protein (*Mbp*). *Plp* and *Mbp* mRNA levels were reduced to 0.169 ± 0.016 fold (*Plp*, mean \pm SEM) and 0.14 ± 0.043 fold (*Mbp*, mean \pm SEM), respectively, after cuprizone-treatment (Fig. 2G), which was confirmed using *in situ* hybridization (ISH) against *Plp* transcript (Fig. 2H).

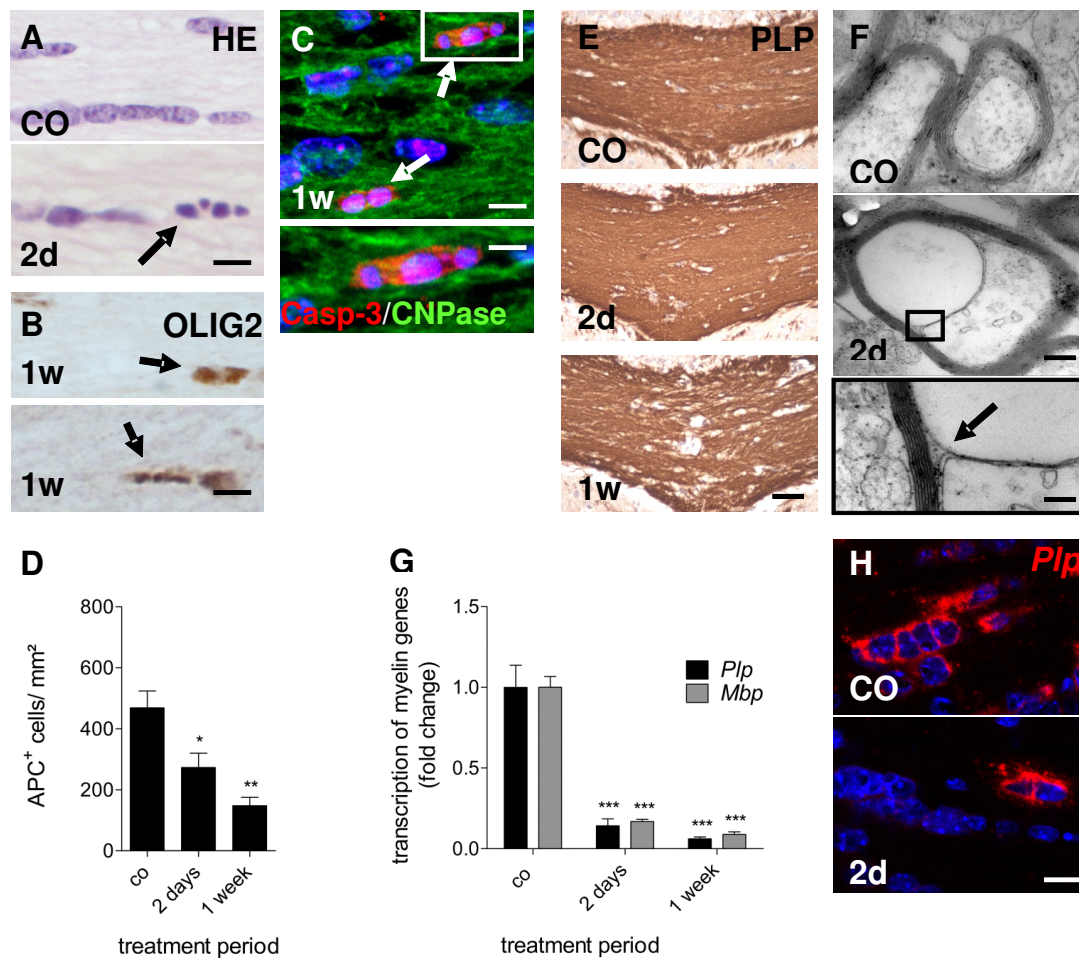


Figure 2 Characterization of early oligodendrocyte stress in cuprizone-treated mice

(A) HE-stained section of the midline of the corpus callosum (CC) in control (CO) mice and two days (2d) after initiation of the cuprizone diet. Note apoptotic oligodendrocytes in cuprizone-treated mice (see arrow). (B) Anti-OLIG2 stained sections of the midline of CC in mice treated with cuprizone for one week (1w). Note OLIG2⁺ nuclei with typical morphological characteristics of apoptosis such as round, condensed and fragmented nuclei (see arrows). Scale bars A and B 10 μ m. (C) Immunofluorescence double labeling for active caspase-3 (red) and CNPase (green). Caspase-3 positive cells can be found in between CNPase positive myelin fibers in interfascicular positioning, typical for oligodendrocytes. The lower picture in C shows higher magnification of the highlighted apoptotic cell. Scale bar 10 μ m (upper panel), 5 μ m (lower panel). Cell nuclei are stained with Hoechst 33342 (blue). (D) Quantification of APC⁺ oligodendrocytes in the midline of the CC of control (CO), two days (2d) and one week (1w) cuprizone-treated mice, respectively. Note lower numbers of APC⁺ cells after two days (273.3 ± 46.73 , $n = 4$) and one week (148.0 ± 27.45 , $n = 4$) compared to control (469 ± 55.32 , $n = 5$) mice. (E) Myelin integrity was determined by immunohistochemistry with anti-PLP antibodies in the CC of control (CO), two days (2d) and one week (1w) cuprizone-treated mice. No gross abnormality in myelin was observed on the histological level. Scale bar 50 μ m. (F) Electron microscopy of the midline of the CC was performed in control (CO) and two days (2d) cuprizone-treated mice. Note the splitting of innermost myelin lamella (arrow). Scale bars 1 μ m; higher magnification 400 nm. (G) Gene transcript levels for *Plp* and *Mbp* were analyzed by *rt*RT-PCR from tissue obtained from the midline of the CC of control (CO), two days and one week cuprizone-treated mice. Values were normalized against the reference gene *18s* and each bar represents the averaged fold induction over untreated controls. Note reduced mRNA levels of *Plp* and *Mbp* already two days after initiation of the cuprizone diet (*Plp* 0.14 ± 0.043 , *Mbp* 0.169 ± 0.016 , $n = 4$). (H) ISH against *Plp* transcript (red) on tissue sections from control (CO) and 2 days (2d) cuprizone-treated mice. Pictures show the midline of the CC. Note the strong expression of *Plp* transcript in control tissue located around nuclei (blue) in chain-like interfascicular positioning indicative for oligodendrocytes. Expression of *Plp* is strongly reduced after 2 days

curpizone treatment. Scale bar 10 μm . Male mice used. Values are given as arithmetic means \pm SEM; * = $p < 0.05$; ** = $p < 0.01$; *** = $p < 0.001$ (One-way ANOVA with Tukey's post hoc test).

To study the relationship between oligodendrocyte stress and early microglia activation, the number of microglial cells was quantified in histological sections by antibodies directed against the microglia marker protein ionized calcium binding adaptor molecule-1 (IBA1). Microglial cell numbers gradually increased after initiation of the cuprizone-treatment (Figs. 3A and 3B). At week 1, the number of IBA1⁺ cells was 6-times higher compared to controls. Besides microglia hyperplasia, microglia hypertrophy was detected at week one (Fig. 3C). In contrast, the number of glial fibrillary acidic protein (GFAP)-expressing astrocytes was not significantly altered till week one (Figs. 3D and 3E).

In summary, short-term cuprizone-treatment resulted in early oligodendrocyte stress with concomitant microglial activation in the absence of overt demyelination.

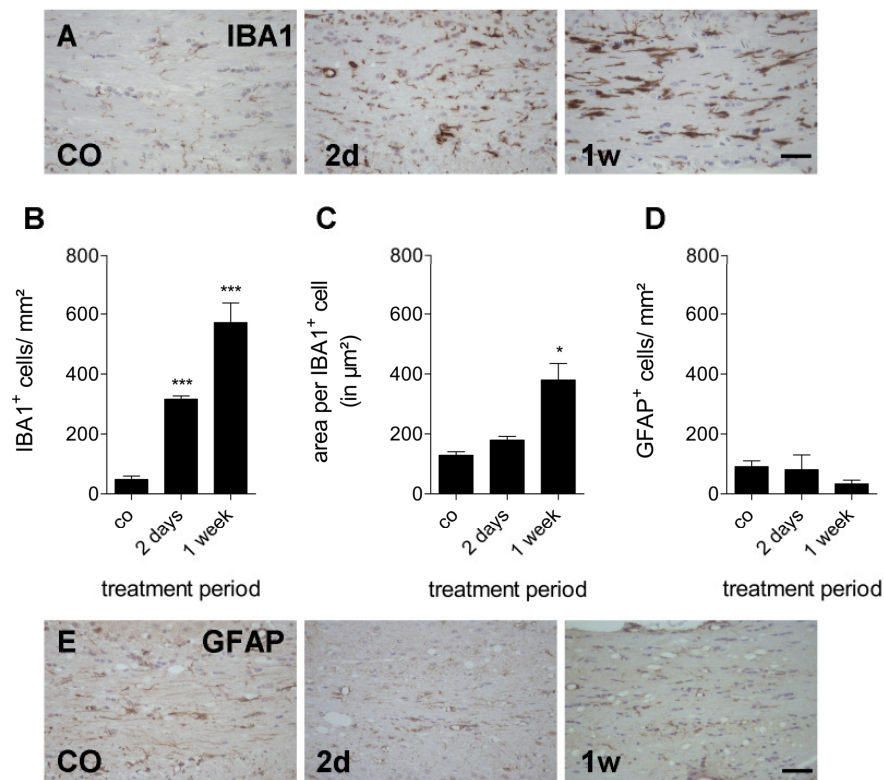


Figure 3 Characterization of early microglia and astrocyte responses

(A) Immunohistochemistry with antibodies directed against the microglial protein IBA1. Note overt microgliosis in the midline of the CC in mice treated with cuprizone for two days or one week (2d and 1w). Scale bar 50 µm. (B) Quantification of IBA1⁺ cells within the CC revealed a strong increase of microglial cell numbers after two days (316.0 ± 10.87 , $n = 4$) and one week cuprizone treatment (571.4 ± 65.62 , $n = 4$) compared to controls (CO, 48.29 ± 11.27 , $n = 5$). (C) ImageJ based morphometrical quantification of microglial cell area within the CC demonstrates a beginning hypertrophy of IBA⁺ cells (CO: 129 ± 11.5 , $n = 3$; two days: 179.1 ± 12.62 , $n = 4$; one week: 379.8 ± 55.12 , $n = 4$). (D) Quantification of GFAP⁺ astrocytes within the CC revealed no increase in astrocyte numbers at day two (81.09 ± 48.63 , $n = 4$) or week one (33.47 ± 12.44 , $n = 4$) compared to controls (CO, 90.87 ± 19.55 , $n = 5$). (E) Immunohistochemistry with antibodies against the astrocytic protein GFAP in control (CO), two days (2d) and one week (1w) cuprizone-treated mice. Scale bar 50 µm. Male mice used. Values are given as arithmetic means \pm SEM; * = $p < 0.05$; ** = $p < 0.01$; *** = $p < 0.001$ (One-way ANOVA with Tukey's post hoc test).

4.1.2 Chemokines are dynamically regulated in cuprizone-treated mice

In a next set of experiments I aimed to identify factors that are involved in early microglia activation. Total mRNA samples from the CC of mice fed with cuprizone for two days were analyzed using Affymetrix GeneChip® arrays. My analysis revealed an increased transcription of numerous pro-inflammatory genes, including genes coding for chemokines (Fig. 4A). From the 21 evaluated CCL-chemokines in the array, three were significantly increased, namely *Ccl2* (*Mcp1*), *Ccl3* (*Mip1a*) and *Ccl7* (*Mcp3*); from the 13 evaluated CXCL- chemokines, only *Cxcl10* (*Ip10*) displayed an increased expression after two days of cuprizone treatment. To confirm these results in more detail, *rt*RT-PCR was performed to specify the gene transcript levels of the three most induced chemokines *Ccl2*, *Ccl3* and *Cxcl10* (Fig. 4B). In line with the microarray data, mRNA levels of these three chemokines were increased after cuprizone exposure compared to untreated controls, with CXCL10 revealing the most prominent fold change (~170 fold upregulation). Furthermore, higher levels of CXCL10 protein were detected by ELISA in brain lysates from cuprizone-treated animals compared to control mice (Fig. 4C). To examine the anatomical distribution of the cells expressing these chemokines, brain sections from cuprizone-treated mice were analyzed by ISH. *Ccl2* mRNA was evenly distributed in the CC, including the myelin- and oligodendrocyte-rich deep cortical layers (arrows in Fig. 4D). Within the hippocampal formation, the polymorph layer of the dentate gyrus displayed some positive signals (arrowheads in Fig. 4D). *Ccl2* signal intensity was weak in superficial cortical layers. In general, the hybridization signal for *Ccl3* was much weaker. I detected some spots in the CC and adjacent Cx region (Fig. 4E). The strongest *in situ* hybridization signal was evident for *Cxcl10*. Strong expression was found in the CC, deep cortical layers and distinct hippocampal sub-regions, such as the polymorph layer of the dentate gyrus (arrowheads in Fig. 4F) or the stratum oriens and radiatum of the hippocampal cornu ammonis region (arrows in Fig. 4F). Remarkably, no *Cxcl10* signal was observed in the neuronal granule cell layer of the dentate gyrus or the pyramidal layer of the cornu ammonis (stars in Fig. 4F), suggesting that neurons are not the major source of CXCL10 in this animal model. In summary, I found a selective upregulation of CXCL10, CCL2 and CCL3 chemokines in response to cuprizone-induced oligodendrocyte stress, and I assume that these chemokines might orchestrate the observed concomitant microglia attraction/activation.

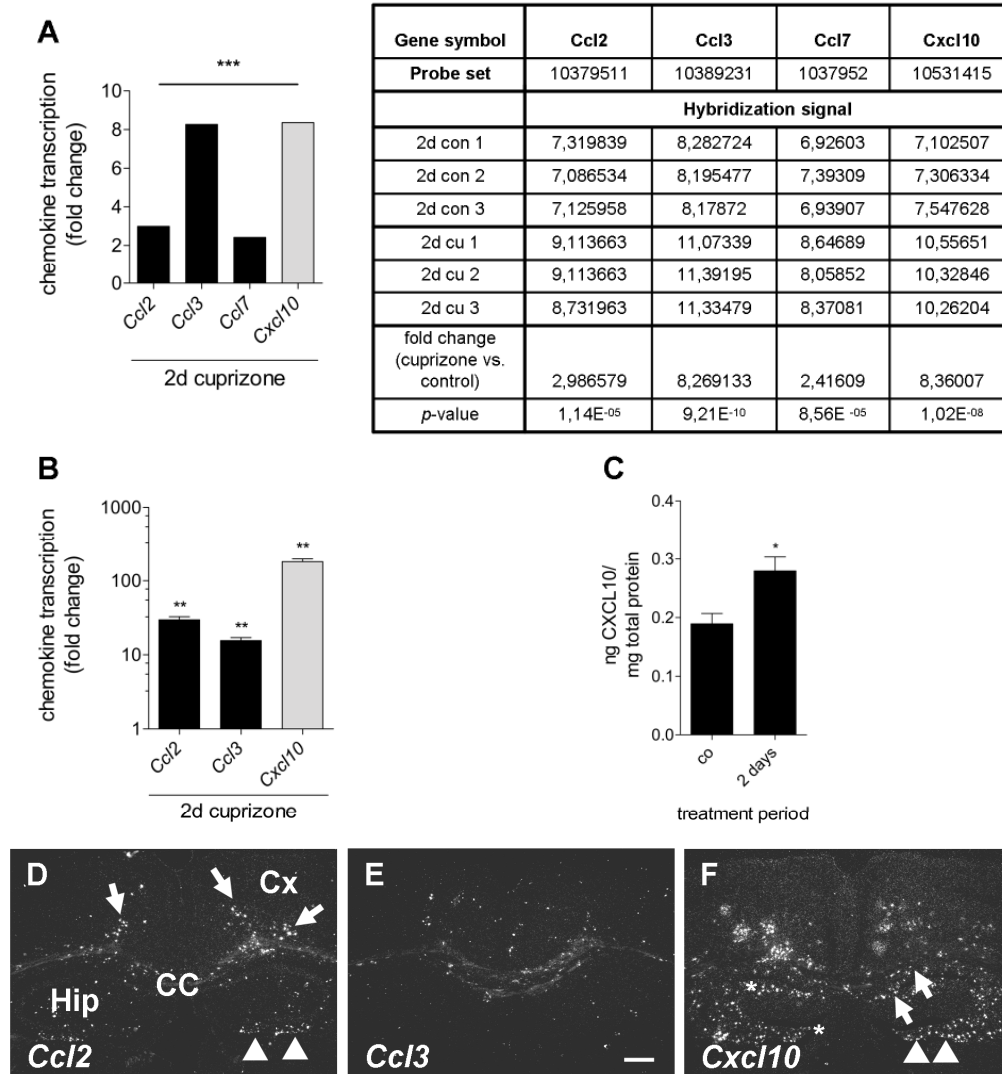


Figure 4 Gene transcription and protein expression of chemokines in cuprizone- treated mice

(A) Evaluation of whole mouse genome Affymetrix GeneChip® array shows that *Ccl2*, *Ccl3*, *Ccl7* and *Cxcl10* transcripts are up-regulated in the CC after two days (2d) cuprizone exposure. Values are given as fold change over control. Hybridization signals for each mice and relative transcription levels (fold change = cuprizone vs. control), together with corresponding *p*-values are presented in the table (*n* = 3 mice per group). (B) mRNA expression levels of *Ccl2*, *Ccl3* and *Cxcl10* after two days (2d) cuprizone-treatment (fold induction over control: *Ccl2*: 29.74 ± 2.98 ; *Ccl3*: 15.54 ± 1.57 ; *Cxcl10*: 180.7 ± 17.44 , *n* = 4), determined by *rt*RT-PCR. Note the strong upregulation of *Cxcl10* expression (~170 fold; unpaired t-test with Welch's correction). (C) CXCL10 protein levels in homogenized brain samples were determined by ELISA in control (CO) and two days cuprizone-treated mice (CO: 0.189 ± 0.0177 ; two days: 0.28 ± 0.024 ; *n* = 3, unpaired t-test). ELISA results were normalized against 1 mg total protein. (D-F) Dark-field photographs of *in situ* hybridization-labeled brain sections (two days cuprizone) for the respective chemokines *Ccl2* (D), *Ccl3* (E), *Cxcl10* (F) taken at the level of the dorsal hippocampus (Hip). Scale bar 300 μ m. Hybridization signals are shown as white grains. (D) Arrows mark the deep cortical layer 6, arrowheads the hippocampal polymorph layer of the dentate gyrus. (F) Arrows indicate strati oriens and radiatum of the hippocampal cornu ammonis region, arrowheads the polymorph layer of the dentate gyrus. Note that a signal is neither observed in the stratum granulare nor in the neuronal granule cell layer of the dentate gyrus or the pyramidal layer of the cornu ammonis (stars in F). Male mice used. Values are given as arithmetic means \pm SEM; * = *p* < 0.05; ** = *p* < 0.01.

4.1.3 CXCL10- but not CCL2- or CCL3-deficient mice display less severe early microglia activation

To examine whether chemokines contribute to early microglia activation in this model, CCL2^{-/-}, CCL3^{-/-} and CXCL10^{-/-} mice were fed cuprizone for one week, and the extent of microgliosis was determined in IBA1-stained sections. While numbers of IBA1⁺ microglia were comparable in CCL2^{-/-}, CCL3^{-/-} and wild type animals, a ~ 40% reduction in the number of IBA1⁺ cells was found in CXCL10-deficient mice (Figs. 5A-C). In detail, the number of microglia was reduced in the CC from 448.131 ± 15.53 cells in wild type mice to 285.816 ± 18.33 cells in the CXCL10^{-/-} mice (Fig. 5C). Thus, CXCL10, but not CCL2 or CCL3, regulates early microgliosis in this model.

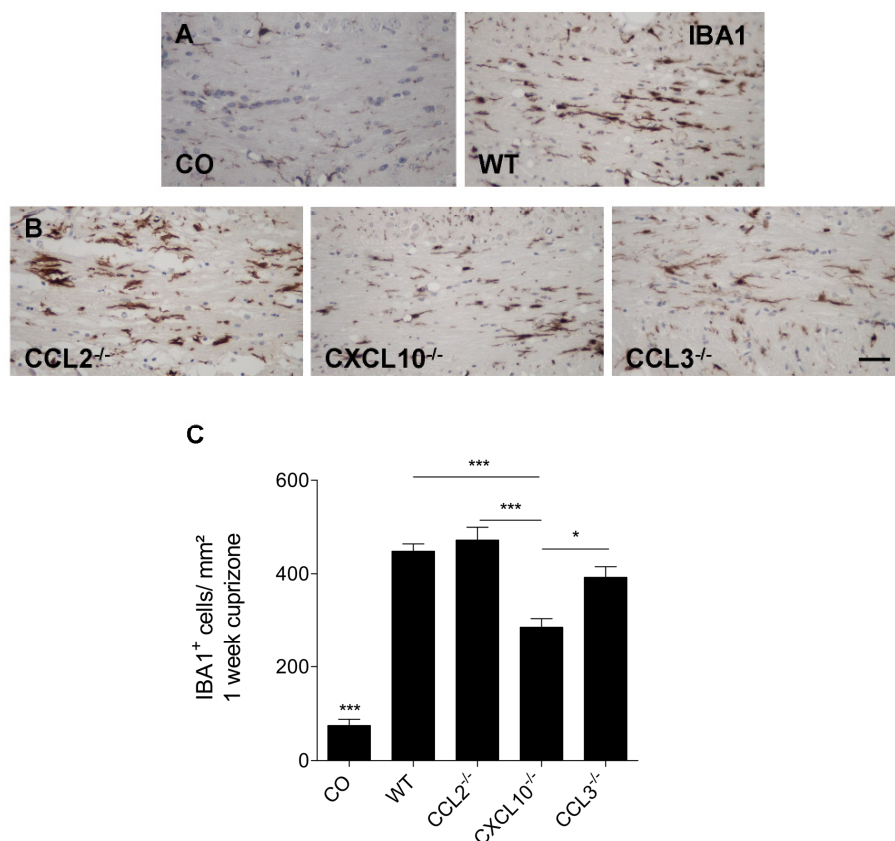


Figure 5 Cuprizone-induced microglia activation in chemokine deficient mice

(A) Anti-IBA1-immunostaining of the CC in control (CO) and one week cuprizone-treated wild type (WT) mice. (B) Sections of the midline of the CC stained with anti-IBA1 antibodies in CCL2^{-/-}, CXCL10^{-/-} and CCL3^{-/-} mice after one week cuprizone exposure. Scale bar 50 µm. (C) Quantification of IBA1-expressing cells within the CC of wild type (WT) and knockout mice (CCL2^{-/-}, CXCL10^{-/-}, CCL3^{-/-}) after one week cuprizone exposure (CO = wild type without treatment). All cuprizone-treated groups show increased numbers of IBA1⁺ microglia within the CC compared to control mice. Note reduced microgliosis in CXCL10^{-/-} (285.8 ± 18.33, n = 11) compared to wild type mice (448.1 ± 15.53, n = 31). Male mice used. Values are given as arithmetic means ± SEM, * = $p < 0.05$; *** = $p < 0.001$ (One-way ANOVA with Tukey's post hoc test).

4.1.4 CXCL10 is expressed and secreted by oligodendrocytes

Oligodendrocytes have been suggested to modulate neuroinflammatory processes in the brain of MS patients [33, 171]. To examine whether oligodendrocytes can be a source of CXCL10 *in vitro*, I analyzed brain sections from cuprizone-treated mice labeled for *Cxcl10* mRNA by *in situ* hybridization and analyzed the tissue in the CC for cells with typical oligodendrocyte distribution (i.e. cells in chain-like formation in interfascicular positioning). As shown in Figure 6, *Cxcl10* mRNA was detected in cuprizone-treated mice in cells with typical oligodendrocyte morphology (Fig. 6A arrowheads, Fig. 6C higher magnification). However *Cxcl10* positive cells were found that did not display typical oligodendrocyte distribution, but may likely be astrocytes or microglial cells (Fig. 6A arrow, Fig. 6D higher magnification). No *Cxcl10* mRNA expression was found in control mice (Fig. 6B). Furthermore, co-localization experiments with *Cxcl10* ISH and subsequent immunohistochemistry against different cellular markers was performed (Fig. 7). *Cxcl10* mRNA co-localized with the oligodendrocyte marker protein carbonic anhydrase-2 (CA2) (Fig. 7A) but neither with the microglia marker IBA1 (Fig. 7B), the astrocyte marker GFAP (Fig. 7C) nor the endothelial marker CD31 (Fig. 7D). Nevertheless, the CA2⁺ cells did not display typical oligodendrocyte morphology. Taken together oligodendrocytes are a likely source of *Cxcl10* expression in the cuprizone model and may thus play important roles in microgliosis and lesion development.

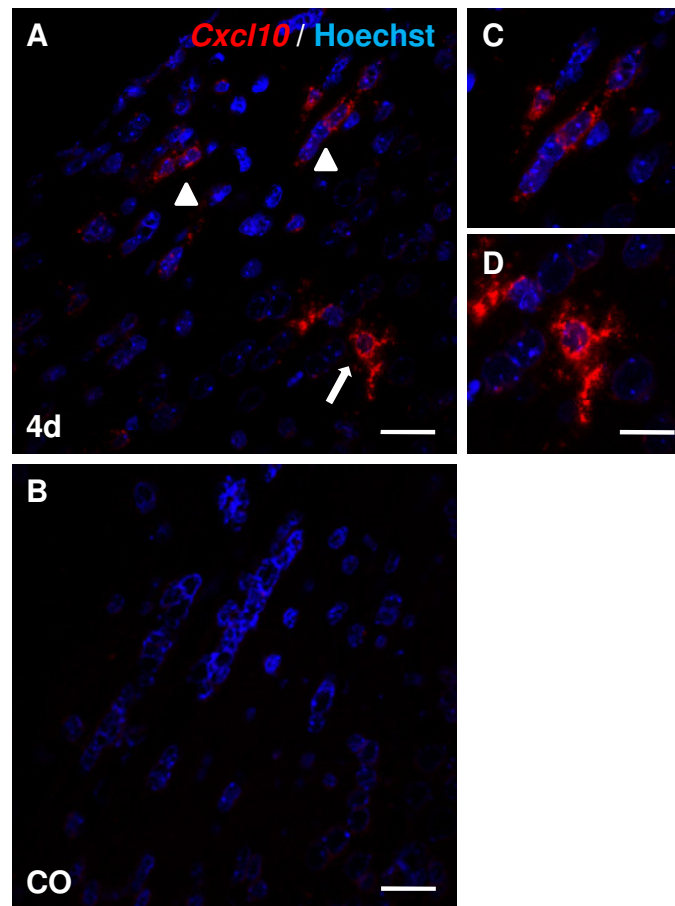


Figure 6 Cxcl10 mRNA is expressed in oligodendrocyte-like cells (A) In situ hybridization for Cxcl10 mRNA in four days cuprizone-treated male mice (4d). Arrowheads indicate cells with typical oligodendrocyte-like morphology e.g. chain-like formation in interfascicular positioning in the lateral corpus callosum. Cxcl10 mRNA was also detected in cells with non-oligodendrocyte-like spatial distribution (arrow). Scale bar 50 μ m. Both cell types are shown in higher magnification in (C) and (D). Scale bar 15 μ m. Note that the hybridization signal for Cxcl10 (red dots) can be found both, in the perinuclear compartment as well as in cell processes. Cell nuclei were counter stained with Hoechst 33342. (B) Cxcl10 expression in control mice. Note that there is no signal for Cxcl10 mRNA in untreated mice. Scale bar 50 μ m.

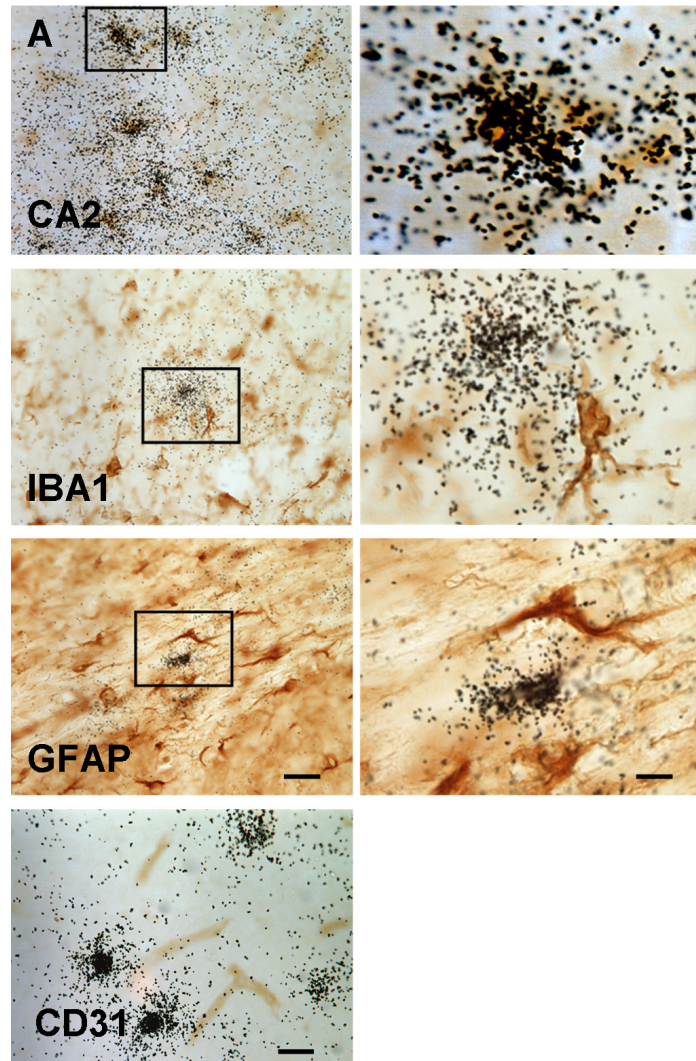


Figure 7 Cxcl10 is expressed by oligodendrocytes in cuprizone- treated mice

(A) Double labeling experiments for *Cxcl10* mRNA (black dots) and the oligodendrocytes marker protein carbonic anhydrase-2 (CA2), the microglial marker protein IBA1, the astrocyte marker protein GFAP or the endothelial marker CD31, of male mice treated for two days with cuprizone. Scale bar 50 μ m. Cells indicated by inserts in the left pictures are shown in a higher magnification on the right (brown, immunoperoxidase staining). Scale bar 10 μ m. Note that *Cxcl10* mRNA co-localizes in the CC with the oligodendrocyte marker CA2, but not with the marker proteins for microglia/macrophages, astrocytes or endothelial cells.

To further understand the relationship between oligodendrocyte stress and CXCL10 expression, I performed cell culture experiments with primary rat oligodendrocytes and the oligodendrocyte cell line OLN93. Primary oligodendrocytes were purified from rat pups and cultured either in the presence of the growth factors FGF-2 and PDGF α to obtain oligodendrocyte precursor cells (OPCs) or in the presence of triiodo-L-thyronine (T3) and ciliary neurotrophic factor (CNTF) to obtain mature oligodendrocytes (mOL). As demonstrated via immunocytochemistry and semi-quantitative reverse transcriptase-polymerase chain reaction (*sq*RT-PCR), this culture protocol results in either highly enriched OPCs (low *Cnp* = 2',3'-Cyclic-nucleotide 3'-phosphodiesterase, *Plp* and *Mbp* mRNA levels; bi-polar morphology) or mature oligodendrocytes (low *Pdgfra* mRNA expression levels; ramified morphology with membrane formation; Fig. 8A). The stimulation of oligodendrocytes with interferon- γ (IFN γ) in non-cytotoxic concentrations, as determined by metabolic activity and lactate-dehydrogenase (LDH) release, resulted in a significant increase in CXCL10 protein levels in the cell culture supernatant (Fig. 8B). The extent of IFN γ -induced CXCL10 release was comparable in OPCs and mOL. In line with my findings using primary cultures, IFN γ -stimulated OLN93 cells up-regulated CXCL10 at the mRNA (Fig. 8C) and protein levels (Fig. 8B/D). CXCL10 expression was also stimulated by the pro-inflammatory molecules lipopolysaccharide (LPS) and tumor necrosis factor- α (TNF α), although to a lesser extent than IFN γ , but not by glutamate and hydrogen peroxide (Fig. 8D). Taken together my results clearly show that oligodendrocytes release CXCL10 *in vitro* under inflammatory conditions.

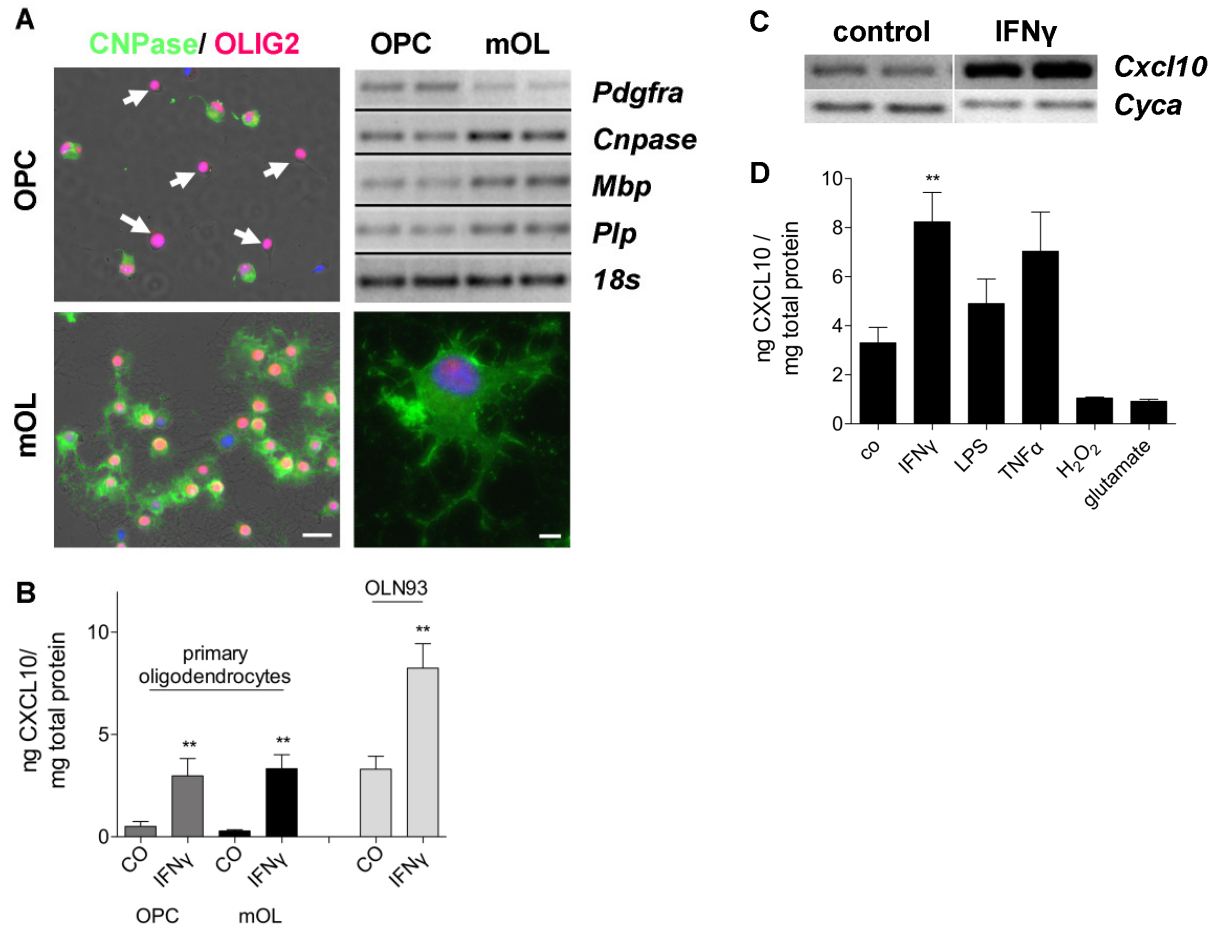


Figure 8 Stressed oligodendrocytes express CXCL10 in vitro

(A) Primary rat oligodendrocyte cultures were either cultured in the presence of growth factors (FGF-2 and PDGF α) or triiodo-L-thyronine and CNTF to obtain oligodendrocyte progenitor cells (OPCs) or mature oligodendrocytes (mOL), respectively. Note the stronger expression of CNPase and the highly branched morphology of mOLs compared to OPCs. Scale bar 50 μ m (left panel) or 5 μ m (right panel). *Sq*-RT-PCR confirmed induction of myelin-associated genes (*Plp*, *Mbp* and *Cnpase*) in mOLs and lower expression of the OPC-marker gene *Pdgfra*. (B) CXCL10 protein levels in the supernatant of cultured OPCs, mOL cells and the rat oligodendrocyte cell line OLN93 treated with IFN γ for 24 hours. ELISA results were normalized against whole cell protein. Results obtained from primary-cultured OPCs and mOL were analyzed with one-way ANOVA followed by Tukey's post hoc test and compared to respective controls. Results obtained from OLN93 cells were analyzed with unpaired t-test with Welch's correction. ** = $p < 0.01$. (C) *Sq*-RT-PCR was performed from cultured OLN93 cells either untreated or treated with IFN γ for 24 hours. Note the increased level of *Cxcl10* mRNA in IFN γ -treated OLN93 cells. The reference gene Cyclophilin A (*Cyca*) served as an internal control. (D) CXCL10 protein levels in the supernatant of cultured rat OLN93 cells treated with IFN γ , LPS, TNF α , H $_2$ O $_2$, or glutamate. Note increased CXCL10 levels after stimulation with inflammatory cytokines and LPS, predominantly after IFN γ stimulation (CO: 3.3 ± 0.63 , IFN γ : 8.23 ± 1.2). ELISA results were normalized against whole cell protein. Values are given as arithmetic means \pm SEM. ** = $p < 0.01$ (One-Way ANOVA with Tukey's post hoc test).

4.1.5 CXCL10 does not affect mature oligodendrocyte cell death

Recently, it has been reported that cultured oligodendrocytes die when exposed to CXCL10 in a concentration-dependent manner [172]. The lower extent of microglia activation I found in CXCL10^{-/-} mice after cuprizone-treatment might simply be due to less severe oligodendrocyte loss in the absence of CXCL10. To investigate, whether CXCL10 influences oligodendrocyte death during cuprizone-treatment, the number of oligodendrocytes was quantified in the CC of wild type and CXCL10^{-/-} mice after one week of cuprizone exposure. As shown in Fig. 9A, the cuprizone-induced loss of oligodendrocyte transcription factor 2-expressing (OLIG2) oligodendrocytes was comparable between both genotypes. In line with these findings, the number of apoptotic cells (as determined in HE-stained sections) was not significantly different in both strains (Fig. 9B). Furthermore, treatment of primary oligodendrocyte cultures (OPCs and mOL) with recombinant CXCL10 for 24 hours did not induce cell death as determined by LDH release (Fig. 9C). Thus, CXCL10 is not a master regulator of oligodendrocyte loss, at least in the applied model(s).

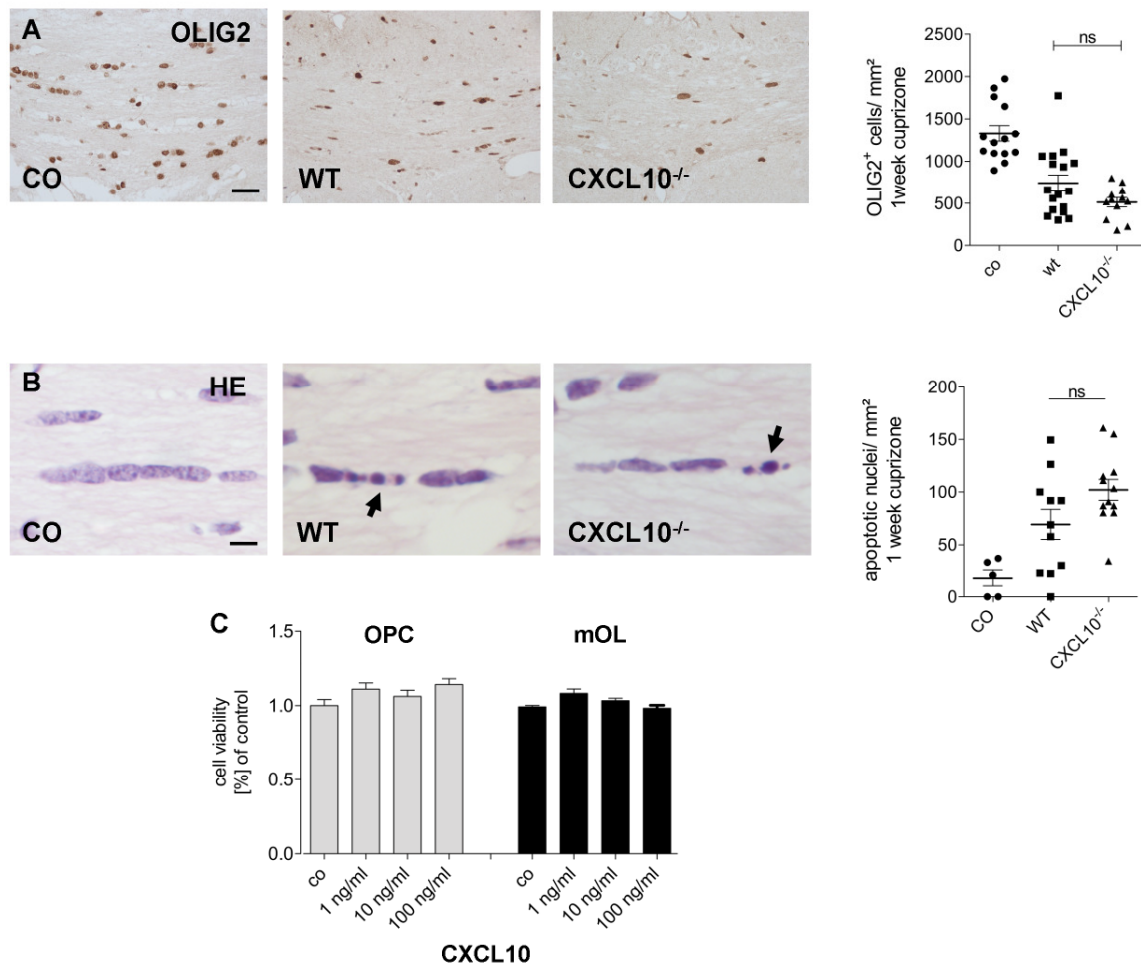


Figure 9 *CXCL10 does not affect oligodendrocyte apoptosis*

(A) Anti-OLIG2 stained sections of the midline of CC in control (CO), wild type (WT) and CXCL10^{-/-} mice after one week of cuprizone exposure. Scale bar 50 μ m. Note that wild type (740.4 ± 94.75 , $n = 17$) and CXCL10^{-/-} (513.2 ± 55.6 , $n = 12$) mice showed similar reduced cell numbers compared to control mice (1331 ± 91.49 , $n = 14$). (B) Evaluation of apoptotic cells in HE-stained sections within the CC one week after cuprizone-treatment. Scale bar 10 μ m. Note that no significant difference is evident between wild type (69.34 ± 14.27 , $n = 11$) and CXCL10^{-/-} (102.1 ± 9.89 , $n = 12$) mice compared to control mice (18.33 ± 7.92 , $n=5$). (C) Primary cultures of rat OPCs and mOL were treated with recombinant CXCL10 for 24 hours. Note that treatment of primary rat oligodendrocyte cultures with CXCL10 (1 ng/ml to 100 ng/ml, OPC = oligodendrocyte precursor cell, mOL = mature oligodendrocyte) did not induce cell death as determined by LDH release. Male mice used. Values are given as arithmetic means \pm SEM; ns = not significant (One-way ANOVA with Tukey's post hoc test).

4.1.6 CXCL10 does not regulate microglia proliferation

The lower number of IBA1⁺ cells found in CXCL10^{-/-} mice (compare Fig. 5C) might be due to a reduction of microglia attraction (i.e. chemotaxis) or proliferation. To address this question, brain sections from wild type and CXCL10^{-/-} mice were double-stained for the proliferation marker proliferating cell nuclear antigen (PCNA) and the microglia marker IBA1. Representative pictures of the staining are shown in Figure 10A. Note that CXCL10^{-/-} mice show less IBA1⁺ and PCNA⁺ cells as well as double positive cells compared to wild type mice. To determine if CXCL10 in fact promotes the proliferation of microglial cells, I normalized the number of proliferating microglia (double positive for IBA1 and PCNA) to the number of total microglia (IBA1⁺) in each mouse. Thus I excluded that the differences seen are due to lower total microglia numbers in CXCL10^{-/-} mice. Interestingly, the percentage of proliferating microglia, out of the total microglia population was comparable in WT and CXCL10^{-/-} mice (Fig. 10B; ~50%). Additional *in vitro* experiments showed that CXCL10 treatment does not result in increased metabolic activity in microglial cells, indicating that CXCL10 does not induce microglia proliferation *in vitro* (Fig. 10C). My *in vivo* and *in vitro* data thus indicate that CXCL10 does not directly affect microglia proliferation although the overall number of microglial cells is reduced in CXCL10^{-/-} mice.

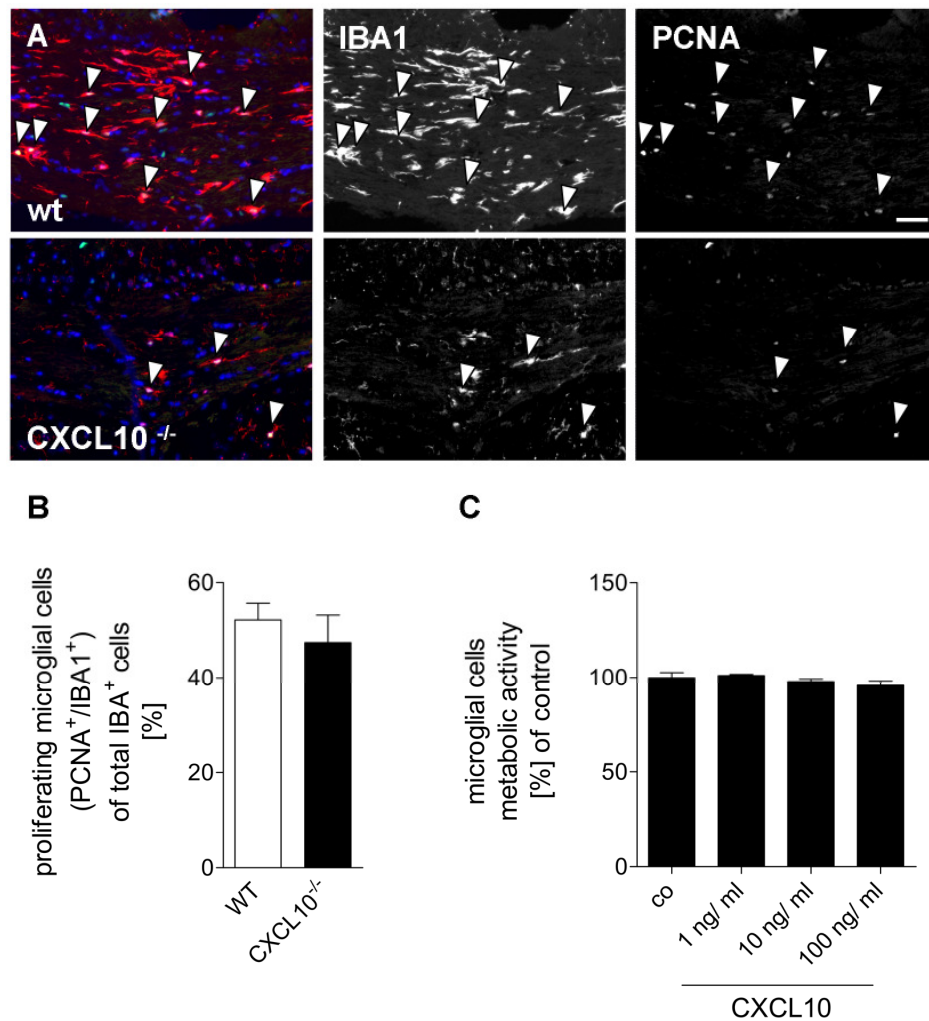


Figure 10 CXCL10 does not increase cuprizone-induced microglia proliferation

(A) Anti-IBA1 (red) and anti-PCNA (green) stained sections of male wild-type and CXCL10^{-/-} mice CC after one week cuprizone-treatment (arrowheads indicate double positive cells; nuclei are marked in blue). Immunostaining of IBA1 as well as PCNA was reduced in CXCL10^{-/-} mice. Scale bar 50 μ m. (B) Quantification of proliferating microglia (IBA⁺ and PCNA⁺ cells) in the CC of wild type and CXCL10^{-/-} mice. Values are normalized to total IBA1⁺ microglia present in the analyzed region of the corresponding mice. No significant difference was observed in the percentage of double positive cells between wild type (52.21 \pm 3.48) and CXCL10^{-/-} mice (47.42 \pm 5.8 unpaired t-test). (C) Treatment of cultured mouse microglial cells (ESdM) with CXCL10 for 24 hours. Note that CXCL10 did not change the metabolic activity of cultured microglial cells as determined by the CTB assay (One-Way ANOVA with Tukey's post hoc test). Values are given as arithmetic means \pm SEM.

4.1.7 CXCL10 induces microglia attraction and activation, but not phagocytosis

In further experiments, I addressed the question, whether CXCL10 plays a role in microglia attraction and activation. For this part of the study, I used a microglial cell line for all following experiments [165]. First, pro-migratory effects of CXCL10 on microglial cells were assessed. Both, recombinant CXCL10 and the supernatants of IFN γ -treated OLN93 cells induced directed microglial cell migration (Fig. 11A). To investigate whether CXCL10 is the key molecule leading to microglial attraction, a CXCL10-neutralizing antibody was added to the supernatant of the oligodendrocytes. As shown in figure 11A, oligodendrocyte-induced microglia migration was completely blocked by the addition of the CXCL10 neutralizing antibodies.

The effect of CXCL10 on microglia polarization (i.e. pro-inflammatory phenotype, M1) was tested by *rt*RT-PCR after a 24 hours treatment period. Recombinant CXCL10 induced 18-fold and 7-fold increases in the expression of *inos* and *Tnfa* mRNAs, respectively (Fig. 11B). These effects were blocked by co-incubation with anti-CXCL10 antibodies (not shown). Furthermore, *Cxcl10* expression was also increased, indicating a positive-feedback mechanism (Fig. 11B). To verify that stressed oligodendrocytes could actually induce a pro-inflammatory phenotype in microglia, cultured microglia were stimulated with the supernatant of oligodendrocytes exposed to IFN γ for 24 hours. These experiments showed an induction of *inos* and *Tnfa* mRNA expression in microglia (Fig. 11C, checked bar), whereas the addition of CXCL10 neutralizing antibodies reverses this effect (Fig. 11C, striped bar). Cells incubated in the presence of unspecific IgGs served as a negative control. These results indicate that IFN γ -stimulated oligodendrocytes induce a pro-inflammatory microglial response which is in large part mediated by CXCL10 protein.

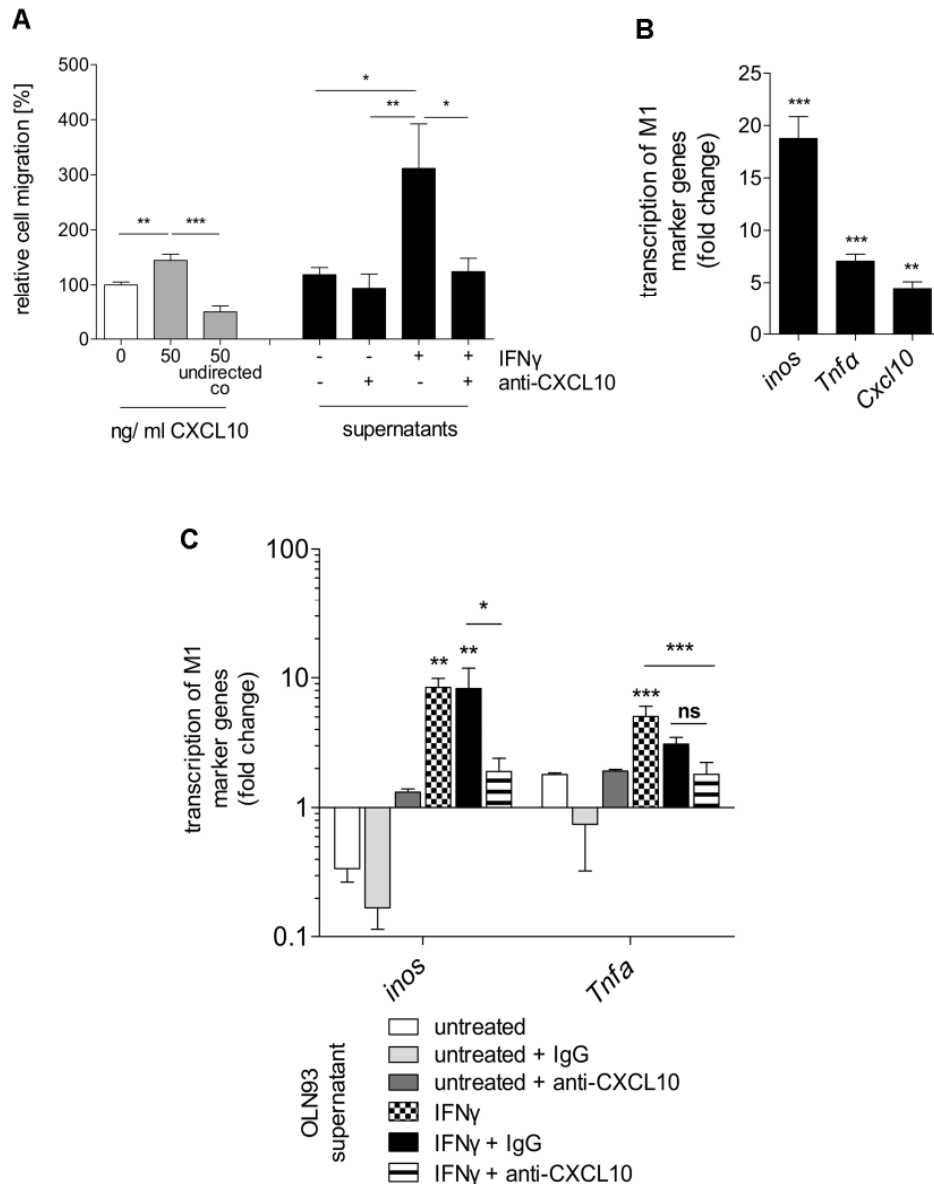


Figure 11 CXCL10 induces chemotaxis and a M1 phenotype in microglial cells

(A) *In vitro* migration two chamber assay of cultured microglial cells (ESdM). Note that recombinant CXCL10 (50 ng/ml) induced directed migration of microglial cells (144.7 ± 11.18) compared to negative control (microglia medium without stimulus, 100 ± 5.38) and undirected control (50 ng/ml CXCL10 in upper and lower chamber, 49.53 ± 10.7). Furthermore, supernatant from IFN γ -treated OLN93 cells (supernatants) induced a ~3 fold increase in migration activity (311.6 ± 80.87) compared to untreated control conditions (supernatant from untreated OLN93 cells 118.6 ± 13.03). This effect was completely blocked by a pre-incubation step with anti-CXCL10 antibodies (124.5 ± 24.14). Results from supernatants were normalized to corresponding negative controls containing microglia medium with or without IFN γ , to exclude direct effects of IFN γ . Data are presented as means \pm SEM of $n = 7$ independent experiments. Differences between groups were tested using ANOVA followed by post hoc Bonferroni. * = $p < 0.05$; ** = $p < 0.01$; *** = $p < 0.001$. (B) *rt*RT-PCR of microglial cells stimulated with CXCL10 for 24 hours. Note the induction of *inos*, *Tnfa* and *Cxcl10* transcripts in CXCL10-stimulated microglia. (C) *rt*RT-PCR of microglial cells stimulated for 24 hours with supernatant (OLN93 supernatant) of untreated or IFN γ -treated OLN93 cells pre-incubated with anti-CXCL10 or control IgG. Stimulated microglia exhibited increased gene transcription of *inos* and *Tnfa*. This effect was partially neutralized with CXCL10 specific antibodies. In both experiments, values are presented as arithmetic means \pm SEM and were normalized against a reference gene (*Gapdh*) and expressed relative to controls, cultured in

standard microglia medium (n = 3 independent experiments). Differences between groups were tested using ANOVA followed by Bonferroni. * = $p < 0.05$; ** = $p < 0.01$; *** = $p < 0.001$; ns = not significant. Since phagocytosis is another cardinal function of microglia, I examined the effect of recombinant CXCL10 on the ability of microglia to phagocytose polystyrene latex beads by flow cytometry [165]. As a positive control, I used LPS which induced a 2-fold increase of microglial phagocytosis activity. I found that CXCL10 did not affect phagocytosis neither under basal conditions nor after LPS stimulation (Figs. 12A and B). These *in vitro* results indicate that CXCL10 does not modulate microglia phagocytosis. To verify these findings *in vivo*, the CC of wild-type and CXCL10^{-/-} mice were stained for the lysosomal-associated membrane protein 2 (MAC-3/LAMP-2) which is a reliable marker for late stage lysosomes and phagocytosis [173-174]. The amount of MAC-3 positive cells was very small in both strains after cuprizone-treatment although higher compared to control mice (Fig. 12C). Statistical evaluation was therefore difficult and I assume that phagocytosis is not a major feature of microglial cells early after cuprizone-treatment. However, this finding is in line with my *in vitro* experiments as I did not see remarkable differences between wild type and CXCL10^{-/-} mice. Taken together, my results indicate that CXCL10, secreted by stressed oligodendrocytes, induces microglia chemotaxis and the induction of a pro-inflammatory (M1) phenotype but does not regulate microglial phagocytosis and proliferation.

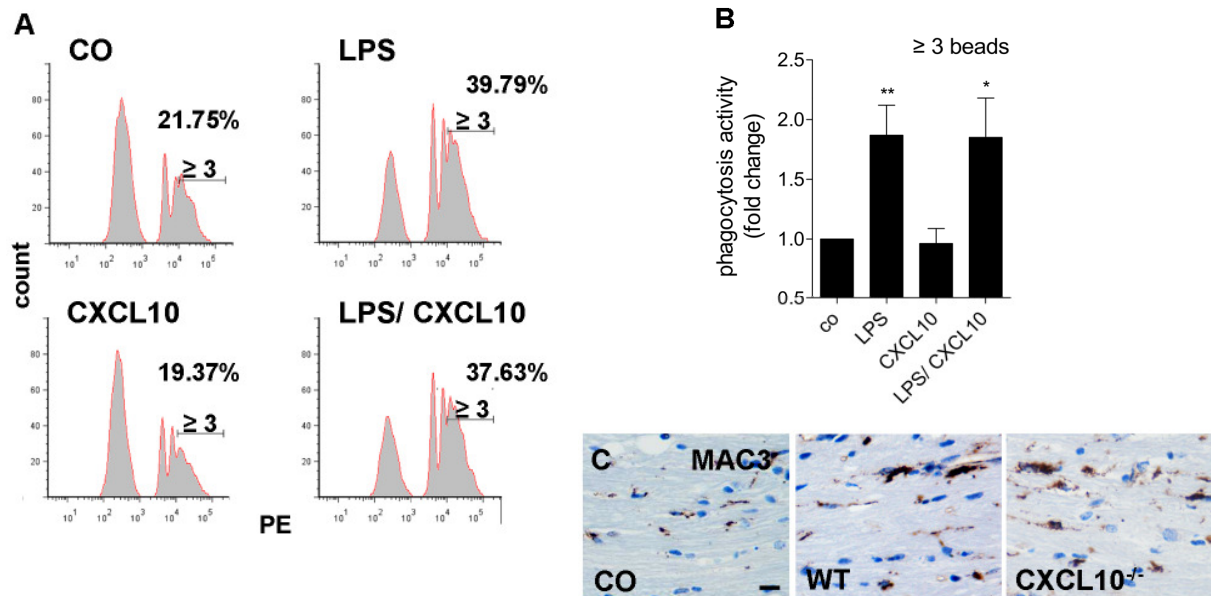


Figure 12 CXCL10 does not induce phagocytosis in microglial cells in vivo nor in vitro

(A) Flow cytometry histograms show representative results obtained with the beads phagocytosis assay. Only cells that phagocytized 3 or more beads were counted as phagocytically active microglial cells (ESdM). Details on calculation are given in the materials and methods section. Numbers in the histograms indicate the percentage of phagocytic active microglial cells. CO: untreated microglia; LPS: microglia treated for 24 hours with 500 ng/ml LPS; CXCL10: microglia treated for 24 hours with 10 ng/ml CXCL10; LPS/CXCL10: microglia treated for 24 hours with both, 500 ng/ml LPS and 10 ng/ml CXCL10. (B) Quantification of phagocytic activity of microglial cells. Note that CXCL10 does not change the phagocytic activity of microglial cells, while LPS increased the uptake of beads by the microglia. Results are presented as fold induction over controls. Graphs represent results of $n = 4$ independent experiments. Differences between groups were tested using ANOVA followed by Tukey's post hoc test. $* = p < 0.05$; $** = p < 0.01$. (C) Anti-MAC3 stained sections of untreated control (CO), wild type (WT) and CXCL10^{-/-} mice treated for one week with cuprizone. Note that MAC3 immunoreactivity is similar in WT and CXCL10^{-/-} animals. Scale bar 20 μm .

4.2 The growth factors FGF-2 and PDGF α are involved in oligodendrocyte maturation and homeostasis *in vitro*

4.2.1 FGF-2 and PDGF α inhibit myelin gene expression in oligodendrocytes possibly via ERK signalling

Oligodendrocyte precursor cells are a multipotent CNS precursor cell population and capable of myelin regeneration after a demyelinating event [175]. Remyelination, an important repair mechanism occurring in MS lesions, can restore axonal function and prevent axonal degeneration [176]. For correct remyelination it is necessary that balanced OPC proliferation and differentiation takes place. In MS patients remyelination is often incomplete at early disease stages and completely fails during chronic phase of the disease. The reason for remyelination failure in MS is still unknown [177]. However, a better understanding of oligodendrocyte biology will help to identify signalling mechanisms, which might be attractive targets for pro-remyelinating therapies in the future. Two important growth factors involved in OPC proliferation and differentiation are FGF-2 and PDGF α (reviewed in [178]). In my experiments FGF-2 and PDGF α -treated OPCs showed very little expression of typical myelin associated genes (i.e. *Plp*, *Mag2*, *Mbp*), indicative of a progenitor phenotype. I investigated in this part of the study if FGF-2 and PDGF α also influence the expression of myelin associated genes in mature oligodendrocytes and what pathways might be involved in FGF-2 and PDGF α signalling. To address the question if FGF-2 and PDGF α play a role in the regulation of myelin gene expression, I treated primary rat oligodendrocytes with basal oligodendrocyte medium containing either 10 ng/ml FGF-2 and/or 10 ng/ml PDGF α or 15 nM triiodo-L-thyronine (T3) and 10 ng/ml CNTF for 48 hours. As expected, stimulation with FGF-2 and/or PDGF α resulted in low expression levels of myelin genes (*Mag2*, *Plp*, *Mbp*) compared to basal medium control as shown in figure 13A-C. In contrast, cells treated with either T3/CNTF or vehicle (basal medium) showed significantly higher expression levels of myelin mRNA, indicative of a more mature cell phenotype. Note that control cells treated with basal oligodendrocyte medium show higher levels of myelin gene expression compared to GF-treated cells indicative of spontaneous differentiation occurring in the absence of FGF-2 and PDGF α . This was confirmed for the myelin protein CNPase in the oligodendrocyte-like cell line OLN93, which showed low expression of CNPase protein after treatment with FGF-2/PDGF α compared to high levels of CNPase protein after T3/CNTF or vehicle treatment (Fig. 13D).

Interestingly, mature oligodendrocytes that were first treated with T3 and CNTF showed reduced myelin mRNA expression after a following treatment with FGF-2 and PDGF α . This result indicates that FGF-2 and PDGF α suppress transcription of myelin genes in mature oligodendrocytes and thus result in a partial de-differentiation of the cells.

In a next step I investigated which pathway might be involved in FGF-2 and PDGF α signalling. As seen in figure 13E, stimulation of rat OLN93 cells with FGF-2 and/or PDGF α lead to increased levels of phosphorylated ERK protein compared to unstimulated cells. Both proteins are described to activate ERK dependent pathways [179-181].

The down regulation of myelin genes is also a characteristic of the cuprizone model (compare Fig. 2G) Therefore, I investigated if cuprizone-treatment leads to an up regulation of the growth factors FGF-2 and PDGF α , which then might lead to down regulation of myelin genes. However, *rt*RT-PCR analysis of FGF-2 and PDGF α expression did not show differences between control and 2 days or 1 week cuprizone-treated mice (data not shown). Taken together, my results show that FGF-2 and PDGF α , beside their role in OPC proliferation, negatively influence maturation of oligodendrocytes *in vitro*. An imbalance in this growth factor system might thus account for some aspects of oligodendrocyte pathology observed in distinct MS lesion subtypes [182] and remyelination failure.

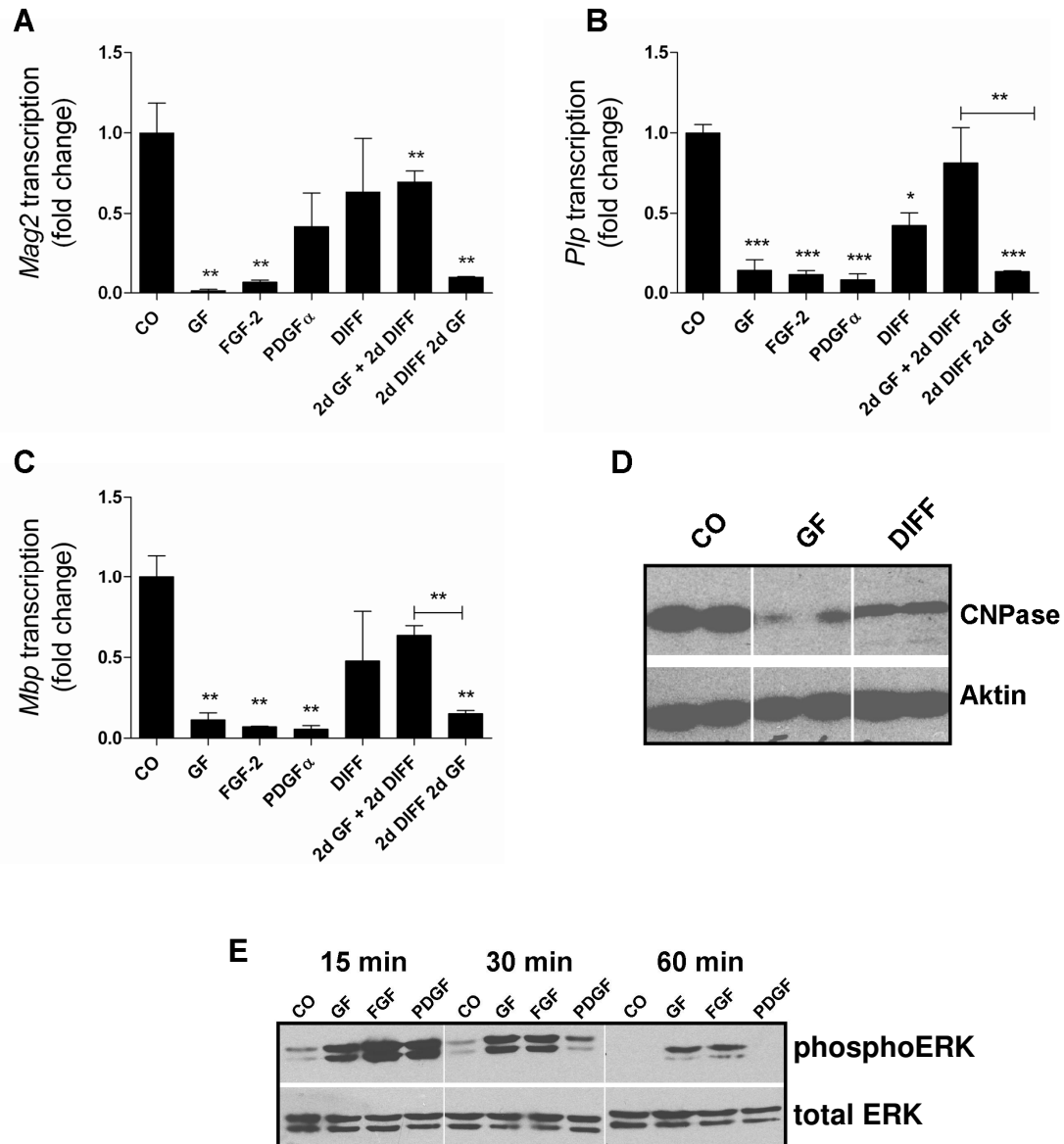


Figure 13 FGF-2 and PDGF α suppress myelin gene transcription in primary oligodendrocytes and activate ERK signalling in OLN93 cells.

(A-C) *rr*RT-PCR of primary rat oligodendrocytes stimulated with basal oligodendrocyte medium alone (CO), or supplemented with 10 ng/ml FGF-2 and 10 ng/ml PDGF α (GF), 10 ng/ml FGF-2 or 10 ng/ml PDGF α alone, 15nM T3 and 10 ng/ml CNTF (DIFF) or alternating with GF and DIFF for 48 hours. Note that the major myelin genes *Mag2* (A), *Plp* (B) and *Mbp* (C) are down regulated by the growths factors FGF-2 and PDGF α , whereas more mature oligodendrocytes show increased myelin gene expression. Furthermore, GF inhibit the expression of myelin genes in mature oligodendrocytes. The graphs show results of $n = 4$ independent experiments. Values are given as arithmetic means \pm SEM. Differences between groups were tested using ANOVA followed by Tukey's post hoc test. * = $p < 0.05$; ** = $p < 0.01$; *** = $p < 0.001$. (D) Western Blot analysis of CNPase expression by rat OLN93 cells after treatment with control medium (CO), 10 ng/ml FGF-2/PDGF α (GF) or 15 nM T3/10 ng/ml CNTF (DIFF) for 48 hours. Note that treatment with GF leads to suppression of CNPase expression. Actin served as a loading control. (E) Western Blot analysis of phosphorylated ERK and total ERK expression in rat OLN93 cells after treatment of cells with basal oligodendrocyte medium alone (CO), or supplemented with 10 ng/ml FGF-2/PDGF α (GF), 10 ng/ml FGF-2 or 10 ng/ml PDGF α alone for 15, 30 and 60 minutes. Total ERK protein served as a loading control. Note that growth factors strongly increase the amount of phosphorylated ERK after 15 min alone and in combination compared to vehicle control. Further note that ERK phosphorylation lasts longer in FGF-2 or FGF2/PDGF α co-treated cells compared with cells only treated with PDGF α .

4.3 The chemokines CCL2 and CCL3 regulate cortical myelin integrity in the cuprizone model

4.3.1 CCL2/3^{-/-} mice are viable, fertile and show no gross physical or behavioural abnormality

The chemokines CCL2 and CCL3 have been described to play important roles during MS disease course and cuprizone-induced demyelination [36, 117, 119]. I already showed that both chemokines, together with CXCL10 and CCL7 are up-regulated early during cuprizone-treatment [183]. To study redundant functions of CCL2 and CCL3, I crossbred a new double knockout strain by mating the commercially available single knockout strains from Jackson laboratory. The F1 generation of heterozygous CCL2^{+/-}/CCL3^{+/-} mice was further mated to obtain homozygous double knockout mice. Both genes are located on chromosome 11 with a distance of 1.24 cM meaning that the genes have a recombination frequency of 1.24 %. Homozygous CCL2/3^{-/-} mice are viable, fertile and do not show any gross abnormalities under normal housing conditions. To identify double knockout mice, I performed a genotyping approach as illustrated in figure 14A. I chose a primer combination which detects a part of the wild type gene, or the transition site between the homologous wild type sequence and an initially introduced neomycin cassette [184-185]. In a semi-quantitative PCR, homozygous wild type mice displayed one band of 287 bp for the *Ccl2* gene and one of 150 bp for the *Ccl3* gene, whereas knockout mice showed a 179 bp band for the disrupted *Ccl2* and a 600 bp band for the disrupted *Ccl3* gene (compare figure 14B). In contrast, heterozygous CCL2^{+/-} mice showed a 287 bp band for the *Ccl2* wild type gene and a 179 bp band for the *Ccl2* knockout gene as they possess both gene variants, one on each chromosome 11. This also applies for CCL3^{+/-} heterozygous mice, which showed two bands with 150 bp and 600 bp for the *Ccl3* wild type and *Ccl3* knockout gene, respectively.

To further verify the knockout on the DNA level, the PCR products of the knockout genotyping PCR were sequenced and compared to the wild type sequence of *Ccl2* and *Ccl3* as published at ENSEMBL (*Ccl2*: ENSMUSG00000035385 and *Ccl3*: ENSMUSG00000000982). Figure 14C shows a part of the sequencing result at the transition site of the neomycin cassette and the homologous recombination site of the mutant sequences paired with the wild type sequence of *Ccl2* (upper sequence) or *Ccl3* (lower sequence). I found that the sequenced DNA is partly homologous to the *Ccl2* or *Ccl3* gene representing the homologous recombination sites present in the vector, which was used to insert the disrupted sequence into the genome of the single knockout mice [184-185]. The adjacent non-

homologous sequence did not give a specific result in a BLAST search and very likely represents a part of the neomycin cassette present in the disrupted gene (sequence of the neomycin cassette is not available).

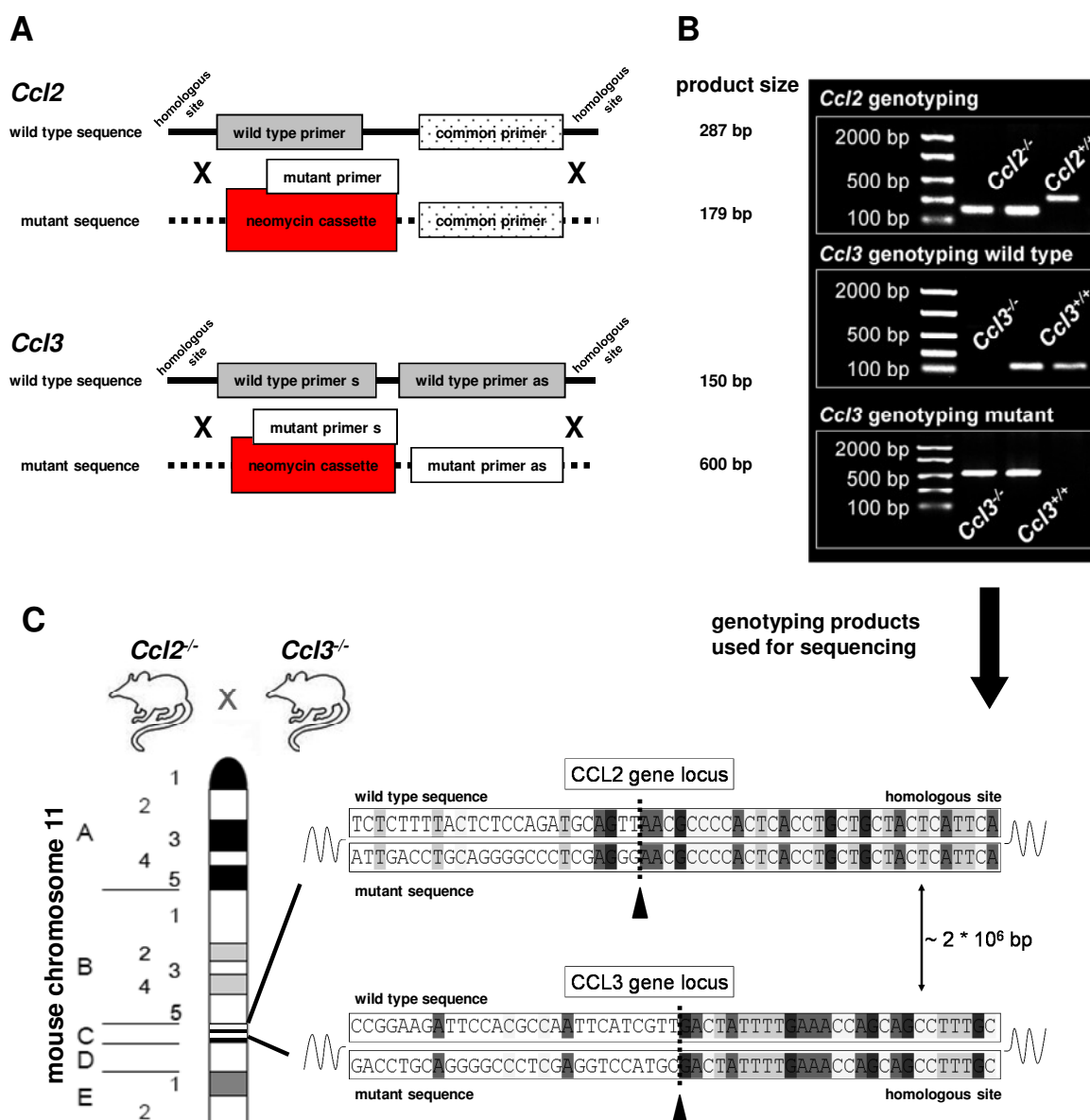


Figure 14 Genotyping strategy and DNA sequencing of *CCL2/3*^{-/-} mice

(A) Genotyping strategy for wild type and *CCL2/3* deficient (*CCL2/3*^{-/-}) mice is presented. Note that the sense primer detecting the knockout is placed in the neomycin cassette which was inserted into the gene of interest when generating the original single knockout mouse. (B) Gel electrophoresis of semi-quantitative PCR genotyping of *CCL2/3*^{-/-} mice and expected product size. (C) Breeding scheme and gene sequence obtained by sequencing the genotyping PCR products. Both genes are located on chromosome 11 with a distance of 1.24 cM (recombination frequency = 1.24%). Note that the mutant sequence is partially homologous to the wild type sequence representing the sites of homologous recombination during initial generation of the single knockout mice. The non-homologous part of the mutant sequence likely represents a part of the neomycin cassette and did not give a specific result in a BLAST mouse genome search.

4.3.2 CCL2 and CCL3 expression is disrupted in CCL2/3^{-/-} mice

In a next step, I verified in the mice the knockout of *Ccl2* and *Ccl3* on the mRNA and protein level. To study mRNA levels of *Ccl2* and *Ccl3* in double knockout mice, I fed wild type as well as CCL2/3^{-/-} mice with 0.2% cuprizone for eight days. As shown in figure 15A, wild type mice display a strong expression of *Ccl2* and *Ccl3* transcripts after cuprizone-treatment compared to wild type control mice, whereas mRNA levels of *Ccl2* and *Ccl3* in CCL2/3^{-/-} mice were almost not detectable. To examine protein levels of CCL2 and CCL3 in CCL2/3^{-/-} mice, I performed ELISA experiments with primary astrocytes and peritoneal macrophages. Astrocytes and macrophages were treated with LPS as indicated in the figure legend and CCL2 and CCL3 protein levels were quantified in the cell culture supernatant. As shown in figures 15B and 15C both wild type cultures release significantly more CCL2 and CCL3 after LPS treatment compared to untreated wild type cells. This was not evident in cells obtained from CCL2/3^{-/-} mice, confirming the absence of both proteins. Taken together, I could confirm that CCL2/3^{-/-} mice do not express CCL2 and CCL3.

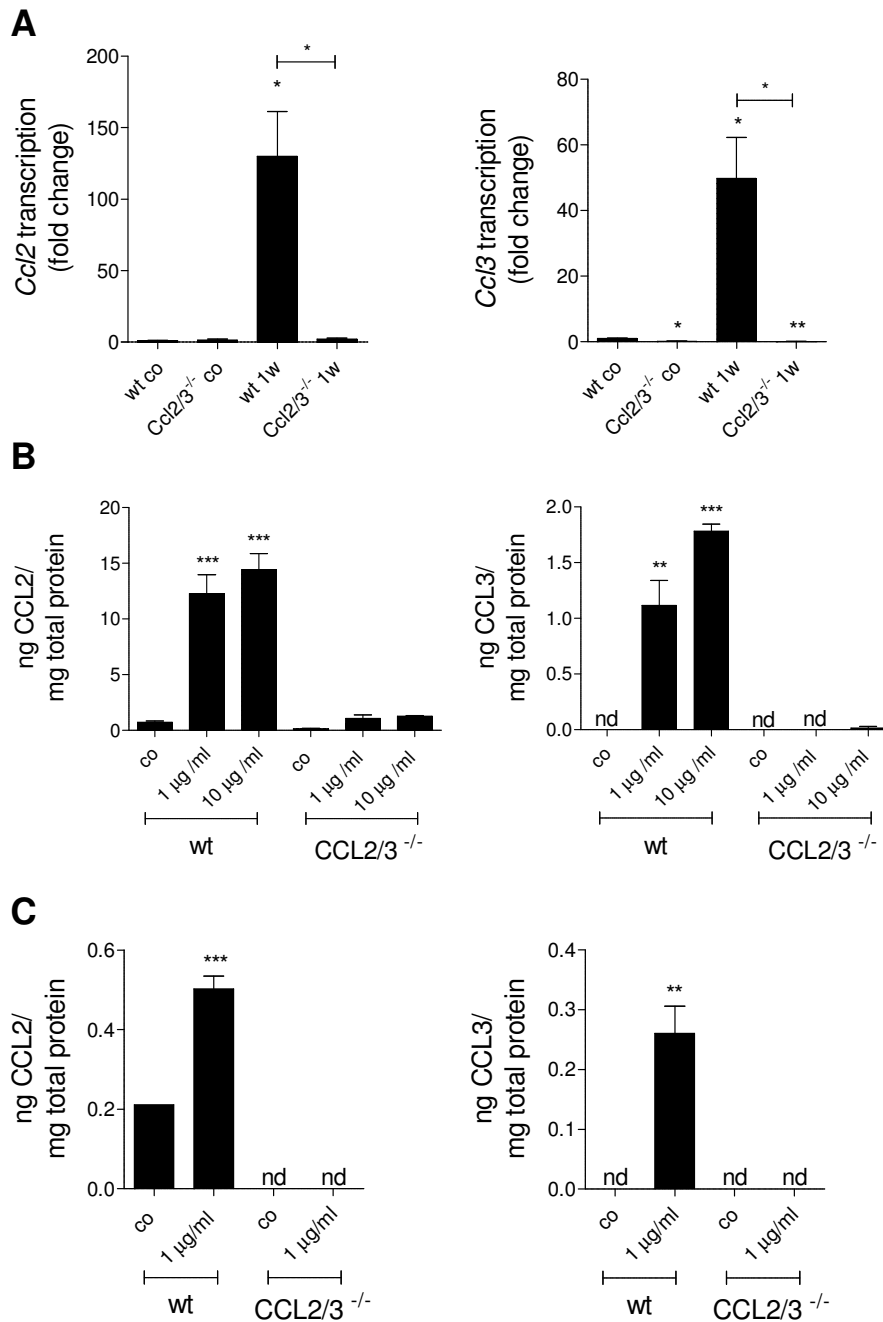


Figure 15 *CCL2/3*^{-/-} mice do not express CCL2 and CCL3 protein

(A) Expression of *Ccl2* and *Ccl3* mRNA in wild type (wt) and *CCL2/3*^{-/-} mice after one week cuprizone-treatment. Levels of *Ccl2* and *Ccl3* transcripts are strongly induced in wild type mice after one week (1w) cuprizone-treatment compared to controls (*Ccl2* co: 1 ± 0.25, 1w: 130 ± 31.3; *Ccl3* co: 1 ± 0.15, 1w: 50 ± 12.5), but not in *CCL2/3*^{-/-} mice (*Ccl2* co: 1.5 ± 0.5, 1w: 2.2 ± 0.7; *Ccl3* co: 0.2 ± 0.05, 1w: 0.1 ± 0.04, n= 4 mice per group). Melting curve analysis revealed that *CCL2/3*^{-/-} cDNA causes unspecific PCR products in the *rt*RT-PCR. (B) CCL2 and CCL3 protein levels in supernatant of control, 1 µg/ml and 10 µg/ml LPS stimulated wild type (*Ccl2* co: 0.7 ± 0.1, 1 µg/ml: 12.3 ± 1.7, 10 µg/ml: 14.5 ± 1.4; *Ccl3* co: not detectable = nd, 1 µg/ml: 1.1 ± 0.2, 10 µg/ml: 1.8 ± 0.06) and *CCL2/3*^{-/-} (*Ccl2* co: 0.15 ± 0.1, 1 µg/ml: 1.1 ± 0.3, 10 µg/ml: 1.3 ± 0.07; *Ccl3* co: nd, 1 µg/ml: nd, 10 µg/ml: 0.013 ± 0.01) astrocytes. Note that protein levels of CCL2 and CCL3 are almost not detectable. (C) CCL2 and CCL3 protein levels in supernatant of control and 1 µg/ml LPS stimulated wild type (*Ccl2* co: 0.2 ± 10⁻⁸, 1 µg/ml: 0.5 ± 0.032; *Ccl3* co: nd, 1 µg/ml: 0.26 ± 0.05) and *CCL2/3*^{-/-} (*Ccl2* co: nd, 1 µg/ml: nd; *Ccl3* co: nd, 1 µg/ml: nd) peritoneal macrophages. No protein was detected in cells from *CCL2/3*^{-/-}

mice. Male and female mice used. Values are given as arithmetic means \pm SEM. Differences between groups were tested using ANOVA followed by Tukey's post hoc test. * = $p < 0.05$; ** = $p < 0.01$; *** = $p < 0.001$.

4.3.3 *CCL2/3^{-/-} mice display normal brain morphology*

To address the morphology and histology of the brain of CCL2/3^{-/-} mice, coronary sections of 6 week old male wild type and knockout mice were investigated using immunohistochemistry (Figs. 16A-D). Brains were sectioned from the levels 215-525 according to the mouse brain atlas of Sidman *et al.* (<http://www.hms.harvard.edu/research/brain/atlas.html>). Figure 16 shows representative pictures of the level 305 from wild type and CCL2/3^{-/-} mice. The main regions of interest were the medial corpus callosum (CC) and the layer 4 of the somatosensory cortex (Cx) as indicated in the haematoxylin eosin stained overview. No gross abnormality was detected on the cellular level regarding GFAP⁺ astrocytes (Fig. 16A), IBA1⁺ microglia (Fig. 16B), OLIG2⁺ oligodendrocytes (Fig. 16C) or PLP⁺ myelin fibres (Fig. 16D). The number of astrocytes, microglia and oligodendrocytes was also statistically evaluated at all investigated brain levels and regions of interest (medial and lateral CC, Cx, gyrus dentatus and cerebellar white matter), but no significant differences were observed between wild type and CCL2/3^{-/-} mice (data not shown). Furthermore, I investigated the morphology of the liver, spleen and kidney using haematoxylin eosin stain, but did not find any gross abnormalities (data not shown). Taken together, CCL2/3^{-/-} mice show normal brain morphology and histology and no abnormalities in a basic investigation of three major organs.

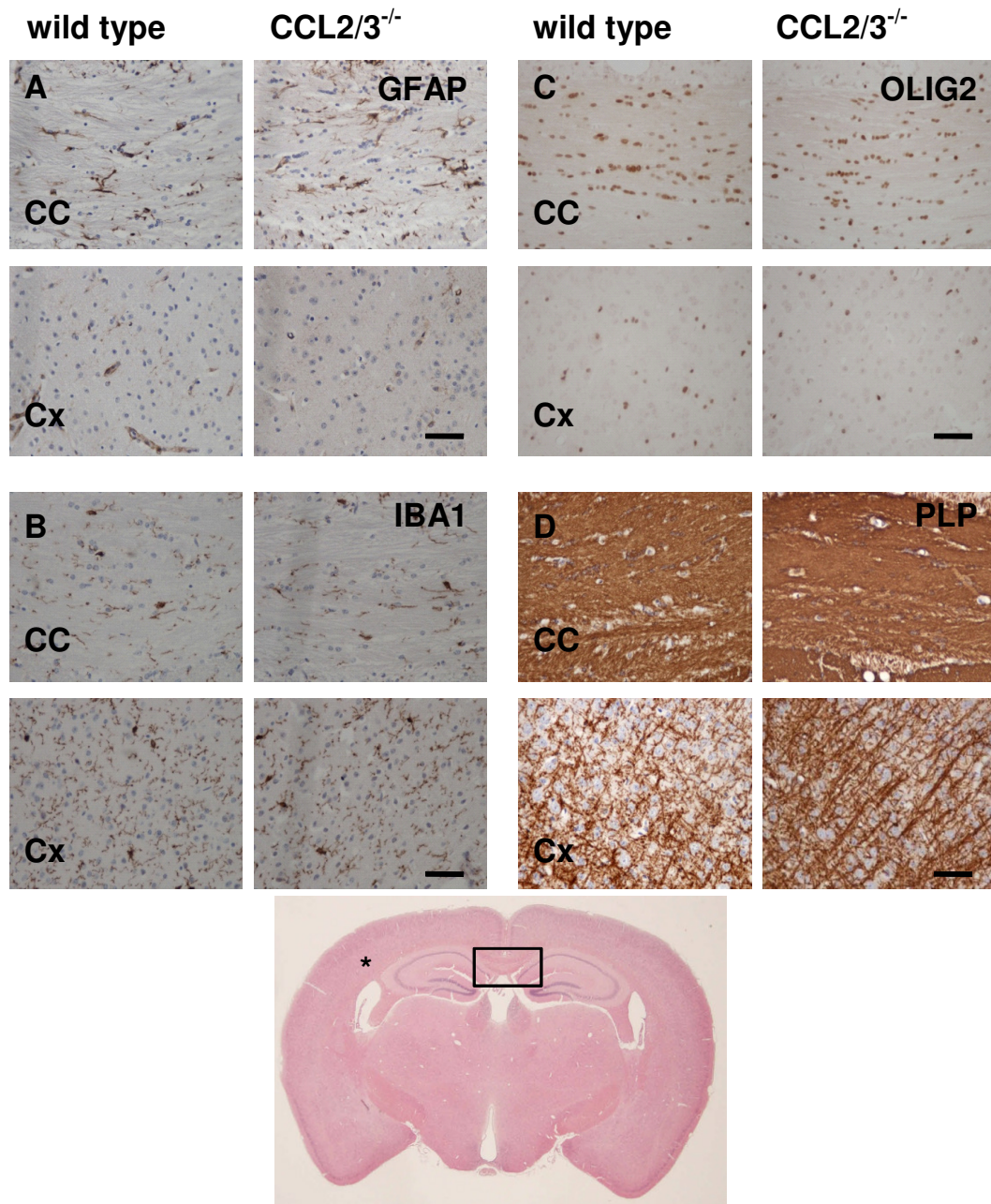


Figure 16 CCL2/3^{-/-} mice have normal brain morphology and histology

Immunohistochemical and histochemical characterization of non-treated CCL2/3^{-/-} mice compared to wild type controls. GFAP (A), IBA1(B), OLIG2 (C) and PLP (D) immunohistochemistry of CCL2/3^{-/-} mice and wild type mice at the level 305 according to the mouse brain atlas of Sidman et. al. Regions of interest are indicated in the haematoxylin stained overview picture (rectangle indicates medial corpus callosum = CC, asterisk indicates layer 4 of the somatosensory cortex = Cx). No gross abnormality was observed in CCL2/3^{-/-} mice compared to wild type controls. Scale bar 50 μ m.

4.3.4 CCL2/3^{-/-} mice display less severe demyelination, astrogliosis and oligodendrocyte loss in the cortex after cuprizone-induced acute demyelination

To address the role of CCL2 and CCL3 in cuprizone-induced demyelination, female mice were fed five weeks with 0.25 % cuprizone. Control animals received normal chow. This cuprizone-experiments were performed together with Cand. med. Mira Rickert. I found that CCL2/3^{-/-} mice show significantly less severe demyelination (Fig. 17A) in the cortex compared to wild type mice which was paralleled by higher numbers of OLIG2⁺ oligodendrocytes (Fig. 17B) and less severe astrogliosis (Fig. 17C). No difference in the number of IBA1⁺ microglial cells was observed (Fig. 17D). In contrast, cellular and myelination parameters of the white matter tract corpus callosum were not different between wild type and CCL2/3^{-/-} mice (Fig. 18A-D). These results suggest a region specific effect of chemokines in the cuprizone model.

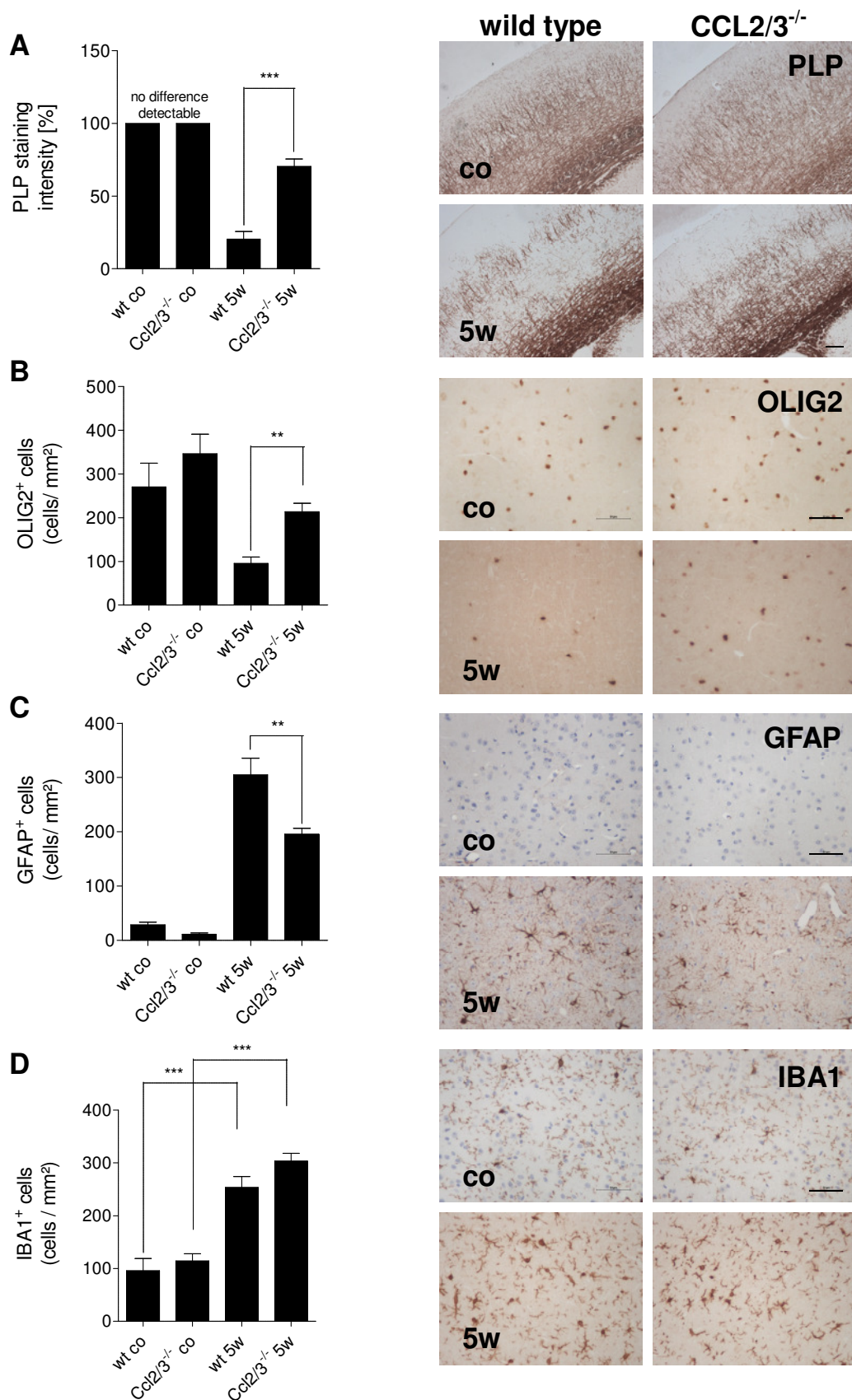


Figure 17 *Ccl2/3^{-/-}* mice show less severe demyelination after cuprizone- treatment in the cortex

(A) Evaluation of anti-PLP staining intensity in wild type and CCL2/3^{-/-} mice after 5 weeks cuprizone. CCL2/3^{-/-} mice show considerably less demyelination in the cortex region after cuprizone-treatment compared to wild type (wt) mice (wt and CCL2/3^{-/-} co: 100, wt 5w: 20.5 ± 5.3, CCL2/3^{-/-} 5w: 70.5 ± 5.1). The right panel shows

representative pictures of anti-PLP stained sections of control (co) and five weeks (5w) cuprizone-treated wild type and CCL2/3^{-/-} mice. Scale bar 100 μ m (B) Analysis of anti-OLIG2 stained sections of control and cuprizone-treated wild type and CCL2/3^{-/-} mice (left panel) and representative pictures of anti-OLIG2 stained sections of cuprizone-treated and control wild type and CCL2/3^{-/-} mice (right panel). Note that CCL2/3^{-/-} mice show more OLIG2⁺ cells in the cortex area compared to wild type mice after 5 weeks (5w) cuprizone-treatment (wt co: 269.9 ± 54.6 n = 3, CCL2/3^{-/-} co: 346 ± 45.2 n = 4, wt 5w: 95.2 ± 14.7 n = 10, CCL2/3^{-/-} 5w: 213.3 ± 19.4 n = 9). (C) Evaluation of GFAP⁺ cells in the cortex of cuprizone-treated CCL2/3^{-/-} and wild type mice and representative pictures of anti-GFAP immunohistochemistry. Note that CCL2/3^{-/-} mice clearly have less GFAP⁺ astrocytes after five weeks (5w) cuprizone-treatment in the cortex compared to wild type mice (wt co: 29 ± 4.6 , CCL2/3^{-/-} co: 11.3 ± 2.4 , wt 5w: 305 ± 30.5 , CCL2/3^{-/-} 5w: 195.8 ± 10.4). (D) Analysis of IBA1⁺ cells in the cortex of wild type and CCL2/3^{-/-} mice treated five weeks with cuprizone and representative pictures of anti-IBA1 immunohistochemistry. Cuprizone-treatment induces similar microgliosis in both wild type and CCL2/3^{-/-} mice (wt co: 96.2 ± 22.9 , CCL2/3^{-/-} co: 114.4 ± 13.7 , wt 5w: 254 ± 20.5 , CCL2/3^{-/-} 5w: 304 ± 14.2). Pictures of the cortex were taken at layer 4 of the primary somatosensory cortex. Scale bar (B-D) 50 μ m. Values are given as arithmetic means \pm SEM. Differences between groups were tested using ANOVA followed by Tukey's post hoc test. * = $p < 0.05$; ** = $p < 0.01$; *** = $p < 0.001$.

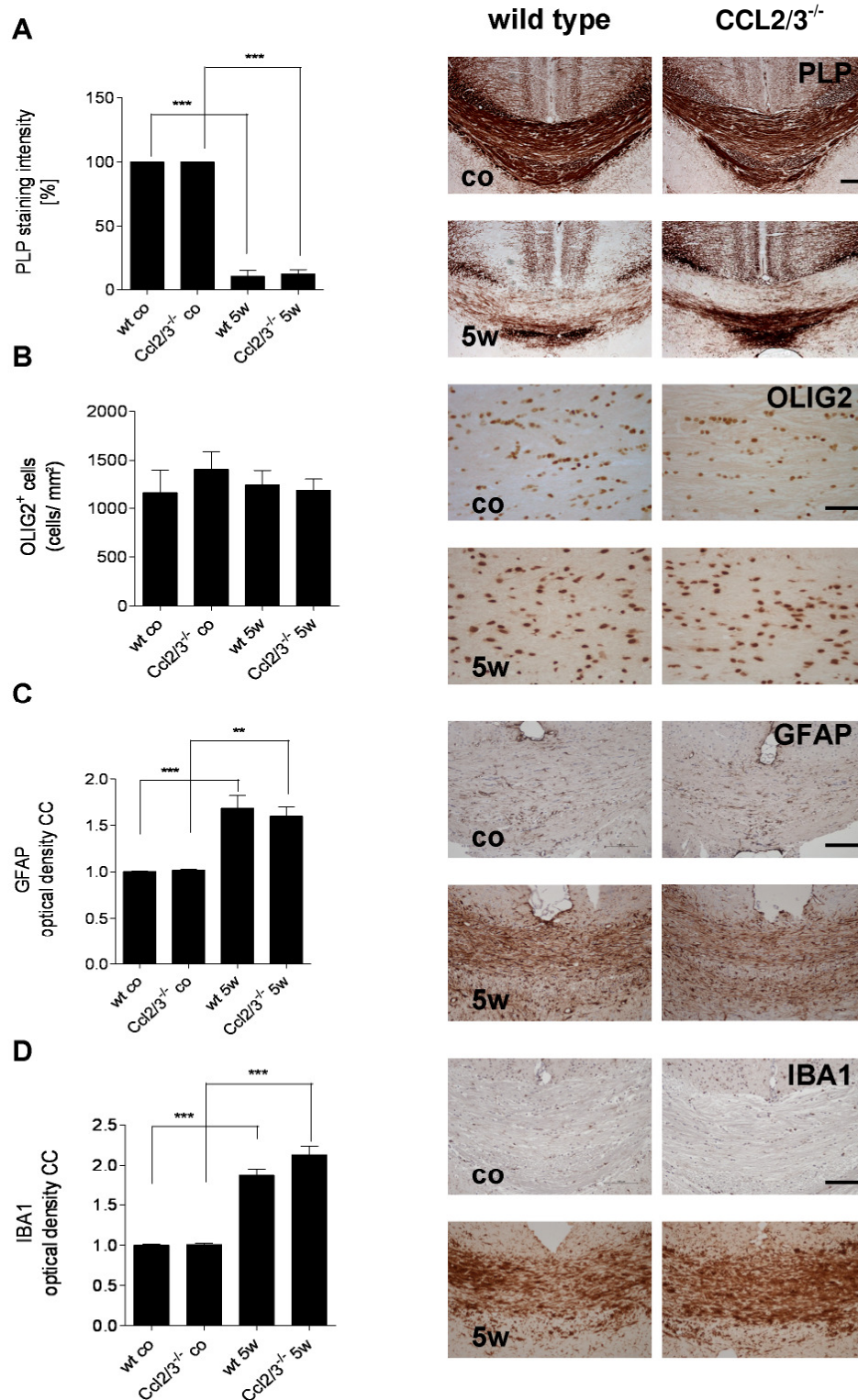


Figure 18 No difference between Ccl2/3^{-/-} mice and wild type mice was observed in the corpus callosum after 5 weeks cuprizone-treatment

(A) Evaluation of anti-PLP staining intensity in wild type and CCL2/3^{-/-} mice after 5 weeks (5w) cuprizone-treatment in the corpus callosum. Scale bar 100 μm. CCL2/3^{-/-} and wild type mice show a similar degree of demyelination (wt and CCL2/3^{-/-} co: 100, wt 5w: 10.6 ± 4.5, CCL2/3^{-/-} 5w: 12.4 ± 3.2). The right panel shows representative pictures of anti-PLP stained sections of control and five weeks cuprizone-treated wild type and CCL2/3^{-/-} mice at the midline of the corpus callosum. (B) Analysis of anti-OLIG2 stained sections of control and cuprizone-treated wild type and CCL2/3^{-/-} mice (left panel) and representative pictures of anti-OLIG2 stained

sections of cuprizone-treated and control wild type and CCL2/3^{-/-} mice (right panel) in the midline of the corpus callosum (wt co: 1158 ± 231 n = 3, CCL2/3^{-/-} co: 1398 ± 189.4 n= 4, wt 5w: 1238 ± 148.8 n= 10, CCL2/3^{-/-} 5w: 1185 ± 113.5 n = 9). Scale bar 50 µm (C) Evaluation of GFAP staining intensity in the corpus callosum of control and cuprizone-treated CCL2/3^{-/-} and wild type mice and representative pictures of anti-GFAP immunohistochemistry in the midline of the corpus callosum (wt co: 1 ± 0.07, CCL2/3^{-/-} co: 1.02 ± 0.008, wt 5w: 1.68 ± 0.14, CCL2/3^{-/-} 5w: 1.6 ± 0.1). (D) Analysis of IBA1 staining intensity in the midline of the corpus callosum of wild type and CCL2/3^{-/-} mice treated five weeks with cuprizone and representative pictures of anti-IBA1 immunohistochemistry. Cuprizone-treatment induces similar microgliosis in both wild type and CCL2/3^{-/-} mice (wt co: 1 ± 0.01, CCL2/3^{-/-} co: 1.008 ± 0.02, wt 5w: 1.87 ± 0.08, CCL2/3^{-/-} 5w: 2.1 ± 0.1). Intensity of GFAP and IBA1 staining was evaluated using ImageJ software as described in materials and methods. Scale bar 100 µm. Values are given as arithmetic means ± SEM. Differences between groups were tested using ANOVA followed by Tukey's post hoc test. * = $p < 0.05$; ** = $p < 0.01$; *** = $p < 0.001$.

5. Discussion

5.1 Oligodendrocyte-derived chemokine CXCL10 triggers microglial activation in the cuprizone model

In the first part of this thesis I showed that the chemokine CXCL10 is critically involved in early cuprizone-induced microglia activation as demonstrated by lower numbers of IBA1-expressing cells in CXCL10-deficient animals. As I found *Cxcl10* mRNA expressed in interfascicular cells indicative for mature, myelinating oligodendrocytes (compare figure 6), these results suggest that oligodendrocytes are involved in early microglia activation. The assumption that oligodendrocytes express and secrete chemotactic molecules under pathological conditions is highlighted by my finding that cultured oligodendrocytes, exposed to IFN γ , up-regulate CXCL10 expression and release and are able to contribute to an inflammatory environment by activating microglial cells in a CXCL10-dependending manner. CXCL10 expression is classically regulated by IFN γ signalling [186] and was already shown to be present in IFN γ -treated oligodendrocyte cultures by Balabanov and colleagues [187]. Although several efforts were done to visualize CXCL10 protein by using specific antibodies on sections of cuprizone-treated mice, these results were not reliable since signal intensities were comparable in wild type as well as CXCL10-deficient mice (data not shown). Therefore, the active contribution of oligodendrocytes in microglia activation has to be critically evaluated in future studies using for instance double-labeling ISH-techniques to prove the co-localization of *Cxcl10* mRNA and oligodendrocyte-specific mRNA. However, these results provide first evidence that oligodendrocytes are involved in inflammatory signalling in the CNS. The contribution of oligodendrogliopathy to MS pathology as a preceding phenomenon before immune cell invasion is controversially discussed in the literature (reviewed in [6, 188]). A number of experimental studies have demonstrated a strong positive correlation between oligodendrocyte susceptibility to injury and the extent of CNS inflammation in experimental MS models. In mice double heterozygous for the LIFR-null mutation and a gp130 intracellular truncation, absence of LIF signalling increased oligodendrocyte susceptibility to injury and augmented the inflammatory reaction and the severity of symptoms [70]. In addition, mice lacking pro-apoptotic genes or over-expressing anti-apoptotic molecules, exclusively in oligodendrocytes, display resistance to EAE and inflammatory demyelination [71-72]. The critical role of oligodendrocytes in CNS inflammation is further exemplified in mice with peroxisome-deficient oligodendrocytes which develop spontaneous neuroinflammation [189]. The molecular mechanisms linking

oligodendrocyte stress with the regulation of early microgliosis remain poorly understood. However, the results from my work support the findings of these studies that oligodendrocytes regulate neuroinflammatory processes.

In this study CXCL10 is a critical regulator of early microglia activation after cuprizone-treatment. Interestingly, Tirota and colleagues found that CXCL10 had a detrimental effect on oligodendrocyte cultures treated with IFN γ [172]. One might speculate that CXCL10-deficient mice thus display less cuprizone-induced oligodendrocyte apoptosis leading to less microglia activation, which I could not confirm in this study. The differences in the *in vitro* experiments, where I also did not find increased oligodendrocyte apoptosis in the presence of CXCL10, are possibly due to the shorter treatment period used in my protocols or lower levels of CXCL10 compared to the concentrations used in the study of Tirota and colleagues. Furthermore, I did not find an upregulation of IFN γ in the genome-wide array analysis of cuprizone-exposed animals, suggesting that the early expression of CXCL10 by oligodendrocytes is an IFN γ -independent mechanism in the cuprizone model. This might be different at later time points of cuprizone-induced demyelination where IFN γ expression has been described [190]. Nevertheless, activation of microglial cells by oligodendrocyte-derived CXCL10 might result in the expression of IFN γ or other inflammatory cytokines by microglia or astrocytes, contributing to an inflammatory environment and demyelination. In addition, CXCL10 has been described to directly affect the recruitment of peripheral immune cells into the subventricular zone of EAE mice, thus being able to directly increase neuroinflammation [191]. In MS, IFN γ plays a critical role in disease pathogenesis. It is predominantly expressed by activated, self-reactive CD4⁺ and natural killer cells, and positively correlates with disease activity in EAE [192]. Furthermore, IFN γ expression increases in the two weeks preceding attacks of MS [193] suggesting that this cytokine is involved in the development of new MS lesions. I speculate that oligodendrocytes initially activate microglial cells and thus contribute directly or indirectly to T-cell infiltration. In turn, invading T-cells might activate oligodendrocyte-derived chemokine/cytokine release (e.g via IFN γ -signalling) inducing a pro-inflammatory “*circulus vitiosus*”. Finally this would lead to an active, demyelinating brain focus and consequently disease progression.

Results of previous studies suggest that CXCL10 is involved in the pathogenesis of MS [194-195]. Our knowledge which cells express CXCL10 under demyelinating conditions is immature. In one study, CXCL10 was found to be expressed by endothelial cells [196] whereas in another study, CXCL10 staining associated with astrocytic processes [197]. Except for the fact that CXCL10 is expressed after cuprizone-treatment [198] not much is

known about the cellular source and function of CXCL10 during cuprizone-induced oligodendroglial pathology. Although I found CXCL10 expression in oligodendrocytes, other cells possibly contribute to CXCL10 accumulation during early cuprizone-induced oligodendroglial pathology. For instance, Skripuletz and colleagues recently showed that CXCL10 is predominantly expressed by astrocytes after a five weeks cuprizone exposure when inflammation and demyelination is on its peak [199]. Here, it is important to point out that in the present study mice were analyzed very early after oligodendrocyte injury before significant demyelination can be detected and overt astrocyte activation is evident [34, 36]. I speculate that CXCL10 plays a role during early and late stages of lesion development, with a change in the CXCL10-expressing cell population. Nevertheless, I cannot formally rule out that astrocytes participate in early microglia activation in this model. A greater number of studies are aiming to define the role of CXCL10 in the inflammatory demyelination model EAE than in the cuprizone model, but these studies have produced conflicting results. Predicting on one hand positive properties of CXCL10 [125] and on the other hand negative properties [124], for example oligonucleotide-blocking of *Cxcl10* transcript reduced clinical signs in MBP-induced EAE [200], whereas CXCL10 knockout animals show more severe EAE [126]. The relevance of these and my study for MS lesion development has to be addressed in the future.

In summary, my results strongly suggest that stressed oligodendrocytes release CXCL10, which activates microglia suggesting that oligodendrocytes can actively participate in the initiation of neuroinflammatory events.

5.2 The growth factors FGF-2 and PDGF α are involved in oligodendrocyte maturation and homeostasis in vitro

The importance of FGF-2 and PDGF α on OPC proliferation and differentiation has been extensively discussed in the literature [201-204] and both molecules or members of their downstream signalling pathways, respectively, are discussed as possible targets for the treatment of remyelination and remyelination failure in MS [177, 205-206]. In this part of the study I could confirm that FGF-2 and PDGF α significantly suppress the expression of major myelin genes (i.e. *Mag2*, *Plp*, *Mbp* and *Cnp*) in OPCs, thus maintaining the precursor status of the cells. Interestingly, the growth factors also suppress myelin gene expression in already mature, myelin gene expressing oligodendrocytes *in vitro*, leading to a de-differentiated phenotype of the cells with probably impaired myelination capacity. This is in line with findings from Fressinaud and colleagues [207]. In the CNS astrocytes are a major source of

FGF-2 and PDGF α [203, 208]. Since MS lesions show high numbers of activated astrocytes high levels of FGF-2 and PDGF α expression can be expected. Indeed, high levels of FGF-2 have been found in the CSF of MS patients correlating with relapses [209]. Furthermore numbers of PDGF α R-expressing oligodendrocytes are elevated in MS lesions, also indicating a role for PDGF α -dependent OPC proliferation in MS [210]. In principal the process of remyelination taking place in demyelinated brain tissue includes three steps: First, OPCs will proliferate and migrate to the demyelinated lesion; second, differentiate to mature oligodendrocytes; and third, get in contact with demyelinated axons to start the remyelination process [211-212]. This process involves not only FGF-2 and PDGF α , but also a broad variety of cytokines, chemokines, hormones and other growth factors [51, 213]. However, if an imbalance exists between proliferative and maturing signals for instance in the presence of very high numbers of activated astrocytes, the differentiation of OPCs and thus remyelination fails and even mature oligodendrocytes might suffer from the de-differentiating stimulus they encounter. Interestingly, remyelination failure in chronic MS lesions is likely not due to a lack of OPCs, as there generally are sufficient numbers of OPCs for successful remyelination in the lesion area [210], but the maturation of these OPCs seems to be impaired especially at later chronic disease stages [78]. Beside growth factors also other mechanism have been described that might account for disturbed remyelination in chronic MS lesions, among them expression of remyelination inhibiting factors, decreasing susceptibility of axons for remyelination, formation of the glial scar and aging of OPCs [177, 206, 214].

At first glance increasing proliferation of OPCs via FGF-2/PDGF α signalling in demyelinated tissues seems to be a favourable idea to support the remyelination process. However, my results indicate that growth factors play ambivalent roles in the remyelination process, which has also been shown in different animal models of MS (reviewed in [215]). A fact that has to be considered when investigating new disease modifying treatments, addressing OPC proliferation and maturation to promote remyelination in MS patients.

5.3 The chemokines CCL2 and CCL3 regulate cortical myelin integrity in the cuprizone model

CCL2 (MCP1) and CCL3 (MIP1 α) are among the best characterized chemokines and have been described in MS pathology as well as in its various animal models [123, 216]. During this study, analysis of chemokine gene expression levels revealed that *Ccl2* and *Ccl3* mRNA are up-regulated early after cuprizone-treatment (compare figure 4). Nevertheless, when investigating the role of CCL2 and CCL3 in early cuprizone-induced microglia activation no

significant differences were found compared to wild type mice. Due to their highly conserved structure many chemokines display redundant functions as they bind to the same receptor [91]. Therefore, we decided to generate a double knockout strain of these two distinct chemokines. By extensive cross-breeding of the commercially available single knockout strains I was able to generate a new strain that does not show expression of CCL2 or CCL3 protein. Since the mice are viable, fertile and do not display any gross abnormality or pathology, they provide an interesting tool to study redundant functions of CCL2 and CCL3 not only in the context of MS, but also in other disease conditions linked to inflammation and/or cell migration.

When conducting a first five week cuprizone trial I found interesting differences between CCL2/3^{-/-} mice compared to wild type mice in the cortex (Cx) but not in the corpus callosum (CC). The demyelination of the Cx of cuprizone-treated C57BL/6 mice has already been described [217]. Interestingly, CCL2/3^{-/-} mice showed less demyelination together with higher numbers of OLIG2⁺ oligodendrocytes indicating a role of these chemokines, either directly or indirectly, in acute cuprizone-induced demyelination. Whether the higher number of oligodendrocytes is due to less oligodendrocyte apoptosis or increased proliferation of OPCs is still an open question. Furthermore, it was not investigated if the mice truly display less demyelination or if they show simultaneously increased remyelination. One might speculate that less demyelination in these mice is caused by less inflammation in the Cx area, but I did not find significantly less microglia activation in CCL2/3^{-/-} mice compared to wild type mice, indicating similar levels of inflammation. However, astrocyte activation was less severe in CCL2/3^{-/-} mice indicating a role for astrocyte-mediated pathways in demyelination and oligodendrocyte survival/proliferation. Since astrocytes are described to secrete growth factors important for oligodendrocyte proliferation [203, 208]), less astrocyte activation might lead to increased oligodendrocyte maturation and thus remyelination. When demyelination and remyelination processes take place at the same time, histopathological investigation might lead to the impression that less demyelination is occurring in the mice. To answer this question other methods like electron microscopy have to be used to distinguish between normally myelinated and remyelinated axons. Ongoing studies will address the question if one of the two chemokines or both together account for the described changes.

It is remarkable that the deletion of two chemokines has such a strong region-specific effect in cuprizone-treated mice. One major difference between the CC and the Cx is the content of myelin. That myelin debris is at least partially responsible for the differences in inflammatory white and gray matter demyelination has already been described in MS and in the cuprizone

model by our group [218]. Here, I speculate that the enormous amount of myelin debris in the CC covers the effects of CCL2 and CCL3 deficiency as inflammation is tremendously high. The myelin-poor Cx, showing a priori less inflammation [36, 217] is thus more receptive for changes in the molecular composition. In MS, the pathology of gray matter lesions is believed to differ from white matter lesions in several aspects, such as less pronounced lymphocyte infiltration, macrophage activity, complement composition, or blood-brain-barrier (BBB) alterations [219-222]. The observed differences could be due to differences in the composition and function of the BBB or other elements of the cytoarchitecture of the cerebral Cx, that makes it more resistant to inflammation [219]. Taking together these results demonstrate that white and gray matter regions differ in their response to pathological challenges of the cuprizone-treatment. With respect to MS pathology, future studies have to take into consideration that white and gray matter display different regions not only in their cytoarchitecture, but also in terms of their molecular composition.

6. Work contribution

6.1 External collaboration partners

Prof. Luc Vallières (*Department of Neurosciences, Laval University Hospital Research Center, Quebec G1V 4G2, QC, Canada*) performed radioisotopic labelled *in situ* hybridization.

Prof. Harald Neumann, Dr. Clara Beutner and Dr. Bettina Linnartz-Gerlach (*Neural Regeneration Group, Institute of Reconstructive Neurobiology, University of Bonn, 53127 Bonn, Germany*) performed *rt*RT-PCR and migration assays on mouse embryonic stem cell derived microglial cells.

6.2 Collaboration partners at RWTH Aachen University

Prof. Werner Baumgartner (*Department of Cellular Neurobiology, Institute for Biology II RWTH Aachen, 52056 Aachen, Germany*) performed the electron microscopy experiments in cuprizone-treated mice.

Dr. Bernd Denecke (*Interdisciplinary Centre for Clinical Research (IZKF) Aachen, RWTH Aachen University, 52074 Aachen, Germany*) performed microarray analysis of tissue from cuprizone-treated mice.

6.3 Contribution of colleagues from the Institute of Neuroanatomy, RWTH Aachen University

M.Sc. Tobias Reiß was involved in the basic immunohistochemical characterization of CCL2/3^{-/-} mice.

Cand. med. Mira Rickert was involved in the conduction and immunohistochemical evaluation of the 5 weeks cuprizone experiment with CCL2/3^{-/-} wild type mice.

MD Barbara Krauspe was involved in the cuprizone experiments used for microarray analysis and together with Dr. Jan-Phillip Buschmann performed the immunohistochemical and molecular characterization of short-term cuprizone-treated mice (wild type mice treated for 2 days and 1 week).

7. References

1. van der Valk, P. and C.J. De Groot, *Staging of multiple sclerosis (MS) lesions: pathology of the time frame of MS*. Neuropathol Appl Neurobiol, 2000. **26**(1): p. 2-10.
2. Compston, A. and A. Coles, *Multiple sclerosis*. Lancet, 2002. **359**(9313): p. 1221-31.
3. Friedrich, D., *Multiple Sklerose*. 2008: Stuttgart: Trias Verlag. .
4. Sellner, J., et al., *The increasing incidence and prevalence of female multiple sclerosis--a critical analysis of potential environmental factors*. Autoimmun Rev, 2011. **10**(8): p. 495-502.
5. Lassmann, H., *Multiple sclerosis pathology: evolution of pathogenetic concepts*. Brain Pathol, 2005. **15**(3): p. 217-22.
6. van Noort, J.M., et al., *Preactive multiple sclerosis lesions offer novel clues for neuroprotective therapeutic strategies*. CNS Neurol Disord Drug Targets, 2011. **10**(1): p. 68-81.
7. Kabat, E.A., A. Wolf, and A.E. Bezer, *Rapid Production of Acute Disseminated Encephalomyelitis in Rhesus Monkeys by Injection of Brain Tissue With Adjuvants*. Science, 1946. **104**(2703): p. 362-3.
8. Lorentzen, J.C., et al., *Protracted, relapsing and demyelinating experimental autoimmune encephalomyelitis in DA rats immunized with syngeneic spinal cord and incomplete Freund's adjuvant*. J Neuroimmunol, 1995. **63**(2): p. 193-205.
9. van der Star, B.J., et al., *In vitro and in vivo models of multiple sclerosis*. CNS Neurol Disord Drug Targets, 2012. **11**(5): p. 570-88.
10. Corthals, A.P., *Multiple sclerosis is not a disease of the immune system*. Q Rev Biol, 2011. **86**(4): p. 287-321.
11. Nakahara, J., et al., *Current concepts in multiple sclerosis: autoimmunity versus oligodendroglipathy*. Clin Rev Allergy Immunol, 2012. **42**(1): p. 26-34.
12. Nakahara, J., S. Aiso, and N. Suzuki, *Autoimmune versus oligodendroglipathy: the pathogenesis of multiple sclerosis*. Arch Immunol Ther Exp (Warsz), 2010. **58**(5): p. 325-33.
13. Stys, P.K., *Pathoetiology of multiple sclerosis: are we barking up the wrong tree?* F1000Prime Rep, 2013. **5**: p. 20.
14. Sanders, V., A.J. Conrad, and W.W. Tourtellotte, *On classification of post-mortem multiple sclerosis plaques for neuroscientists*. J Neuroimmunol, 1993. **46**(1-2): p. 207-16.
15. Gay, F.W., et al., *The application of multifactorial cluster analysis in the staging of plaques in early multiple sclerosis. Identification and characterization of the primary demyelinating lesion*. Brain, 1997. **120** (Pt 8): p. 1461-83.
16. Prineas, J.W., et al., *Immunopathology of secondary-progressive multiple sclerosis*. Ann Neurol, 2001. **50**(5): p. 646-57.
17. Marik, C., et al., *Lesion genesis in a subset of patients with multiple sclerosis: a role for innate immunity?* Brain, 2007. **130**(Pt 11): p. 2800-15.
18. Lassmann, H., *Hypoxia-like tissue injury as a component of multiple sclerosis lesions*. J Neurol Sci, 2003. **206**(2): p. 187-91.
19. Barnett, M.H. and J.W. Prineas, *Relapsing and remitting multiple sclerosis: pathology of the newly forming lesion*. Ann Neurol, 2004. **55**(4): p. 458-68.
20. van der Valk, P. and S. Amor, *Preactive lesions in multiple sclerosis*. Curr Opin Neurol, 2009. **22**(3): p. 207-13.
21. Li, H., et al., *Characterization and distribution of phagocytic macrophages in multiple sclerosis plaques*. Neuropathol Appl Neurobiol, 1993. **19**(3): p. 214-23.
22. Kuhlmann, T., et al., *Bcl-2-expressing oligodendrocytes in multiple sclerosis lesions*. Glia, 1999. **28**(1): p. 34-9.

23. Lucchinetti, C., et al., *Heterogeneity of multiple sclerosis lesions: implications for the pathogenesis of demyelination*. Ann Neurol, 2000. **47**(6): p. 707-17.
24. Ascherio, A., K.L. Munger, and K.C. Simon, *Vitamin D and multiple sclerosis*. Lancet Neurol, 2010. **9**(6): p. 599-612.
25. Challoner, P.B., et al., *Plaque-associated expression of human herpesvirus 6 in multiple sclerosis*. Proc Natl Acad Sci U S A, 1995. **92**(16): p. 7440-4.
26. Fensterl, V. and G.C. Sen, *Interferons and viral infections*. Biofactors, 2009. **35**(1): p. 14-20.
27. Kim, B., S.D. Kaistha, and B.T. Rouse, *Viruses and autoimmunity*. Autoimmunity, 2006. **39**(1): p. 71-7.
28. Lunemann, J.D., et al., *Elevated Epstein-Barr virus-encoded nuclear antigen-1 immune responses predict conversion to multiple sclerosis*. Ann Neurol, 2010. **67**(2): p. 159-69.
29. Marrie, R.A., *Environmental risk factors in multiple sclerosis aetiology*. Lancet Neurol, 2004. **3**(12): p. 709-18.
30. Soulet, D. and S. Rivest, *Microglia*. Curr Biol, 2008. **18**(12): p. R506-8.
31. Neumann, H., M.R. Kotter, and R.J. Franklin, *Debris clearance by microglia: an essential link between degeneration and regeneration*. Brain, 2009. **132**(Pt 2): p. 288-95.
32. Ransohoff, R.M. and V.H. Perry, *Microglial physiology: unique stimuli, specialized responses*. Annu Rev Immunol, 2009. **27**: p. 119-45.
33. van Noort, J.M., et al., *Alphab-crystallin is a target for adaptive immune responses and a trigger of innate responses in preactive multiple sclerosis lesions*. J Neuropathol Exp Neurol, 2010. **69**(7): p. 694-703.
34. Kipp, M., et al., *The cuprizone animal model: new insights into an old story*. Acta Neuropathol, 2009. **118**(6): p. 723-36.
35. Kipp, M., et al., *The hippocampal fimbria of cuprizone-treated animals as a structure for studying neuroprotection in multiple sclerosis*. Inflamm Res, 2011. **60**(8): p. 723-6.
36. Buschmann, J.P., et al., *Inflammatory Response and Chemokine Expression in the White Matter Corpus Callosum and Gray Matter Cortex Region During Cuprizone-Induced Demyelination*. J Mol Neurosci, 2012. **48**(1): p. 66-76.
37. Acs, P., et al., *17beta-estradiol and progesterone prevent cuprizone provoked demyelination of corpus callosum in male mice*. Glia, 2009. **57**(8): p. 807-14.
38. Clarner, T., et al., *Corticosteroids impair remyelination in the corpus callosum of cuprizone-treated mice*. J Neuroendocrinol, 2011. **23**(7): p. 601-11.
39. Groebe, A., et al., *Cuprizone treatment induces distinct demyelination, astrogliosis, and microglia cell invasion or proliferation in the mouse cerebellum*. Cerebellum, 2009. **8**(3): p. 163-74.
40. Gudi, V., et al., *Regional differences between grey and white matter in cuprizone induced demyelination*. Brain Res, 2009. **1283**: p. 127-38.
41. Skripuletz, T., et al., *De- and remyelination in the CNS white and grey matter induced by cuprizone: the old, the new, and the unexpected*. Histol Histopathol, 2011. **26**(12): p. 1585-97.
42. Noll, E. and R.H. Miller, *Oligodendrocyte precursors originate at the ventral ventricular zone dorsal to the ventral midline region in the embryonic rat spinal cord*. Development, 1993. **118**(2): p. 563-73.
43. Pringle, N.P., et al., *Dorsal spinal cord neuroepithelium generates astrocytes but not oligodendrocytes*. Neuron, 1998. **20**(5): p. 883-93.
44. Fu, H., et al., *Dual origin of spinal oligodendrocyte progenitors and evidence for the cooperative role of Olig2 and Nkx2.2 in the control of oligodendrocyte differentiation*. Development, 2002. **129**(3): p. 681-93.

45. Cai, J., et al., *Generation of oligodendrocyte precursor cells from mouse dorsal spinal cord independent of Nkx6 regulation and Shh signaling*. Neuron, 2005. **45**(1): p. 41-53.
46. Vallstedt, A., J.M. Klos, and J. Ericson, *Multiple dorsoventral origins of oligodendrocyte generation in the spinal cord and hindbrain*. Neuron, 2005. **45**(1): p. 55-67.
47. Kessaris, N., et al., *Competing waves of oligodendrocytes in the forebrain and postnatal elimination of an embryonic lineage*. Nat Neurosci, 2006. **9**(2): p. 173-9.
48. Noble, M., et al., *Development and regeneration in the central nervous system*. Philos Trans R Soc Lond B Biol Sci, 1990. **327**(1239): p. 127-43.
49. Fok-Seang, J. and R.H. Miller, *Distribution and differentiation of A2B5+ glial precursors in the developing rat spinal cord*. J Neurosci Res, 1994. **37**(2): p. 219-35.
50. Richardson, R.M., et al., *Isolation of neuronal progenitor cells from the adult human neocortex*. Acta Neurochir (Wien), 2006. **148**(7): p. 773-7.
51. Baumann, N. and D. Pham-Dinh, *Biology of oligodendrocyte and myelin in the mammalian central nervous system*. Physiol Rev, 2001. **81**(2): p. 871-927.
52. Miller, R.H., *Regulation of oligodendrocyte development in the vertebrate CNS*. Prog Neurobiol, 2002. **67**(6): p. 451-67.
53. Duchala, C.S., K. Asotra, and W.B. Macklin, *Expression of cell surface markers and myelin proteins in cultured oligodendrocytes from neonatal brain of rat and mouse: a comparative study*. Dev Neurosci, 1995. **17**(2): p. 70-80.
54. Pedraza, L., J.K. Huang, and D.R. Colman, *Organizing principles of the axoglial apparatus*. Neuron, 2001. **30**(2): p. 335-44.
55. Kursula, P., *Structural properties of proteins specific to the myelin sheath*. Amino Acids, 2008. **34**(2): p. 175-85.
56. Simons, M. and K. Trajkovic, *Neuron-glia communication in the control of oligodendrocyte function and myelin biogenesis*. J Cell Sci, 2006. **119**(Pt 21): p. 4381-9.
57. Pfeiffer, S.E., A.E. Warrington, and R. Bansal, *The oligodendrocyte and its many cellular processes*. Trends Cell Biol, 1993. **3**(6): p. 191-7.
58. Lajtha, A., et al., *Turnover of myelin proteins in mouse brain in vivo*. Biochem J, 1977. **164**(2): p. 323-9.
59. LeBaron, F.N., S. Sanyal, and F.B. Jungalwala, *Turnover rate of molecular species of sphingomyelin in rat brain*. Neurochem Res, 1981. **6**(10): p. 1081-9.
60. McTigue, D.M. and R.B. Tripathi, *The life, death, and replacement of oligodendrocytes in the adult CNS*. J Neurochem, 2008. **107**(1): p. 1-19.
61. Connor, J.R. and S.L. Menzies, *Relationship of iron to oligodendrocytes and myelination*. Glia, 1996. **17**(2): p. 83-93.
62. Braughler, J.M., L.A. Duncan, and R.L. Chase, *The involvement of iron in lipid peroxidation. Importance of ferric to ferrous ratios in initiation*. J Biol Chem, 1986. **261**(22): p. 10282-9.
63. Juurlink, B.H., *Response of glial cells to ischemia: roles of reactive oxygen species and glutathione*. Neurosci Biobehav Rev, 1997. **21**(2): p. 151-66.
64. Thorburne, S.K. and B.H. Juurlink, *Low glutathione and high iron govern the susceptibility of oligodendroglial precursors to oxidative stress*. J Neurochem, 1996. **67**(3): p. 1014-22.
65. Bauer, J., et al., *Endoplasmic reticulum stress in PLP-overexpressing transgenic rats: gray matter oligodendrocytes are more vulnerable than white matter oligodendrocytes*. J Neuropathol Exp Neurol, 2002. **61**(1): p. 12-22.

66. Bradl, M., et al., *Transgenic Lewis rats overexpressing the proteolipid protein gene: myelin degeneration and its effect on T cell-mediated experimental autoimmune encephalomyelitis*. Acta Neuropathol, 1999. **97**(6): p. 595-606.
67. Lin, W. and B. Popko, *Endoplasmic reticulum stress in disorders of myelinating cells*. Nat Neurosci, 2009. **12**(4): p. 379-85.
68. Dowling, P., et al., *Cell death and birth in multiple sclerosis brain*. J Neurol Sci, 1997. **149**(1): p. 1-11.
69. Prineas, J.W. and J.D. Parratt, *Oligodendrocytes and the early multiple sclerosis lesion*. Ann Neurol, 2012. **72**(1): p. 18-31.
70. Butzkueven, H., et al., *LIF receptor signaling limits immune-mediated demyelination by enhancing oligodendrocyte survival*. Nat Med, 2002. **8**(6): p. 613-9.
71. Hisahara, S., et al., *Targeted expression of baculovirus p35 caspase inhibitor in oligodendrocytes protects mice against autoimmune-mediated demyelination*. EMBO J, 2000. **19**(3): p. 341-8.
72. Hovelmeier, N., et al., *Apoptosis of oligodendrocytes via Fas and TNF-RI is a key event in the induction of experimental autoimmune encephalomyelitis*. J Immunol, 2005. **175**(9): p. 5875-84.
73. Zendedel, A., C. Beyer, and M. Kipp, *Cuprizone-Induced Demyelination as a Tool to Study Remyelination and Axonal Protection*. J Mol Neurosci, 2013.
74. Dubois-Dalcq, M., C. Ffrench-Constant, and R.J. Franklin, *Enhancing central nervous system remyelination in multiple sclerosis*. Neuron, 2005. **48**(1): p. 9-12.
75. Nishiyama, A., *Glial progenitor cells in normal and pathological states*. Keio J Med, 1998. **47**(4): p. 205-8.
76. Nishiyama, A., *Polydendrocytes: NG2 cells with many roles in development and repair of the CNS*. Neuroscientist, 2007. **13**(1): p. 62-76.
77. Franklin, R.J., *Why does remyelination fail in multiple sclerosis?* Nat Rev Neurosci, 2002. **3**(9): p. 705-14.
78. Chang, A., et al., *Premyelinating oligodendrocytes in chronic lesions of multiple sclerosis*. N Engl J Med, 2002. **346**(3): p. 165-73.
79. Calver, A.R., et al., *Oligodendrocyte population dynamics and the role of PDGF in vivo*. Neuron, 1998. **20**(5): p. 869-82.
80. Noble, M., et al., *Platelet-derived growth factor promotes division and motility and inhibits premature differentiation of the oligodendrocyte/type-2 astrocyte progenitor cell*. Nature, 1988. **333**(6173): p. 560-2.
81. Richardson, W.D., et al., *A role for platelet-derived growth factor in normal gliogenesis in the central nervous system*. Cell, 1988. **53**(2): p. 309-19.
82. Engel, U. and G. Wolswijk, *Oligodendrocyte-type-2 astrocyte (O-2A) progenitor cells derived from adult rat spinal cord: in vitro characteristics and response to PDGF, bFGF and NT-3*. Glia, 1996. **16**(1): p. 16-26.
83. Gard, A.L. and S.E. Pfeiffer, *Two proliferative stages of the oligodendrocyte lineage (A2B5+O4- and O4+GalC-) under different mitogenic control*. Neuron, 1990. **5**(5): p. 615-25.
84. Wang, Z., H. Colognato, and C. Ffrench-Constant, *Contrasting effects of mitogenic growth factors on myelination in neuron-oligodendrocyte co-cultures*. Glia, 2007. **55**(5): p. 537-45.
85. Hinks, G.L. and R.J. Franklin, *Distinctive patterns of PDGF-A, FGF-2, IGF-I, and TGF-beta1 gene expression during remyelination of experimentally-induced spinal cord demyelination*. Mol Cell Neurosci, 1999. **14**(2): p. 153-68.
86. Baggiolini, M., *Chemokines and leukocyte traffic*. Nature, 1998. **392**(6676): p. 565-8.
87. Luster, A.D., *Chemokines--chemotactic cytokines that mediate inflammation*. N Engl J Med, 1998. **338**(7): p. 436-45.

88. Ubogu, E.E., M.B. Cossoy, and R.M. Ransohoff, *The expression and function of chemokines involved in CNS inflammation*. Trends Pharmacol Sci, 2006. **27**(1): p. 48-55.
89. Charo, I.F. and R.M. Ransohoff, *The many roles of chemokines and chemokine receptors in inflammation*. N Engl J Med, 2006. **354**(6): p. 610-21.
90. Fernandez, E.J. and E. Lolis, *Structure, function, and inhibition of chemokines*. Annu Rev Pharmacol Toxicol, 2002. **42**: p. 469-99.
91. Rossi, D. and A. Zlotnik, *The biology of chemokines and their receptors*. Annu Rev Immunol, 2000. **18**: p. 217-42.
92. Laing, K.J. and C.J. Secombes, *Chemokines*. Dev Comp Immunol, 2004. **28**(5): p. 443-60.
93. Murphy, P.M., *International Union of Pharmacology. XXX. Update on chemokine receptor nomenclature*. Pharmacol Rev, 2002. **54**(2): p. 227-9.
94. Mackay, C.R., *Chemokines: immunology's high impact factors*. Nat Immunol, 2001. **2**(2): p. 95-101.
95. Ransohoff, R.M., L. Liu, and A.E. Cardona, *Chemokines and chemokine receptors: multipurpose players in neuroinflammation*. Int Rev Neurobiol, 2007. **82**: p. 187-204.
96. Laudanna, C. and R. Alon, *Right on the spot. Chemokine triggering of integrin-mediated arrest of rolling leukocytes*. Thromb Haemost, 2006. **95**(1): p. 5-11.
97. Rittner, H.L. and A. Brack, *Chemokines and pain*. Curr Opin Investig Drugs, 2006. **7**(7): p. 643-6.
98. Nibbs, R.J., et al., *Cloning and characterization of a novel promiscuous human beta-chemokine receptor D6*. J Biol Chem, 1997. **272**(51): p. 32078-83.
99. Blackburn, P.E., et al., *Purification and biochemical characterization of the D6 chemokine receptor*. Biochem J, 2004. **379**(Pt 2): p. 263-72.
100. Hansell, C.A., C.V. Simpson, and R.J. Nibbs, *Chemokine sequestration by atypical chemokine receptors*. Biochem Soc Trans, 2006. **34**(Pt 6): p. 1009-13.
101. Mueller, A., E. Kelly, and P.G. Strange, *Pathways for internalization and recycling of the chemokine receptor CCR5*. Blood, 2002. **99**(3): p. 785-91.
102. Neel, N.F., et al., *Chemokine receptor internalization and intracellular trafficking*. Cytokine Growth Factor Rev, 2005. **16**(6): p. 637-58.
103. Belmadani, A., et al., *The chemokine stromal cell-derived factor-1 regulates the migration of sensory neuron progenitors*. J Neurosci, 2005. **25**(16): p. 3995-4003.
104. Li, M. and R.M. Ransohoff, *Multiple roles of chemokine CXCL12 in the central nervous system: a migration from immunology to neurobiology*. Prog Neurobiol, 2008. **84**(2): p. 116-31.
105. Lieberam, I., et al., *A Cxcl12-CXCR4 chemokine signaling pathway defines the initial trajectory of mammalian motor axons*. Neuron, 2005. **47**(5): p. 667-79.
106. Pujol, F., P. Kitabgi, and H. Boudin, *The chemokine SDF-1 differentially regulates axonal elongation and branching in hippocampal neurons*. J Cell Sci, 2005. **118**(Pt 5): p. 1071-80.
107. Guyon, A., et al., *Stromal cell-derived factor-1alpha modulation of the excitability of rat substantia nigra dopaminergic neurones: presynaptic mechanisms*. J Neurochem, 2006. **96**(6): p. 1540-50.
108. Skrzydelski, D., et al., *The chemokine stromal cell-derived factor-1/CXCL12 activates the nigrostriatal dopamine system*. J Neurochem, 2007. **102**(4): p. 1175-83.
109. Biber, K., et al., *Neuronal 'On' and 'Off' signals control microglia*. Trends Neurosci, 2007. **30**(11): p. 596-602.
110. Flynn, G., et al., *Regulation of chemokine receptor expression in human microglia and astrocytes*. J Neuroimmunol, 2003. **136**(1-2): p. 84-93.

111. Rezaie, P., et al., *Expression of beta-chemokines and chemokine receptors in human fetal astrocyte and microglial co-cultures: potential role of chemokines in the developing CNS*. *Glia*, 2002. **37**(1): p. 64-75.
112. Andjelkovic, A.V., et al., *Functional expression of CCR2 by human fetal astrocytes*. *J Neurosci Res*, 2002. **70**(2): p. 219-31.
113. Biber, K., et al., *Functional expression of CXCR3 in cultured mouse and human astrocytes and microglia*. *Neuroscience*, 2002. **112**(3): p. 487-97.
114. Tanabe, S., et al., *Functional expression of the CXC-chemokine receptor-4/fusin on mouse microglial cells and astrocytes*. *J Immunol*, 1997. **159**(2): p. 905-11.
115. Heesen, M., et al., *Mouse astrocytes respond to the chemokines MCP-1 and KC, but reverse transcriptase-polymerase chain reaction does not detect mRNA for the KC or new MCP-1 receptor*. *J Neurosci Res*, 1996. **45**(4): p. 382-91.
116. Odemis, V., et al., *Interleukin-6 and cAMP induce stromal cell-derived factor-1 chemotaxis in astroglia by up-regulating CXCR4 cell surface expression. Implications for brain inflammation*. *J Biol Chem*, 2002. **277**(42): p. 39801-8.
117. McMahon, E.J., et al., *Absence of macrophage-inflammatory protein-1alpha delays central nervous system demyelination in the presence of an intact blood-brain barrier*. *J Immunol*, 2001. **167**(5): p. 2964-71.
118. Glabinski, A.R., et al., *Synchronous synthesis of alpha- and beta-chemokines by cells of diverse lineage in the central nervous system of mice with relapses of chronic experimental autoimmune encephalomyelitis*. *Am J Pathol*, 1997. **150**(2): p. 617-30.
119. Szczucinski, A. and J. Losy, *Chemokines and chemokine receptors in multiple sclerosis. Potential targets for new therapies*. *Acta Neurol Scand*, 2007. **115**(3): p. 137-46.
120. Huang, D.R., et al., *Absence of monocyte chemoattractant protein 1 in mice leads to decreased local macrophage recruitment and antigen-specific T helper cell type 1 immune response in experimental autoimmune encephalomyelitis*. *J Exp Med*, 2001. **193**(6): p. 713-26.
121. Karpus, W.J. and R.M. Ransohoff, *Chemokine regulation of experimental autoimmune encephalomyelitis: temporal and spatial expression patterns govern disease pathogenesis*. *J Immunol*, 1998. **161**(6): p. 2667-71.
122. Karpus, W.J., et al., *An important role for the chemokine macrophage inflammatory protein-1 alpha in the pathogenesis of the T cell-mediated autoimmune disease, experimental autoimmune encephalomyelitis*. *J Immunol*, 1995. **155**(10): p. 5003-10.
123. Karpus, W.J. and K.J. Kennedy, *MIP-1alpha and MCP-1 differentially regulate acute and relapsing autoimmune encephalomyelitis as well as Th1/Th2 lymphocyte differentiation*. *J Leukoc Biol*, 1997. **62**(5): p. 681-7.
124. Fife, B.T., et al., *CXCL10 (IFN-gamma-inducible protein-10) control of encephalitogenic CD4+ T cell accumulation in the central nervous system during experimental autoimmune encephalomyelitis*. *J Immunol*, 2001. **166**(12): p. 7617-24.
125. Narumi, S., et al., *Neutralization of IFN-inducible protein 10/CXCL10 exacerbates experimental autoimmune encephalomyelitis*. *Eur J Immunol*, 2002. **32**(6): p. 1784-91.
126. Klein, R.S., et al., *IFN-inducible protein 10/CXC chemokine ligand 10-independent induction of experimental autoimmune encephalomyelitis*. *J Immunol*, 2004. **172**(1): p. 550-9.
127. Tsunoda, I., et al., *Distinct roles for IP-10/CXCL10 in three animal models, Theiler's virus infection, EAE, and MHV infection, for multiple sclerosis: implication of differing roles for IP-10*. *Mult Scler*, 2004. **10**(1): p. 26-34.
128. dos Santos, A.C., et al., *CCL2 and CCL5 mediate leukocyte adhesion in experimental autoimmune encephalomyelitis--an intravital microscopy study*. *J Neuroimmunol*, 2005. **162**(1-2): p. 122-9.

129. Sellebjerg, F. and T.L. Sorensen, *Chemokines and matrix metalloproteinase-9 in leukocyte recruitment to the central nervous system*. Brain Res Bull, 2003. **61**(3): p. 347-55.
130. Opdenakker, G., I. Nelissen, and J. Van Damme, *Functional roles and therapeutic targeting of gelatinase B and chemokines in multiple sclerosis*. Lancet Neurol, 2003. **2**(12): p. 747-56.
131. Kaur, C., et al., *Origin of microglia*. Microsc Res Tech, 2001. **54**(1): p. 2-9.
132. Ajami, B., et al., *Local self-renewal can sustain CNS microglia maintenance and function throughout adult life*. Nat Neurosci, 2007. **10**(12): p. 1538-43.
133. Lawson, L.J., V.H. Perry, and S. Gordon, *Turnover of resident microglia in the normal adult mouse brain*. Neuroscience, 1992. **48**(2): p. 405-15.
134. Nimmerjahn, A., F. Kirchhoff, and F. Helmchen, *Resting microglial cells are highly dynamic surveillants of brain parenchyma in vivo*. Science, 2005. **308**(5726): p. 1314-8.
135. Davalos, D., et al., *ATP mediates rapid microglial response to local brain injury in vivo*. Nat Neurosci, 2005. **8**(6): p. 752-8.
136. Carbonell, W.S., et al., *Migration of perilesional microglia after focal brain injury and modulation by CC chemokine receptor 5: an in situ time-lapse confocal imaging study*. J Neurosci, 2005. **25**(30): p. 7040-7.
137. Streit, W.J., M.B. Graeber, and G.W. Kreutzberg, *Functional plasticity of microglia: a review*. Glia, 1988. **1**(5): p. 301-7.
138. Kim, S.U. and J. de Vellis, *Microglia in health and disease*. J Neurosci Res, 2005. **81**(3): p. 302-13.
139. Dheen, S.T., C. Kaur, and E.A. Ling, *Microglial activation and its implications in the brain diseases*. Curr Med Chem, 2007. **14**(11): p. 1189-97.
140. Gonzalez-Scarano, F. and G. Baltuch, *Microglia as mediators of inflammatory and degenerative diseases*. Annu Rev Neurosci, 1999. **22**: p. 219-40.
141. Donnelly, D.J. and P.G. Popovich, *Inflammation and its role in neuroprotection, axonal regeneration and functional recovery after spinal cord injury*. Exp Neurol, 2008. **209**(2): p. 378-88.
142. King, I.L., T.L. Dickendesher, and B.M. Segal, *Circulating Ly-6C⁺ myeloid precursors migrate to the CNS and play a pathogenic role during autoimmune demyelinating disease*. Blood, 2009. **113**(14): p. 3190-7.
143. Tran, E.H., et al., *Immune invasion of the central nervous system parenchyma and experimental allergic encephalomyelitis, but not leukocyte extravasation from blood, are prevented in macrophage-depleted mice*. J Immunol, 1998. **161**(7): p. 3767-75.
144. Berger, T., et al., *Experimental autoimmune encephalomyelitis: the antigen specificity of T lymphocytes determines the topography of lesions in the central and peripheral nervous system*. Lab Invest, 1997. **76**(3): p. 355-64.
145. Prineas, J.W. and F. Connell, *The fine structure of chronically active multiple sclerosis plaques*. Neurology, 1978. **28**(9 Pt 2): p. 68-75.
146. Prineas, J.W. and R.G. Wright, *Macrophages, lymphocytes, and plasma cells in the perivascular compartment in chronic multiple sclerosis*. Lab Invest, 1978. **38**(4): p. 409-21.
147. Prineas, J.W., et al., *Multiple sclerosis: remyelination of nascent lesions*. Ann Neurol, 1993. **33**(2): p. 137-51.
148. Merrill, J.E., et al., *Microglial cell cytotoxicity of oligodendrocytes is mediated through nitric oxide*. J Immunol, 1993. **151**(4): p. 2132-41.
149. Merrill, J.E. and R.P. Zimmerman, *Natural and induced cytotoxicity of oligodendrocytes by microglia is inhibitable by TGF beta*. Glia, 1991. **4**(3): p. 327-31.

150. Trapp, B.D., et al., *Axonal transection in the lesions of multiple sclerosis*. N Engl J Med, 1998. **338**(5): p. 278-85.
151. Peterson, J.W., et al., *VCAM-1-positive microglia target oligodendrocytes at the border of multiple sclerosis lesions*. J Neuropathol Exp Neurol, 2002. **61**(6): p. 539-46.
152. Arnett, H.A., et al., *TNF alpha promotes proliferation of oligodendrocyte progenitors and remyelination*. Nat Neurosci, 2001. **4**(11): p. 1116-22.
153. Foote, A.K. and W.F. Blakemore, *Inflammation stimulates remyelination in areas of chronic demyelination*. Brain, 2005. **128**(Pt 3): p. 528-39.
154. Kotter, M.R., et al., *Macrophage-depletion induced impairment of experimental CNS remyelination is associated with a reduced oligodendrocyte progenitor cell response and altered growth factor expression*. Neurobiol Dis, 2005. **18**(1): p. 166-75.
155. Kotter, M.R., et al., *Macrophage depletion impairs oligodendrocyte remyelination following lyssolecithin-induced demyelination*. Glia, 2001. **35**(3): p. 204-12.
156. Hintermann, E., et al., *CXCL10 promotes liver fibrosis by prevention of NK cell mediated hepatic stellate cell inactivation*. J Autoimmun, 2010. **35**(4): p. 424-35.
157. Kipp, M., et al., *Brain lipid binding protein (FABP7) as modulator of astrocyte function*. Physiol Res, 2011. **60 Suppl 1**: p. S49-60.
158. Hesse, A., et al., *In toxic demyelination oligodendroglial cell death occurs early and is FAS independent*. Neurobiol Dis, 2010. **37**(2): p. 362-9.
159. Norkute, A., et al., *Cuprizone treatment induces demyelination and astrogliosis in the mouse hippocampus*. J Neurosci Res, 2009. **87**(6): p. 1343-55.
160. Villeneuve, J., P. Tremblay, and L. Vallieres, *Tumor necrosis factor reduces brain tumor growth by enhancing macrophage recruitment and microcyst formation*. Cancer Res, 2005. **65**(9): p. 3928-36.
161. Chen, Y., et al., *Isolation and culture of rat and mouse oligodendrocyte precursor cells*. Nat Protoc, 2007. **2**(5): p. 1044-51.
162. Richter-Landsberg, C. and U. Vollgraf, *Mode of cell injury and death after hydrogen peroxide exposure in cultured oligodendroglia cells*. Exp Cell Res, 1998. **244**(1): p. 218-29.
163. Richter-Landsberg, C. and M. Gorath, *Developmental regulation of alternatively spliced isoforms of mRNA encoding MAP2 and tau in rat brain oligodendrocytes during culture maturation*. J Neurosci Res, 1999. **56**(3): p. 259-70.
164. Richter-Landsberg, C. and M. Heinrich, *OLN-93: a new permanent oligodendroglia cell line derived from primary rat brain glial cultures*. J Neurosci Res, 1996. **45**(2): p. 161-73.
165. Beutner, C., et al., *Generation of microglial cells from mouse embryonic stem cells*. Nat Protoc, 2010. **5**(9): p. 1481-94.
166. Braun, A., et al., *Selective regulation of growth factor expression in cultured cortical astrocytes by neuro-pathological toxins*. Neurochem Int, 2009. **55**(7): p. 610-8.
167. Kipp, M., et al., *Brain-region-specific astroglial responses in vitro after LPS exposure*. J Mol Neurosci, 2008. **35**(2): p. 235-43.
168. Johann, S., et al., *Expression of enzymes involved in the prostanoid metabolism by cortical astrocytes after LPS-induced inflammation*. J Mol Neurosci, 2008. **34**(2): p. 177-85.
169. Kipp, M., et al., *BLBP-expression in astrocytes during experimental demyelination and in human multiple sclerosis lesions*. Brain Behav Immun, 2011. **25**(8): p. 1554-68.
170. Irizarry, R.A., et al., *Summaries of Affymetrix GeneChip probe level data*. Nucleic Acids Res, 2003. **31**(4): p. e15.

171. Zeis, T., et al., *Normal-appearing white matter in multiple sclerosis is in a subtle balance between inflammation and neuroprotection*. Brain, 2008. **131**(Pt 1): p. 288-303.
172. Tirotta, E., R.M. Ransohoff, and T.E. Lane, *CXCR2 signaling protects oligodendrocyte progenitor cells from IFN-gamma/CXCL10-mediated apoptosis*. Glia, 2011. **59**(10): p. 1518-28.
173. Huynh, K.K., et al., *LAMP proteins are required for fusion of lysosomes with phagosomes*. EMBO J, 2007. **26**(2): p. 313-24.
174. Eskelinen, E.L., Y. Tanaka, and P. Saftig, *At the acidic edge: emerging functions for lysosomal membrane proteins*. Trends Cell Biol, 2003. **13**(3): p. 137-45.
175. Ffrench-Constant, C. and M.C. Raff, *Proliferating bipotential glial progenitor cells in adult rat optic nerve*. Nature, 1986. **319**(6053): p. 499-502.
176. Lassmann, H., et al., *Remyelination in multiple sclerosis*. Mult Scler, 1997. **3**(2): p. 133-6.
177. Wootla, B., et al., *The road to remyelination in demyelinating diseases: current status and prospects for clinical treatment*. Expert Rev Clin Immunol, 2013. **9**(6): p. 535-49.
178. Watzlawik, J., A.E. Warrington, and M. Rodriguez, *Importance of oligodendrocyte protection, BBB breakdown and inflammation for remyelination*. Expert Rev Neurother, 2010. **10**(3): p. 441-57.
179. Frost, E.E., et al., *Initiation of oligodendrocyte progenitor cell migration by a PDGF-A activated extracellular regulated kinase (ERK) signaling pathway*. Neurochem Res, 2009. **34**(1): p. 169-81.
180. Besser, D., M. Presta, and Y. Nagamine, *Elucidation of a signaling pathway induced by FGF-2 leading to uPA gene expression in NIH 3T3 fibroblasts*. Cell Growth Differ, 1995. **6**(8): p. 1009-17.
181. Vora, P., et al., *Differential effects of growth factors on oligodendrocyte progenitor migration*. Eur J Cell Biol, 2011. **90**(8): p. 649-56.
182. Aboul-Enein, F., et al., *Preferential loss of myelin-associated glycoprotein reflects hypoxia-like white matter damage in stroke and inflammatory brain diseases*. J Neuropathol Exp Neurol, 2003. **62**(1): p. 25-33.
183. Berger, K., et al., *Oligodendrocyte-derived chemokine CXCL10 triggers microglial activation in the cuprizone animal model of multiple sclerosis* 2013, Institute of Neuroanatomy: Aachen.
184. Lu, B., et al., *Abnormalities in monocyte recruitment and cytokine expression in monocyte chemoattractant protein 1-deficient mice*. J Exp Med, 1998. **187**(4): p. 601-8.
185. Cook, D.N., et al., *Requirement of MIP-1 alpha for an inflammatory response to viral infection*. Science, 1995. **269**(5230): p. 1583-5.
186. Luster, A.D., J.C. Unkeless, and J.V. Ravetch, *Gamma-interferon transcriptionally regulates an early-response gene containing homology to platelet proteins*. Nature, 1985. **315**(6021): p. 672-6.
187. Balabanov, R., et al., *Interferon-gamma-oligodendrocyte interactions in the regulation of experimental autoimmune encephalomyelitis*. J Neurosci, 2007. **27**(8): p. 2013-24.
188. Trapp, B.D. and K.A. Nave, *Multiple sclerosis: an immune or neurodegenerative disorder?* Annu Rev Neurosci, 2008. **31**: p. 247-69.
189. Kassmann, C.M., et al., *Axonal loss and neuroinflammation caused by peroxisome-deficient oligodendrocytes*. Nat Genet, 2007. **39**(8): p. 969-76.
190. Mana, P., et al., *Deleterious role of IFNgamma in a toxic model of central nervous system demyelination*. Am J Pathol, 2006. **168**(5): p. 1464-73.

191. Muzio, L., et al., *Cxcl10 enhances blood cells migration in the sub-ventricular zone of mice affected by experimental autoimmune encephalomyelitis*. Mol Cell Neurosci, 2010. **43**(3): p. 268-80.
192. Renno, T., et al., *Interferon-gamma in progression to chronic demyelination and neurological deficit following acute EAE*. Mol Cell Neurosci, 1998. **12**(6): p. 376-89.
193. Beck, J., et al., *Increased production of interferon gamma and tumor necrosis factor precedes clinical manifestation in multiple sclerosis: do cytokines trigger off exacerbations?* Acta Neurol Scand, 1988. **78**(4): p. 318-23.
194. Szczucinski, A. and J. Losy, *CCL5, CXCL10 and CXCL11 chemokines in patients with active and stable relapsing-remitting multiple sclerosis*. Neuroimmunomodulation, 2011. **18**(1): p. 67-72.
195. Muzio, L., et al., *Cxcl10 enhances blood cells migration in the sub-ventricular zone of mice affected by experimental autoimmune encephalomyelitis*. Mol Cell Neurosci, 2009. **43**(3): p. 268-80.
196. Subileau, E.A., et al., *Expression of chemokines and their receptors by human brain endothelium: implications for multiple sclerosis*. J Neuropathol Exp Neurol, 2009. **68**(3): p. 227-40.
197. Sorensen, T.L., et al., *Multiple sclerosis: a study of CXCL10 and CXCR3 co-localization in the inflamed central nervous system*. J Neuroimmunol, 2002. **127**(1-2): p. 59-68.
198. Biancotti, J.C., S. Kumar, and J. de Vellis, *Activation of inflammatory response by a combination of growth factors in cuprizone-induced demyelinated brain leads to myelin repair*. Neurochem Res, 2008. **33**(12): p. 2615-28.
199. Skripuletz, T., et al., *Astrocytes regulate myelin clearance through recruitment of microglia during cuprizone-induced demyelination*. Brain, 2013. **136**(Pt 1): p. 147-67.
200. Wojcik, W.J., et al., *Chronic intrathecal infusion of phosphorothioate or phosphodiester antisense oligonucleotides against cytokine responsive gene-2/IP-10 in experimental allergic encephalomyelitis of lewis rat*. J Pharmacol Exp Ther, 1996. **278**(1): p. 404-10.
201. Bogler, O., et al., *Cooperation between two growth factors promotes extended self-renewal and inhibits differentiation of oligodendrocyte-type-2 astrocyte (O-2A) progenitor cells*. Proc Natl Acad Sci U S A, 1990. **87**(16): p. 6368-72.
202. McKinnon, R.D., et al., *A role for fibroblast growth factor in oligodendrocyte development*. Ann N Y Acad Sci, 1991. **638**: p. 378-86.
203. Pringle, N., et al., *PDGF A chain homodimers drive proliferation of bipotential (O-2A) glial progenitor cells in the developing rat optic nerve*. EMBO J, 1989. **8**(4): p. 1049-56.
204. Raff, M.C., R.H. Miller, and M. Noble, *A glial progenitor cell that develops in vitro into an astrocyte or an oligodendrocyte depending on culture medium*. Nature, 1983. **303**(5916): p. 390-6.
205. Webster, H.D., *Growth factors and myelin regeneration in multiple sclerosis*. Mult Scler, 1997. **3**(2): p. 113-20.
206. Stangel, M. and C. Trebst, *Remyelination strategies: new advancements toward a regenerative treatment in multiple sclerosis*. Curr Neurol Neurosci Rep, 2006. **6**(3): p. 229-35.
207. Fressinaud, C., J.M. Vallat, and G. Labourdette, *Basic fibroblast growth factor down-regulates myelin basic protein gene expression and alters myelin compaction of mature oligodendrocytes in vitro*. J Neurosci Res, 1995. **40**(3): p. 285-93.
208. Messersmith, D.J., et al., *Fibroblast growth factor 2 (FGF2) and FGF receptor expression in an experimental demyelinating disease with extensive remyelination*. J Neurosci Res, 2000. **62**(2): p. 241-56.

209. Sarchielli, P., et al., *Fibroblast growth factor-2 levels are elevated in the cerebrospinal fluid of multiple sclerosis patients*. *Neurosci Lett*, 2008. **435**(3): p. 223-8.
210. Maeda, Y., et al., *Platelet-derived growth factor-alpha receptor-positive oligodendroglia are frequent in multiple sclerosis lesions*. *Ann Neurol*, 2001. **49**(6): p. 776-85.
211. Stangel, M. and H.P. Hartung, *Remyelinating strategies for the treatment of multiple sclerosis*. *Prog Neurobiol*, 2002. **68**(5): p. 361-76.
212. Zhao, C., et al., *Mechanisms of CNS remyelination--the key to therapeutic advances*. *J Neurol Sci*, 2005. **233**(1-2): p. 87-91.
213. Stangel, M., *Remyelinating and neuroprotective treatments in multiple sclerosis*. *Expert Opin Investig Drugs*, 2004. **13**(4): p. 331-47.
214. Kotter, M.R., C. Stadelmann, and H.P. Hartung, *Enhancing remyelination in disease--can we wrap it up?* *Brain*, 2011. **134**(Pt 7): p. 1882-900.
215. Moore, C.S., et al., *How factors secreted from astrocytes impact myelin repair*. *J Neurosci Res*, 2011. **89**(1): p. 13-21.
216. Zou, L.P., et al., *Dynamics of production of MIP-1alpha, MCP-1 and MIP-2 and potential role of neutralization of these chemokines in the regulation of immune responses during experimental autoimmune neuritis in Lewis rats*. *J Neuroimmunol*, 1999. **98**(2): p. 168-75.
217. Skripuletz, T., et al., *Cortical demyelination is prominent in the murine cuprizone model and is strain-dependent*. *Am J Pathol*, 2008. **172**(4): p. 1053-61.
218. Clarner, T., et al., *Myelin debris regulates inflammatory responses in an experimental demyelination animal model and multiple sclerosis lesions*. *Glia*, 2012. **60**(10): p. 1468-80.
219. Bo, L., et al., *Intracortical multiple sclerosis lesions are not associated with increased lymphocyte infiltration*. *Mult Scler*, 2003. **9**(4): p. 323-31.
220. Breij, E.C., et al., *Homogeneity of active demyelinating lesions in established multiple sclerosis*. *Ann Neurol*, 2008. **63**(1): p. 16-25.
221. van Horssen, J., et al., *The blood-brain barrier in cortical multiple sclerosis lesions*. *J Neuropathol Exp Neurol*, 2007. **66**(4): p. 321-8.
222. Peterson, J.W., et al., *Transected neurites, apoptotic neurons, and reduced inflammation in cortical multiple sclerosis lesions*. *Ann Neurol*, 2001. **50**(3): p. 389-400.

8. Summary

Multiple sclerosis (MS) is a demyelinating disorder of the central nervous system classically discussed as an autoimmune disease. However, recent neuropathological evidence suggests that primary oligodendroglipathy might trigger the inflammatory response during MS lesion development. In my thesis I showed that cuprizone-treatment induced a distal oligodendroglipathy within days that was paralleled by early microgliosis. The chemokines CXCL10, CCL2 and CCL3 were found to be upregulated in this tissue. In CXCL10, but not CCL2 and CCL3 deficient mice, microglia recruitment was decreased indicating a pivotal role of CXCL10 in the initiation of inflammatory foci. CXCL10 was found to be predominantly expressed by damaged oligodendrocytes. Further *in vitro* studies confirmed that oligodendrocyte-derived CXCL10 induced microglia migration and a pro-inflammatory M1-phenotype. In summary, my results show that stressed oligodendrocytes release CXCL10, which activates microglia suggesting that oligodendrocytes can actively participate in the initiation of neuroinflammatory events.

In the second part of my thesis I investigated the role of the growth factors FGF-2 and PDGF α on oligodendrocyte precursor cell (OPC) maturation, a process necessary to achieve correct and sufficient remyelination in MS lesions. FGF-2 and PDGF α treatment of primary OPCs showed that both growth factors negatively influence maturation of oligodendrocytes *in vitro*. An imbalance in this growth factor system might thus account for some aspects of oligodendrocyte pathology observed in distinct MS lesion subtypes and remyelination failure. In the last part of my thesis I investigated redundant functions of the chemokines CCL2 and CCL3 using a newly bred double knockout mouse strain (CCL2/3^{-/-}) deficient in both genes. A basic investigation of the mice confirmed the absence of CCL2 and CCL3 on the mRNA and protein level and revealed that the mice show no gross abnormalities in brain tissue morphology and histology. Interestingly, a 5 weeks cuprizone-trial showed that CCL2/3^{-/-} mice display regional differences with less severe demyelination, oligodendrocyte loss and astroglia activation in the cortex, but not in the corpus callosum compared to wild type mice. With respect to MS pathology, future studies have to take into consideration that white and gray matter display different regions with respect to their cytoarchitecture and molecular composition.

Zusammenfassung

Die multiple Sklerose (MS) ist eine demyelinisierende Erkrankung des zentralen Nervensystems, die klassischerweise als Autoimmunerkrankung angesehen wird. Eine Reihe neuropathologischer Studien deuten jedoch drauf hin, dass eine primäre Oligodendrogliepathie ein Trigger der Immunantwort während der MS Läsionsentstehung ist. In meiner Arbeit konnte ich zeigen, dass die Behandlung mit Cuprizone in kurzer Zeit zu einer distalen Oligodendrogliepathie führt, die mit einer frühen Mikroglie einhergeht. Dabei sind die Chemokine CXCL10, CCL2 und CCL3 im Gewebe hochreguliert. Weitere Untersuchungen mit CXCL10, CCL2 und CCL3 defizienten Mäusen zeigten, dass ausschließlich CXCL10 defiziente Mäuse eine verringerte Mikroglia-Rekrutierung nach Cuprizone-Gabe zeigen. Dies verdeutlicht die wichtige Rolle von CXCL10 für die frühe Immunantwort. Es konnte zudem gezeigt werden, dass CXCL10 hauptsächlich von geschädigten Oligodendrozyten exprimiert wird. Weiterführende *in vitro* Versuche bestätigten, dass von Oligodendrozyten produziertes CXCL10 die Migration von Mikrogliazellen stimuliert und zur Aktivierung eines pro-inflammatorischen M1-Phänotyps in den Mikrogliazellen führt. Meine Ergebnisse zeigen, dass gestresste Oligodendrozyten CXCL10 produzieren, welches wiederum Mikrogliazellen aktiviert und somit Oligodendrozyten eine aktive Rolle in der Initiierung neuroinflammatorischer Prozesse übernehmen können.

Im zweiten Teil meiner Arbeit habe ich den Effekt der Wachstumsfaktoren FGF-2 und PDGF α auf die Ausreifung von Oligodendrozytenvorläufern (OPC) untersucht, ein Prozess der notwendig ist eine korrekte und ausreichende Remyelinisierung in MS Läsionen zu erreichen. Die *in vitro* Behandlung von primären OPCs mit FGF-2 und PDGF α zeigte, dass beide Wachstumsfaktoren die Ausreifung der Zellen negativ beeinflussen. Eine Störung dieses Wachstumsfaktor-Systems könnte für einige Aspekte der Oligodendrozytenpathologie bestimmter MS Läsionen verantwortlich sein und eine Rolle beim Versagen der Remyelinisierung spielen.

Im letzten Teil meiner Thesis untersuchte ich redundante Funktionen der Chemokine CCL2 und CCL3 mittels einer neu gezüchteten "knockout" Mauslinie (CCL2/3^{-/-}) der beide Chemokine fehlen. Eine Grundcharakterisierung der Mäuse ergab, dass die Tiere keine CCL2 oder CCL3 mRNA bzw. Proteine produzieren und dass die Mäuse keine besonderen Veränderungen der Hirnmorphologie oder Histologie aufweisen. Interessanterweise zeigte sich nach einem 5 Wochen Cuprizone-Versuch, dass die CCL2/3^{-/-} Mäuse im Vergleich zu Wildtyp Mäusen regionale Unterschiede in der Histopathologie des Cortex, jedoch nicht des

Corpus callosum aufweisen. Dazu zählen eine verringerte Demyelinisierung, weniger Oligodendrozytenapoptose und eine verringerte Astroglie. Zukünftige Studien, die sich mit der MS Pathologie befassen, sollten demnach die zellulären und molekularen Unterschiede der weißen und grauen Substanz stärker berücksichtigen.

9. Curriculum vitae

Katharina Janssen geborene Berger

Deidesheimer Straße 29

68309 Mannheim

E-mail: katharina.janssen@abbvie.com

Zur Person

Geburtsdatum: 20.02.1985

Geburtsort : Witten

Familienstand: verheiratet

Staatsangehörigkeit: deutsch

Beruflicher Werdegang

06/2013 – heute Trainee bei AbbVie Deutschland GmbH & Co KG.

03/2010 – 06/2013 Promotion am Institut für Neuroanatomie, Universitätsklinikum Aachen

08/2009 – 02/2010 Wissenschaftliche Mitarbeiterin, Medizinische Klinik III, Universitätsklinikum Aachen

03/2009 - 07/2009 Englisch- und Biologie-Tutorin bei Schülerhilfe Wetter und Lernstudio Barbarossa Witten

Studium

10/2004-03/2009 Studium der Biologie an der Ruhr-Universität Bochum
Abschluss: Diplom, Note: 1,0

04/2008-03/2009 Diplomarbeit am Lehrstuhl für Zellmorphologie und Molekulare Neurobiologie, Ruhr-Universität Bochum

Schulbildung

08/1991-06/2004 Rudolf Steiner Schule Bochum

06/2004 Abschluss: Allgemeine Hochschulreife, Note 1,9

Mannheim, 07.04.2014

Publications

- Astroglial redistribution of aquaporin 4 during spongy degeneration in a Canavan disease mouse model. Clarner T, Wiczorek N, Krauspe B, **Janssen K**, Beyer C, Kipp M. J Mol Neurosci. 2013 Nov 24 (Epub ahead of print).
- Inflammatory Response and Chemokine Expression in the White Matter Corpus Callosum and Gray Matter Cortex Region During Cuprizone-Induced Demyelination. Buschmann JP*, **Berger K***, Awad H, Clarner T, Beyer C, Kipp M. J Mol Neurosci. Epub 2012 Apr 22. * contributed equally; own data used for dissertation.
- Micro-RNA profiling in human serum reveals compartment-specific roles of miR-571 and miR-652 in liver cirrhosis. Roderburg C, Mollnow T, Bongaerts B, Elfimova N, Vargas Cardenas D, **Berger K**, Zimmermann H, Koch A, Vucur M, Luedde M, Hellerbrand C, Odenthal M, Trautwein C, Tacke F, Luedde T. PLoS One. 2012;7(3):e32999. Epub 2012 Mar 7.
- Sex steroids control neuroinflammatory processes in the brain: relevance for acute ischaemia and degenerative demyelination. Kipp M, **Berger K**, Clarner T, Dang J, Beyer C. J Neuroendocrinol. 2012 Jan; 24(1)
- Myelin debris regulates inflammatory responses in an experimental demyelination animal model and multiple sclerosis lesions. Clarner T, Diederichs F, **Berger K**, Denecke B, Gan L, van der Valk P, Beyer C, Amor S, Kipp M. Glia. 2012 Oct; 60(10):1468-80. doi: 10.1002/glia.22367. Epub 2012 Jun 11.
- The hippocampal fimbria of cuprizone-treated animals as a structure for studying neuroprotection in multiple sclerosis. Kipp M, Norkus A, Krauspe B, Clarner T, **Berger K**, van der Valk P, Amor S, Beyer C. Inflamm Res. 2011 Aug;60(8):723-6. Epub 2011 Apr 24.

10. Danksagung

Eine Doktorarbeit ist natürlich nichts, was man völlig alleine bewerkstelligt. Deshalb möchte ich mich an dieser Stelle bei einigen Personen besonders bedanken.

Zunächst vielen Dank an das Prüfungskomitee, dass Sie sich bereit erklärt haben diese Arbeit zu betreuen.

Herrn Professor Cordian Beyer und Professor Markus Kipp danke ich für die Möglichkeit, dass ich im Rahmen meiner Doktorarbeit dieses spannende Thema bearbeiten durfte, für anregende Diskussionen und für die tolle Unterstützung.

Markus möchte ich noch einmal explizit für die hervorragende Betreuung danken. Ich habe sehr viel bei dir gelernt, ganz besonders eine Lebensweisheit: „Was dich nicht umbringt macht dich härter“!

Helga, Uta und Petra danke ich ganz herzlich für die großartige Hilfe im Labor und ihre Kollegialität.

Und auch bei meinen restlichen ehemaligen Kollegen aus der Neuroanatomie, sowie meinen Freunden hier in Aachen, danke ich für drei spannende, anstrengende aber vor allem lustige Jahre. Ihr seid ein tolles Team mit dem ich immer viel Spaß hatte und hoffentlich auch in Zukunft noch haben werde.

Zu guter Letzt möchte ich mich bei meiner Familie bedanken. Schön das ihr immer für mich da seid, ihr seid das Wichtigste.